Earth-Science Reviews 255 (2024) 104772

Contents lists available at ScienceDirect

Earth-Science Reviews

journal homepage: www.elsevier.com/locate/earth-science-reviews

Invited review

# Complementary classifications of aeolian dunes based on morphology, dynamics, and fluid mechanics

Sylvain Courrech du Pont [a,*], David M. Rubin [b], Clément Narteau [c], Mathieu G.A. Lapôtre [d], Mackenzie Day [e], Philippe Claudin [f], Ian Livingstone [g], Matt W. Telfer [h], Jani Radebaugh [i], Cyril Gadal [j], Andrew Gunn [d,k], Patrick A. Hesp [l], Sabrina Carpy [m], Charles S. Bristow [n], Andreas C.W. Baas [o], Ryan C. Ewing [p], Giles F.S. Wiggs [q]

[a] *Laboratoire Matière et Systèmes Complexes, Université Paris Cité, CNRS, Paris, France*
[b] *Department of Earth and Planetary Sciences, University of Santa Cruz, Santa Cruz, USA*
[c] *Institut de Physique du Globe de Paris, Université Paris Cité, CNRS, Paris, France*
[d] *Department of Earth and Planetary Sciences, Stanford University, Stanford, USA*
[e] *Department of Earth, Planetary, and Space Sciences, University of California Los Angeles, Los Angeles, USA*
[f] *Laboratoire de Physique et Mécanique des Milieux Hétérogènes, CNRS, ESPCI Paris, PSL Research University, Université Paris Cité, Sorbonne Université, Paris, France*
[g] *The Graduate School, The University of Northampton, Northampton, UK*
[h] *SOGEES, University of Plymouth, Plymouth, UK*
[i] *Department of Geological Sciences, Brigham Young University, Provo, USA*
[j] *Department of Mathematics and Manchester Centre for Nonlinear Dynamics, The University of Manchester, Manchester, UK*
[k] *School of Earth, Atmosphere and Environment, Monash University, Clayton, Australia*
[l] *College of Science and Engineering, Flinders University, Bedford Park, Australia*
[m] *Laboratoire de Planétologie et Géosciences, CNRS, Nantes Université, Université Angers, Le Mans Université, Nantes, France*
[n] *Department of Earth and Planetary Sciences, Birkbeck University of London, London, UK*
[o] *Department of Geography, King's College London, London, UK*
[p] *Department of Geology and Geophysics, Texas A&M University, College Station, USA*
[q] *School of Geography and the Environment, University of Oxford, UK*

## ARTICLE INFO

*Keywords:*
Dune classification
Geomorphology
Morphodynamics
Fluid mechanics
Sediment transport
Aeolian bedforms
Desert, coastal, and planetary dune types
Wind-blown landscapes

## ABSTRACT

Dunes form where winds blow over a bed of mobile sediment grains — conditions that are common in our solar system. On Earth, dunes abound in arid continental interiors and along sandy coastlines. Dune fields have also been recognized on Venus, Mars, Saturn's moon Titan, and Pluto. In response to the different boundary conditions and other environmental forcings, dunes adopt a rich diversity of shapes, sizes, and behaviors. Thus, people around the globe and over centuries have developed a rich vocabulary to describe dunes and their complexity. As a result, existing dune nomenclature often includes redundant terms with differing definitions across scientific communities. Previous studies have endeavored to link dune shape to environmental forcing, usually by means of correlation. Although instructive, correlation-based classifications can be misleading if not based on underlying mechanics or if dune morphogenetic classes are not uniquely defined. Here, we synthesize existing dune terminology and use the last two decades of research on dune morphodynamics to propose three complementary dune classification schemes based on: (1) descriptive dune geomorphology, (2) morphodynamic processes, and (3) fluid mechanics and physics of sediment transport. The first classification relates dune types to geomorphic setting, the presence or absence of vegetation or obstacles, and dune shape (including planform shape, and cross-sectional symmetry or asymmetry). Dune classes can be further subdivided where the direction of sand transport is known independently. The second classification relates dune types and shapes to bed properties (sand-covered vs partially starved bed) and wind forcing (directional variability or the relative strengths and directions of wind modes) that together influence dune dynamics (growth, migration, elongation) and select the dominant processes by which dunes are shaped and oriented relative to the resultant transport direction. The third classification relates, for different planetary environments, the range of possible dune sizes, from minimum to maximum wavelength, to fluid

* Corresponding author.
*E-mail address:* sylvain.courrech@u-paris.fr (S. Courrech du Pont).

https://doi.org/10.1016/j.earscirev.2024.104772
Received 2 October 2023; Received in revised form 29 March 2024; Accepted 1 April 2024
Available online 6 April 2024

flow regime (rough or smooth) and the response of sediment flux, which influence the coupling between sand bed topography, fluid flow, and sediment transport. These characteristic lengths are useful scales for comparative geomorphology. The three classification schemes provide complementary information. Together, they form a unified framework for geomorphologists, sedimentologists, geographers, physicists, and others to describe windblown sand dunes on Earth and beyond through their shape, dynamics, and size as a response to winds and boundary conditions.

## 1. Introduction — Previous classifications and aims

Dunes propagate and develop through the action of wind, constrained by other factors such as topography and vegetation. They are not only the result of present winds, but can integrate the history of winds including seasonal wind cycles and longer-term changes. This property helps to explain the richness of shapes and scales observed, and makes dunes witnesses of past winds and environmental conditions. On Earth, dunes are used to study paleoclimates and to test global circulation models (Loope et al., 2001; Preusser et al., 2002; Shozaki and Hasegawa, 2022). Dune stratification, shape and orientation are also used to constrain climate models and the history of celestial bodies such as Venus, Mars, and Titan, for which little climate data are available but where dunes are observed (Lorenz et al., 2006; Fenton, 2006; Hayward et al., 2009; Radebaugh et al., 2010; Bourke et al., 2010; Fenton et al., 2013; Lucas et al., 2014; Charnay et al., 2015; Lapôtre et al., 2016; Fernandez-Cascales et al., 2018; Rubin et al., 2022).

The discovery of planetary dunes and the use of comparative geomorphology (Lapôtre et al., 2020) make it increasingly necessary to define a dune in terms of physical processes, in particular to compare their sizes in different environments. Such physical definitions are especially critical where, for example, the scales and morphologies of different types of bedforms may overlap.

While sand transport mechanisms, sizes, and characteristic times may differ from one environment to another, dune shapes are similar (Fig. 1). General formation processes seem insensitive to the details of sediment transport, and such over-arching processes tend to prevail in the establishment of dune shape and the development of dune patterns and arrangement within fields. This area of research has advanced considerably in recent years through a combination of field studies, laboratory experiments, and models, making it possible to quantitatively relate wind regimes to dune shapes and dynamics.

Following Bagnold, we define an *aeolian dune* as an accumulation of sand resulting from wind deposition, which does not exclude a combination of erosion and deposition (Bagnold, 1941). On a fully covered mobile sand bed, this erosion–deposition process results from the interaction between sand topography, fluid flow, and sand transport (Kennedy, 1969). This three-step feedback mechanism excludes aeolian impact ripples, as observed on Earth, which result primarily from the direct interaction between topography and transport (Anderson, 1987; Csahók et al., 2000; Yizhaq et al., 2004; Andreotti et al., 2006; Durán et al., 2014). Underwater dunes and ripples form from a similar three-step feedback mechanism, so that our conclusions can be based on underwater experiments just as well as on numerical simulations. However, oceans and rivers have some specific boundary conditions that promote a wide range of characteristic patterns, such as wave ripples, antidunes or alternate bars, which have not been observed in aeolian sand landscapes and are outside the scope of this review.

The purpose of classification is to describe the relationship between different objects in such a way as to simplify these relationships and facilitate generalization (Sokal, 1974). Despite the overwhelming variety of terms used to denote dune types (Table 1), there is an assumption that this variety collapses to a much smaller number of common groups, and often that dunes not only look different from each other, but are formed in different ways. Thus classification may help us to use a name to convey morphology and thereby comprehend dune formation processes and dynamics. Defining the categories into which dunes should be classified, however, is challenging. The debate is an old one, and very closely analogous to the long-standing biological taxonomic debates, using Charles Darwin's terms, between 'lumpers' (those that seek to classify into as few categories as possible, allowing for more variability within each class) and '(hair) splitters' (those that tend to permit more categories, but allow for less variability within a class). An ideal classification scheme should be comprehensive, mutually exclusive, internally consistent, unambiguous, and easy to use, with morphology providing information about genesis. These ideals can be hard to reconcile when dealing with natural phenomena.

Often, different terms have developed in separate geographical locations for essentially the same phenomenon. In the early days of the study of dune geomorphology, this was perhaps more understandable, as the true global extent of some landforms would have been unknown, and thus locally-used terms were applied to landforms which were new to the eyes of (largely European) science; hence, for instance, the abundance of terms derived from the Arabic language (*e.g.*, seif, draa). Yet, in some instances, regional terminology has persisted. For instance, the English-language term 'pyramid dune' (to describe a large dune with multiple crestlines, typically leading to a central highpoint) recently has been used almost exclusively in the Chinese-based literature, and the synonymous term 'star dune' is found more commonly elsewhere.

Early classifications of dunes were based primarily on field-based research, and thus were generally based on work in specific geographical locations, such as Sokolow's work in Russia (Sokolòw, 1894), Melton's work in the High Plains, USA (Melton, 1940), Smith's work in Nebraska (Smith, 1965), and Cooper's work along the west coast of the USA (Cooper, 1958, 1967). Some of these early classifications were reviewed by Mainguet (Mainguet, 1984), but in general remained regional in scope and therefore sometimes lacked more general application. That said, Aufrère did attempt some more global qualitative synthesis, based not only on his own studies in the Algerian Sahara, but also on the work of Vaughan Cornish and Richard Oldham (India), Sven Hedin (central Asia), and Cecil Madigan (Australia) (Aufrère, 1935). From the outset, there were frequent endeavors to link formative factors to landform, and one of the first to attempt this semi-quantitatively was Hack, based on his work in northern Arizona, USA (Hack, 1941). The resultant ternary diagram, based on wind strength, sand supply, and vegetation cover worked well in that region, but lacked global applicability.

Developing a global (and possibly universal) classification required the global scope that satellite-borne remote sensing provided. The first attempt at a general characterization of dune forms from global examples was that of McKee and co-workers (McKee, 1979), facilitated by the global coverage of Landsat imagery that became available in the 1970s. McKee also brought a body of work on the internal structure of dunes to this study, which was used to identify sand dune types based on their process of construction. Various versions of the McKee scheme have been subsequently adopted particularly in desert and aeolian geomorphology textbooks (*e.g.*, Greeley and Iversen, 1987). McKee also introduced a terminology to allow for the co-existence of dunes at different scales (McKee, 1979): *simple dunes* — single dunes or a single dune type; *compound dunes*, dunes of the same type at two or more scales; *complex dunes*, dunes of more than one type, usually at different scales.

While McKee's classification distinguished a number of fundamental forms on the basis of morphology and internal structure, other classifications, often developed as pedagogic tools for textbooks, have used a

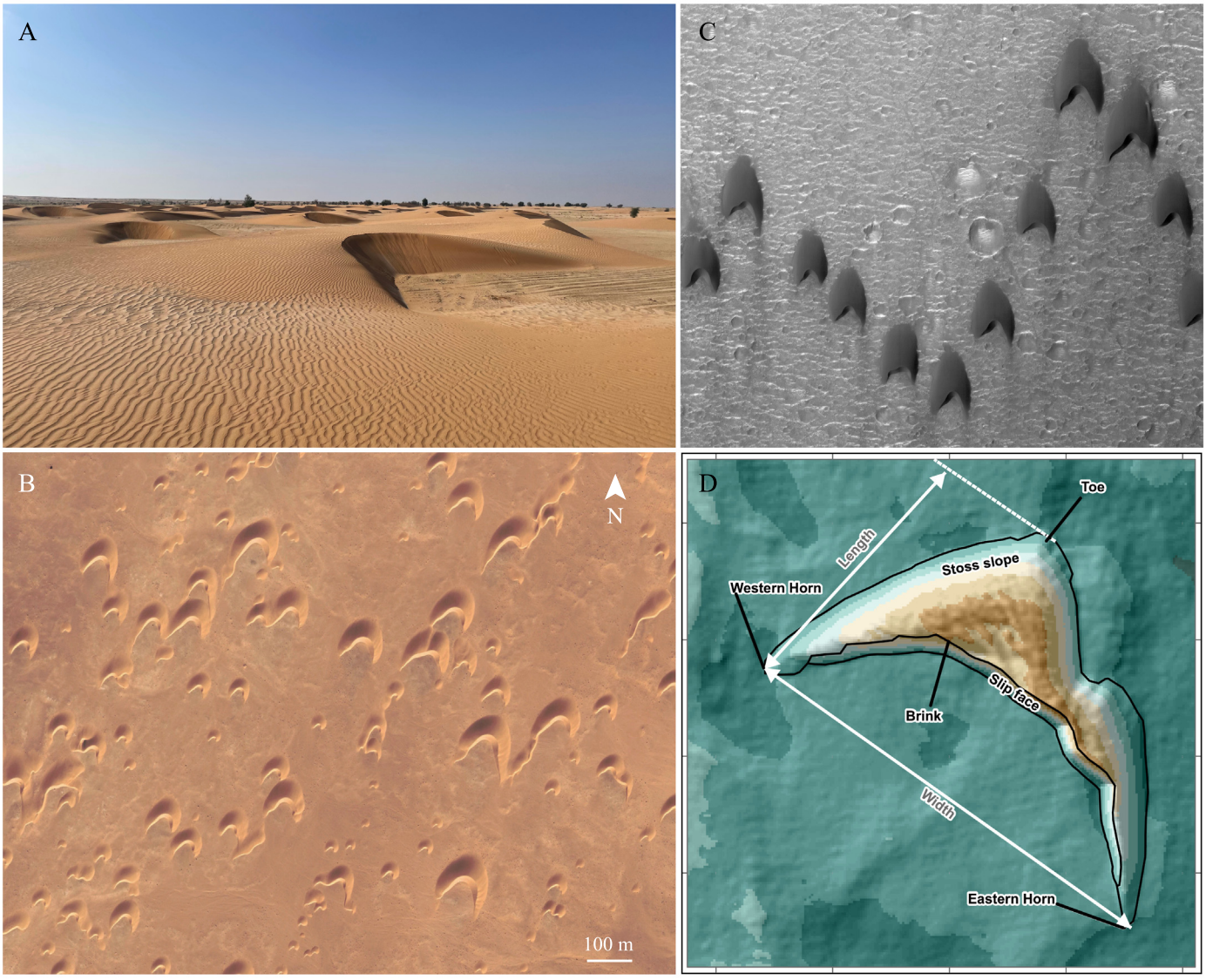


**Fig. 1.** Barchan dunes in different environments. A: Barchan dunes in Oman (20.75°N, 57.61°E), date: 11/2022. B: Barchan dunes in Occidental Sahara (26.76°N, 13.38°W), date: 11/2021. C: Barchan dunes in Oyama crater on Mars (23.19°N, 20.40°W), date: 08/2015 (HiRISE camera). D: Bathymetry image of a marine barchan dune off the east coast of the UK in the North Sea, from Couldrey et al. (2020). The width scale of the image is 410 m. Credits: M. Lapôtre (A), Maxar Technologies (B), NASA/JPL-Caltech/University of Arizona (C), Couldrey et al. (2020) (D).

branching (dendritic) structure to show the interrelationships between dune types. The first of these was developed by Pye and Tsoar (1990, p. 162, Fig. 6.7) and was subsequently modified by Cooke et al. (1993) and then by Livingstone and Warren (1996). Each of these versions uses the distinction between *free* and *anchored* dunes as a starting point. *Free dunes* (called "true dunes" by Bagnold, 1941, p. 188) exist because of a lack of inhibition to the movement of particles. These are fundamental bedforms. Conversely, *anchored dunes* (which Bagnold termed "sand shadows" and "sand drifts") owe their existence to the presence of an inhibition to particle movement, most usually topography or vegetation (see review by Hesp and Smyth p. 157–178 in Livingstone and Warren, 1996).

At the heart of geomorphological studies of dune form is the relationship between morphology and wind regime. The work of Wasson and Hyde (1983), evaluated by Bullard and Livingstone (2002), was a first attempt to use empirical data to distinguish dunes on the basis of available sand (measured by Wasson and Hyde as an estimate of the depth of available sand if spread as a sheet of uniform thickness) and the directional variability of the wind regime. Although this pioneering work provided a useful scheme for future studies, the limited data (largely from Australia), resulted in restricted ranges of dune type. Consequently, as noted by Rubin (1984), their results erroneously suggested that longitudinal dunes were restricted to areas with little sand. Using the same general approach, Livingstone and Warren (1996) and Bishop et al. (2002) revised this conclusion and showed that linear dunes can form where sand coverage is extensive. This scheme was subsequently adapted as the basis for a classification by Lancaster (1994, 2013) who added his own data from a wider range of sand seas to that of Wasson and Hyde (1983). Lancaster added "other key parameters" to sand supply and wind regime.

Although many schemes have related dune form to the 'resultant' wind directions or sand-transport directions, Hunter et al. (1983) and Rubin and Hunter (1985, 1987) were keen to point out that terminologies (and therefore classifications) implying those relationships were problematic. Their contention was that dunes can form with orientations that are neither parallel nor perpendicular to the resultant transport direction. Thus, it is misleading to use terms such as longitudinal and linear interchangeably: *linear* denotes a form in which one planform dimension greatly exceeds the other and is therefore a morphological description, whereas *longitudinal* implies an orientation

**Table 1**
Dune type terminology. Terms are drawn from a number of English-language sources, although some terms used in English originate from other languages. Key sources for terms are McKee (1979), Lancaster (1989), Pye and Tsoar (1990), Livingstone and Warren (1996), and Hesp and Walker (2021).

| | | | | |
|---|---|---|---|---|
| abyssal | aklé | anchored | barchan | barchanoid |
| blowout | chaots | checkerboard | chevron | clay |
| clifftop | climbing | complex | compound | coppice |
| crescentic | demkha | dome | draa | echo |
| ellipsoidal | elongating | embryo | falling | foredune |
| free | frontal | ghourd | hairpin | hummock |
| lee | linear | longitudinal | lunette | megadune |
| nail | nebkha | network | oblique | obstacle |
| oghroud | pancake | parabolic | parallel | pyramidal |
| phytogenetic hillock | polygonal | precipitation ridge | raked | relic/relict |
| retention ridge | rhourd | sand massif | sand mountain | sand ramp |
| shadow | seif | simple | snow | source-bordering |
| star | stellate | straight-crested-asymmetric | teardrop | terminal |
| transverse | true | unvegetated | vegetated | zalib |
| zibar | | | | |

that is approximately parallel to net sand transport. Many linear dunes are not aligned with the resultant transport directions but are oblique, *i.e.*, the planform long axis is at 15–75 degrees from the resultant sand transport direction (Hunter et al., 1983). Rubin and Hunter (1987) showed that dune orientation where the bed is fully covered with sand does not depend on the resultant transport direction, but on what they termed gross bedform normal transport. The more recent experimental and theoretical work of Courrech du Pont et al. (2014) bridged the gap between the older studies that classified dunes at least partially on the basis of sand availability, and the new studies that showed that dune orientation is controlled by two mechanisms, one of which dominates where the bed is fully covered with sand and the other where the bed is partially starved.

Although many of the classification schemes discussed so far owe their origins to inland desert dunefields, throughout this period there was also development of an understanding of coastal dunes, as well as increasingly sophisticated work from the physics community aimed at understanding fluid entrainment, transport and deposition of granular materials, and their coupling with the topography. Despite the fundamental process similarity between coastal and desert environments highlighted by the physical modeling of dunes, some differences in nomenclature had begun to emerge. Thus, whilst parabolic and transverse dunes were frequently discussed in both desert and coastal literature, the term *foredune* is reported almost exclusively from the coastal dune domain (*e.g.*, Hesp, 2013). Conversely, the term *source-bordering dune* (Page, 1971), used commonly in the desert literature to refer to a dune owing its existence to an immediately adjacent sediment supply – which might be said to apply to any coastal dune if it evolves from the backshore like foredunes – is almost absent from the coastal literature.

The observation in the early 1970s of dunes on Mars, tentatively from Mariner 6 (Belcher et al., 1971) and more definitively from Mariner 9 (Cutts and Smith, 1973), opened new opportunities and challenges in dune classification. The subsequent discovery of aeolian bedforms on at least six other solar system bodies (the process of their discovery is reviewed in Diniega et al., 2017) emphasizes the seeming near-ubiquity of dunes and other bedforms — indeed, they have so far been found on every solid planetary body with an atmosphere, and some where the 'atmosphere' is at best extremely thin. Whereas in each case landforms were identified as dunes by analogy with identified and classified terrestrial dunes, in some instances, the planetary dunes have thrown up additional complications for classification. For instance, on Mars, barchans were one of the first types of dunes to be identified, and yet we now know there is greater morphological diversity of Martian barchans than those on Earth, and some Martian dune morphologies do not readily fit into McKee's, or subsequent, classifications (Hayward et al., 2007).

This study aims to provide a comprehensive classification of dunes that can be used both with terrestrial and extra-terrestrial systems, building on recent advances in the understanding of those systems. We propose a new classification of dunes through three distinct and complementary classification-tree diagrams that when combined should answer the fundamental questions of how to describe a shape, relate dune shape and size to the external constraints (the wind regime, the environment, and the boundary conditions), and infer the dune dynamics. The first tree is based on dune morphology where a step-by-step recognition of shapes, possibly interacting with their surroundings, discriminate the main dune types (Section 2). This tree is connected to the second tree, which is based on mechanisms of dune growth and dynamics that links the shapes to external constraints through morphogenetic processes (Section 3). The third tree is based on the fluid mechanics and sediment transport, which set the characteristic scales and the range of possible sizes that can occur in different planetary environments (Section 4). We illustrate the practical use and relevance of those three classifications through several case studies and examples (Section 5). These different classifications involve many concepts and parameters. We present the main ideas as necessary in the description of the trees and refer to the Appendix for detailed development and explanation. It is our intention that together these classifications will lead to a convergence in understanding dune-forming processes and dynamics and will provide a platform and nomenclature for future dune studies on Earth and beyond.

## 2. Classification of aeolian dunes based on dune morphology

### 2.1. Purpose and approach

The morphology of a dune encompasses the three-dimensional geometry defined by the bedform surface. The readily observable characteristics of dune morphology have been the bedrock of previous dune classification schemes (Section 1) and can be investigated either from the ground, or using aerial photography or satellite imaging. Importantly, classifications based on dune morphology do not require *a priori* knowledge of the local winds. We assembled here a morphology-based dune identification tree (Fig. 2) that aims to assist in the categorization of a given dune based on its observable shape, including crestline morphology in plan-view, and environment. The tree is structured with the goal that someone with introductory training in geography, geomorphology, geology, or other related disciplines could identify dune type by answering the series of questions posed in the tree. We attempted to keep the number of questions to the minimum necessary to discriminate between the different types of dunes.

The categorization tree in Fig. 2 is appropriate to the majority of dunes found in nature. Rather than encompassing all possible cases, including niche situations or exotic environments, the classification tree aims to broadly categorize and include the very large majority of the dune types found on Earth (see Section 2.3.1 for discussion of planetary applications and special cases).

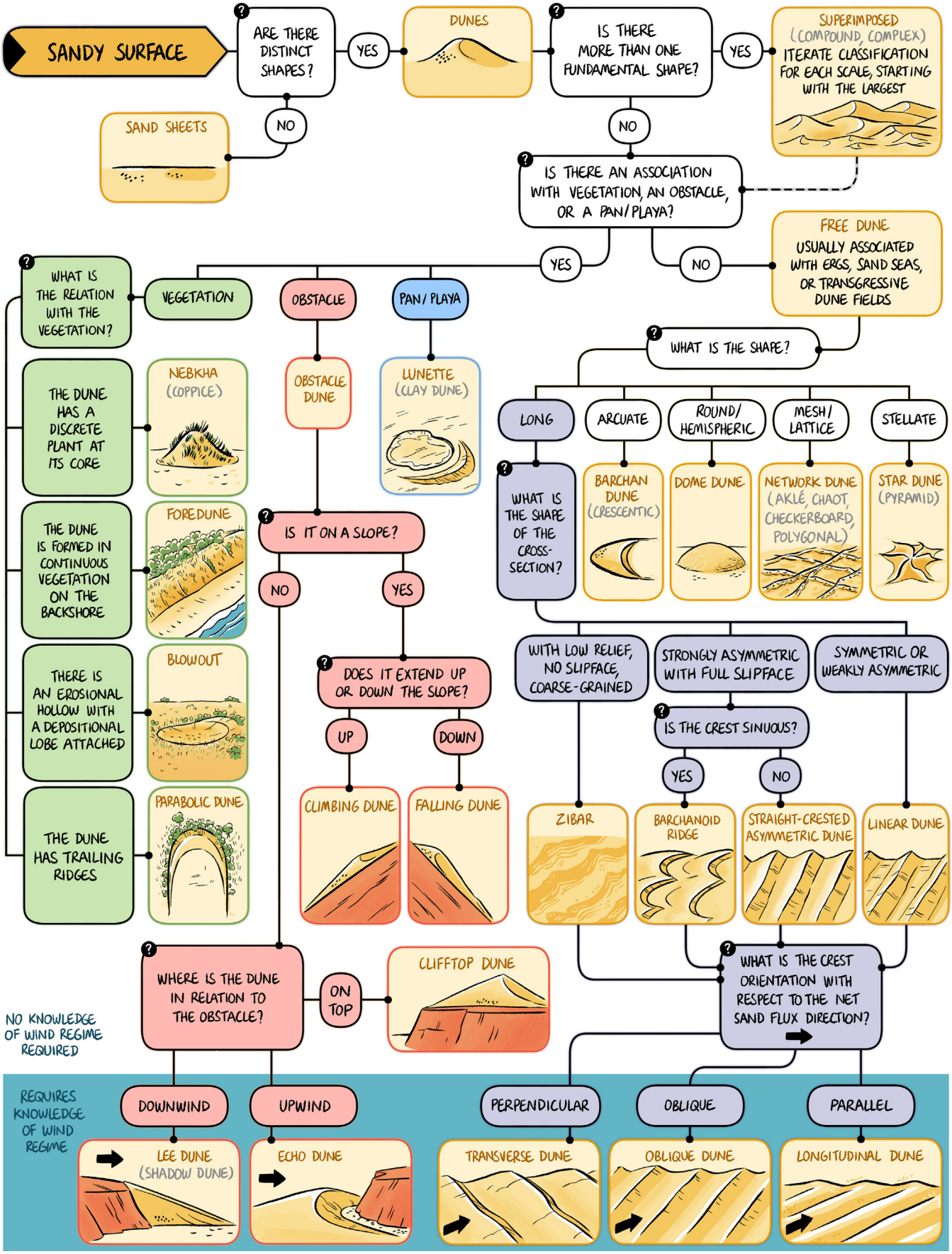


**Fig. 2.** Identification tree for dune classification based on morphology. Terms in parentheses are equivalent, but the yellow main term is preferred.

### 2.2. Tree description — Selection of dune type from shape and interactions with surrounding landscape

Below is a walkthrough of the tree in Fig. 2, highlighting some nuances in the classification where additional description is helpful. We start by requiring a sandy surface, and immediately differentiate between dunes and non-dunes (*e.g.*, sand sheets) using the presence of distinct shapes, and from there use observations about the morphology in plan-view to determine dune type. Although the vertical morphology of dunes holds important information, the plan-view morphology of dunes exhibits more significant global variability and is both more diagnostically useful and more convenient, in part because planform morphology is readily visible in remotely sensed images. In addition, we refer to the crestline of a bedform, which loosely follows the planform morphology. Crestlines are defined by topographic high points along a dune's upper surface and along with brinklines (*i.e.*, the often sharp transition from stoss to lee face), can be easily observed in remote images. Once the dune type has been identified, it may imply information about the local wind regime. The inferred wind direction and/or variability is based on previous research and helps connect the identification in this tree to the growth mechanisms and fluid dynamics outlined in the other two classification trees in this work. Dunes may occur in desert sand seas and ergs (Hesse, 2019; Wiggs, 2019), on beaches of all kinds (*e.g.*, on ocean shores, lake shores, playas, rivers and estuaries), and on coastal transgressive dunefields (coastal sand seas or ergs). For sandy surfaces with distinct shapes (dunes), the classification is intended to be applied individually to a single one of these shapes (morphologies). In many cases, these shapes are likely repeated in the immediate vicinity to form a dunefield. Dunes exhibiting similar shapes at different scales or multiple shapes at different scales are considered compound or complex dunes, respectively (McKee, 1979), and each morphology and scale can be interrogated separately.

Dune types are differentiated by the immediate non-dune boundary conditions that influence the dune morphology. Dunes whose morphology is integrally related to the presence of a local obstacle, vegetation, or playa are differentiated from dunes not directly related to such specific boundary conditions. Although any dune is influenced by boundary conditions such as local topography, water table, and vegetation (Ewing and Kocurek, 2010; Kocurek and Ewing, 2016; Telfer et al., 2017; Hesp and Walker, 2021), we only consider dunes where these local conditions are clearly related to or control the morphology, and consider all other dunes *free dunes*. The former are more commonly found in local settings (*e.g.*, coastal systems, lakes, estuaries, rivers, playa margins), whereas the latter are more likely to populate extensive dune fields, ergs, and sand seas (*e.g.*, as seen in the Rub' al Khali Desert (McKee, 1979; Al-Masrahy and Mountney, 2013), Taklamakan Desert (Wang et al., 2002), or in many coastal transgressive dunefields (Hesp, 2013)).

#### 2.2.1. Free dunes

Free dunes (Figs. 1 & 3) are further subdivided based on their plan-view shape. Stellate morphologies with many arms in radial patterns are considered *star dunes*. Mesh or lattice patterns in dune crests indicate *network dunes*. Many other terms for this morphology also exist, but their defining characteristic is always a network of dune crests crossing one another, commonly at near perpendicular angles and at similar scales. Isolated dunes with arcuate shapes, sometimes called crescent- or half-moon shapes, are *barchan dunes*. Mound-shaped, round, and hemispheric sand bodies are called *dome dunes*. Round landform structures may also develop on sand sheets in early stages of development. These proto-dunes are differentiated from dome dunes by low heights and attachment to a sand sheet source. Proto-dunes are not included in the categorization tree because as transitional features between sand sheets and dunes they may not be identifiable as distinct shapes. However, we note them here for disambiguation and completeness (Kocurek et al., 1992; Nield and Wiggs, 2011; Elbelrhiti, 2012; Delorme et al., 2023).

The remaining categories of free dunes are all morphologically 'long', meaning their length to width ratio is high and the crestline continuity in plan-view is large with respect to the bedform width or wavelength. The term 'elongate' was avoided given the use of the term in the dynamical classification (referring to dune growth in the along-crest direction, Section 3). To differentiate between dune types with long morphologies in plan-view, additional information is needed on the shape of the cross section and in particular on its symmetry with respect to the crest line. Long dunes with a symmetrical or slightly asymmetrical normal-to-crest profile are referred to as *linear dunes*. In dunes with some slight asymmetry in cross section, a slip face may be locally present. Dunes whose cross section has a strong asymmetry with an extended slip face on one side are *barchanoid ridges* if the crest line is sinuous and simply *straight-crested asymmetric dunes* if not. Long dunes with low relief and coarse grains not developing a slipface are termed *zibars* (Holm, 1953; Warren, 1971, 1972; Qian et al., 2015).

Morphologically long dunes can be further classified according to their orientation with respect to the net transport direction. We note that the wind direction discussed when categorizing aeolian dunes should refer specifically to the direction of sand-transporting winds, as sub-threshold winds will not contribute to the mobilization of sand or, therefore, dune development (Appendix A.2). Dunes whose crest is perpendicular to the net transport direction are termed *transverse*. Those that are oriented parallel are referred to as *longitudinal*. *Oblique* dunes are in between. Previous work proposed that oblique dunes be defined differing from parallel or perpendicular orientations by more than 15 degrees (Hunter et al., 1983; Rubin and Hunter, 1987). Such denominations are not morphological in nature. However, linear dunes typically develop in wind regimes that are bi-modal to multi-directional and have longitudinal or oblique orientations (Section 5.2.2; Rubin and Hunter, 1987; Rubin and Ikeda, 1990; Parteli et al., 2009; Courrech du Pont et al., 2014; Gao et al., 2015). In some singular cases as in reversing flows, their orientation may be transverse, analogous to wave ripples or tidal sand waves (Rubin, 2012). Typical barchanoid or straight-crested asymmetric dunes are transverse and develop slipfaces along some or all of the downwind side of their crests, which may allow identification of the dominant sand-transporting wind direction from aerial photograph/satellite images or surface observation.

#### 2.2.2. Dunes coupling to their surroundings

Dunes not considered as free dunes (*i.e.*, those with morphologies controlled by local material boundary conditions) are subdivided into morphologies related to vegetation (Fig. 4), obstacles, or playas and pans (Fig. 5).

Although any dune type can become vegetated (*e.g.*, the Nebraska Sand Hills (Ahlbrandt and Fryberger, 1980) and most coastal dune systems (Hesp, 2013)), here we specifically require that the vegetation be morphologically intrinsic to the dune (Tsoar, 2005; Baas and Nield, 2007; Hesp, 2013; Hesp and Walker, 2021). For example, *nebkha dunes* (nabkha or nebka) form with a core of vegetation and develop as the vegetation traps sand by slowing winds while also continuing to grow in place (Nield and Baas, 2008; Hesp and Smyth, 2017). Various other terms have been used to describe discrete dunes formed in isolated plants such as coppice dunes, bush mounds, phytogenetic hillocks, and others (Hesp and Smyth, 2017). Dunes that are formed by aeolian sand deposition in semi-continuous to continuous vegetation in coastal backshore systems are considered *foredunes* (Arens and Van der Lee, 1995; Hesp, 2002). Note that nebkhas commonly form along the backshore of semi-arid to arid coasts and may also be considered foredunes in these systems (Hernández-Calvento et al., 2017; Hesp et al., 2021). Dunes that form principally by erosion within vegetation forming erosional bowls, troughs, saucers (and other shapes) are called *blowout dunes* or simply *blowouts* (Jungerius, 1984; Hesp, 2002). Blowouts normally display downwind attached depositional lobes thereby fulfilling the definition of a dune; defined by Bagnold (1941) as "a mound or hill of sand which rises to a single summit" (p. 188). Note that erosional depressions in the absence of a depositional lobe may also be

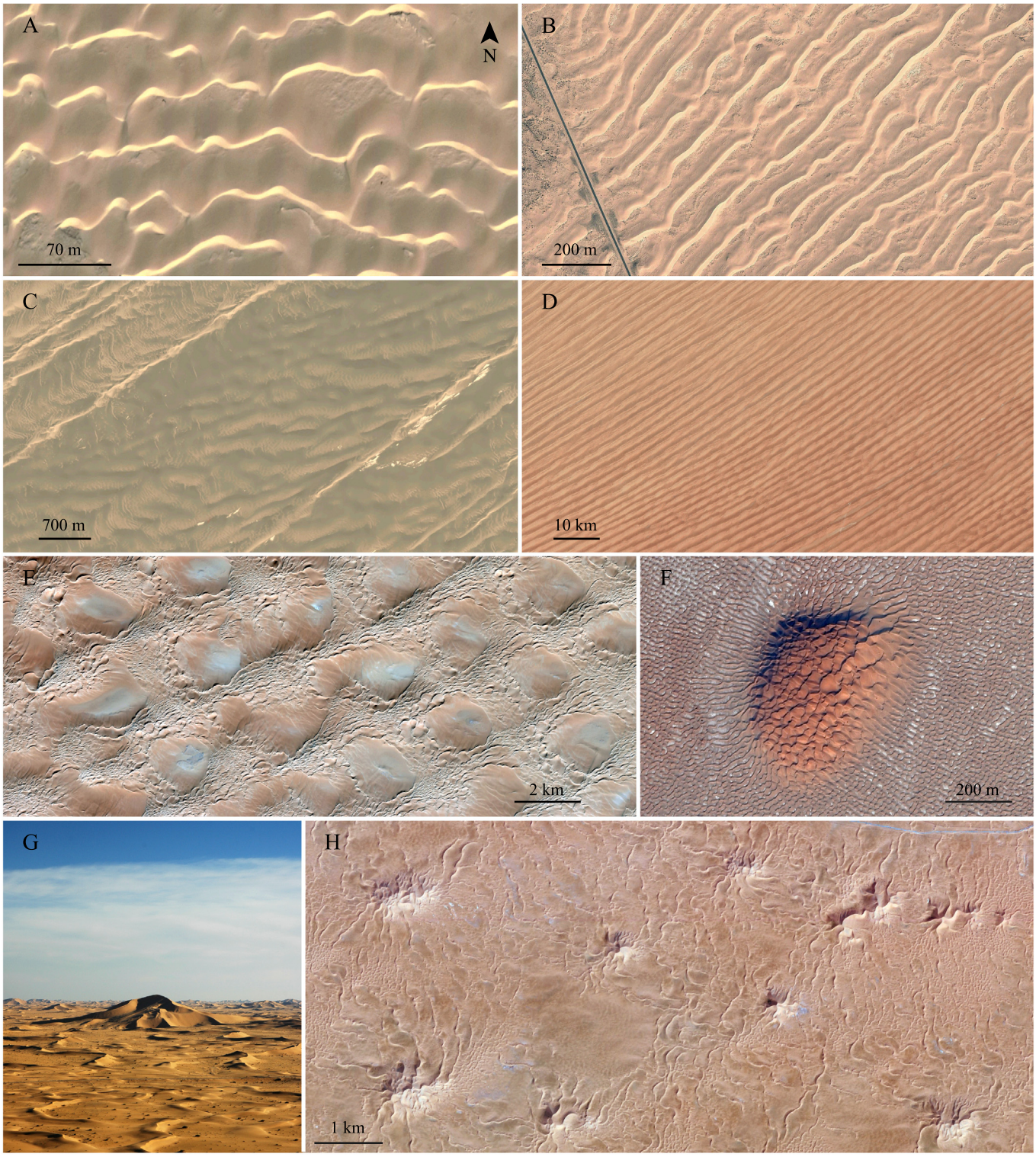


**Fig. 3.** Free dunes. A: Barchanoid ridges in Occidental Sahara (27.17°N, 13.29°W), date: 11/2018. B: Straight-crested asymmetric dunes in the Mu-Us Desert in China (38.76°N, 107.94°E), date: 03/2011. C: Zibars (low relief dunes between linear dunes) in the Kumtagh Desert in China (40.33°N, 92.66°E), date: 03/2021. D: Linear dunes in the Rub' al Khali Desert (18.39°N, 48.06°E), date: 12/2016. E: Network dunes in Libya (25.14°N, 13.08°E), date: 09/2016. F: Dome dune in Oman (18.52°N, 53.55°E), date: 11/2014. G, H: Star dunes in Algeria (31.43°N, 7.30°E), date: 02/2006 (G), 08/2012 (H). Credits: Maxar Technologies (A, B, E, F, H), CNES/Airbus (C), Landsat Copernicus (D), P. Claudin (G).

referred to as blowouts, but then do not meet the definition of a dune. *Parabolic dunes* develop when vegetation stabilizes the lateral margins of the depositional lobes, causing them to develop U- or parabola-shaped (sometimes V-shaped) crestlines and plan view shapes. Parabolic dunes display short to long trailing ridges whereas blowouts do not have trailing ridges (Hesp and Walker, 2021). The trailing ridges in the parabolic dunes point in the opposite direction to the avalanche face, rather than in the same direction, as is the case with barchan dunes.

Although dunes are almost exclusively formed from sand-sized grains, dunes may form with significant clay and silt fractions along the margins of playa, salt lake, and evaporitic pan systems. Much of the clay


**Fig. 4.** Dunes associated with vegetation. A: Foredune at Fort Steven, Oregon (46.18°N, 123.98°W), date: 08/2013. B: Foredune plain comprising multiple foredunes formed by coastal progradation at the south of Perth, western Australia (32.34°S, 115.74°E), date: 1984. C–E: Nebkhas. (C) Southern edge of the Taklamakan Desert (37°N, 80.7°E), date: 10/2017. (D) Port Lincoln, South Australia (34.73°S, 135.87°E), date: 11/2018. (E) East of the Kumtagh Desert (39.9°N, 94.15°E), date: 10/2018. F: Trough blowout 12 m deep and 600 m long on the Tibet plateau (35.99°N, 100.42°E). G: Bowl blowout 3 m deep at Cape Cod (42.08°N, 70.19°W). H & I: Parabolic dune in South Australia (34.91°S, 135.89°E), dates: 02/2020 (H) and 09/2016 (I). Credits: C. Bristow (A), P. Hesp (B, D, F, G, H), C. Narteau (C, E), CNES/Airbus (I).

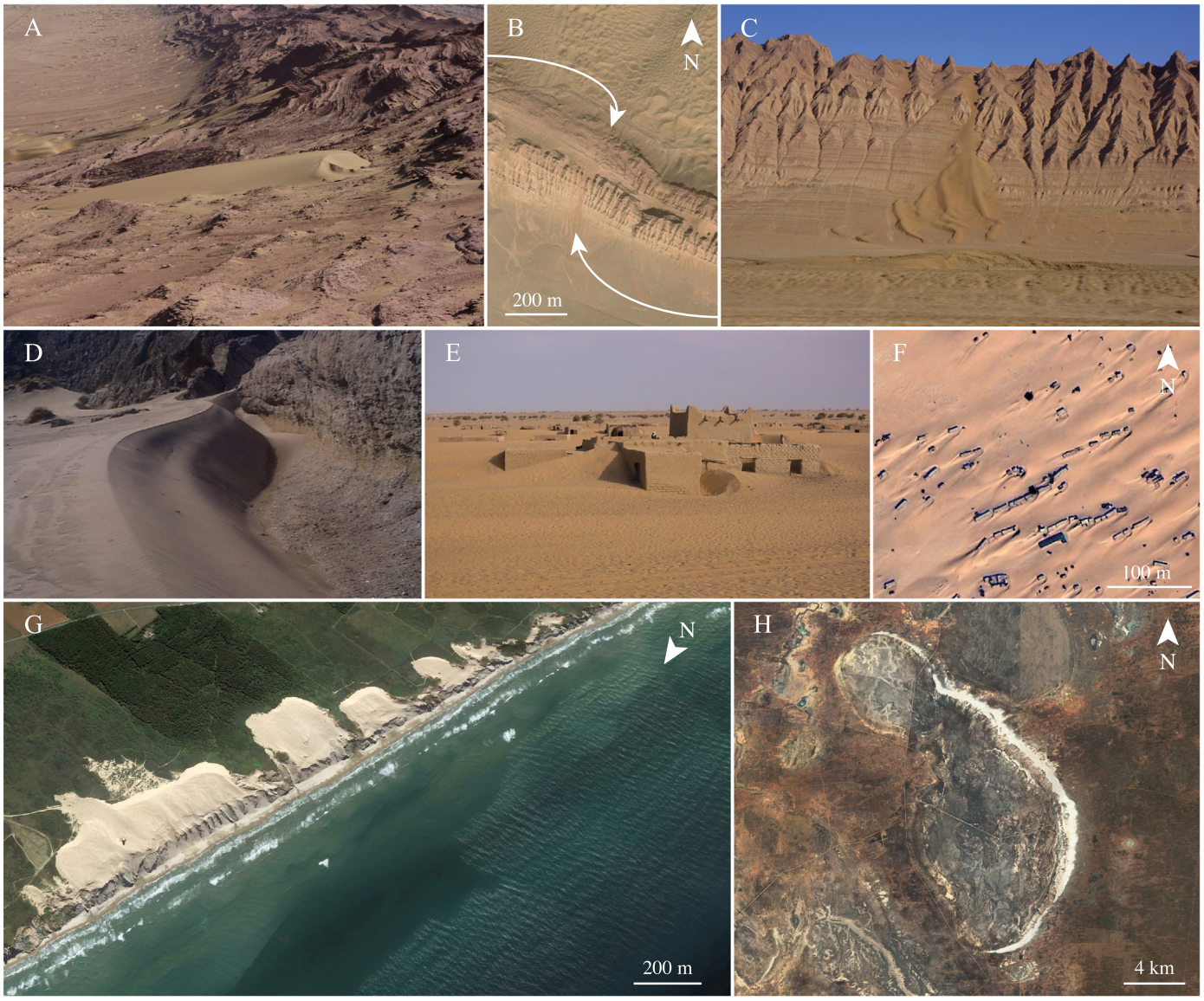


**Fig. 5.** Dunes in association with an obstacle or pan. A–C: Climbing (A) and falling (C) dunes on either side of Mazartagh mountain range (38.68°N, 80.38°E, date 10/2017). B: Aerial view of A and C, date: 09/2019. D: Echo dune at Castlepoint, New Zealand (40.90°S, 176.23°E), date: 08/2003. E: Lee (downwind, left) and echo (upwind, right) dunes on either side of a building from Kouba Olanga in Chad, date: 02/2005. Panel F shows the context (15.75°N, 18.3°E), date: 01/2006. G: Cliff-top dune in Rubjerd Knude, Denmark (57.44°N, 9.77°E), date: 07/2021 (Saye et al., 2006). H: Lunette dune bordering (now dry) Lake Mungo in Australia (33.74°S, 143.13°E), date: 02/2023. Credits: C. Narteau (A, C), CNES/Airbus (B, H), P. Hesp (D), C. Bristow (E), Maxar Technologies (F), Terra Metrics (G).

and silt can occur as sand-sized aggregates that behave dynamically as sand grains. These dunes are intrinsic to the pan/playa and have been termed clay dunes and *lunette dunes* (Hills, 1940; Bowler, 1973; Goudie and Thomas, 1986). The term lunette is preferred here.

Finally, wind and, therefore, aeolian sediment transport respond to topographic obstacles, sometimes generating dunes with morphologies tied to that topography. We refer to these collectively as *obstacle dunes* and differentiate between them using the underlying slope, proximity to an obstacle, and direction of the wind (Livingstone and Warren, 2019). As with some free dunes discussed earlier, assessing the sub-type of an obstacle dune requires either knowledge of the sand-transporting wind direction, or an inference based on the morphology of the dune. *Climbing-* and *falling dunes*, found on slopes less steep than the angle of repose, may or may not exhibit slip faces, but develop in response to sediment transport up- and down slope, respectively. Note that the use of 'climbing' in the geomorphic classification of dunes is distinct from the stratigraphic use of the term (*e.g.*, climbing ripple structures, or bounding surfaces with an angle of climb) which refers to bedform migration accompanied by net deposition. Depending on the local boundary conditions, dunes can also form immediately upwind, downwind, or on top of a topographic obstacle that diverts the wind. Once the position of the dune with respect to the wind direction and the obstacle is known, the dune can be identified as either an *echo dune* (upwind of the obstacle, and approximately echoing the planform or morphology of the adjacent feature), *lee dune* (downwind of the obstacle), or *clifftop dune* (on top of the obstacle). We note that the obstacles controlling dune development in this case are broadly defined. For example, echo dunes might form at the base of scarps, in front of and along the margins of small to large boulders or obstacles, and lee dunes (including shadow dunes) form downwind of obstacles (including vegetation and nebkhas). However, climbing-, falling-, and clifftop-dunes all require topographic slopes to form.

### 2.3. Discussion

#### 2.3.1. Scope of the morphology-based classification

The morphology-based identification tree in Fig. 2 is intended to encompass the majority of aeolian dune types observed on Earth. Other aeolian bedforms, including many varieties of ripples (*e.g.*, impact ripples, megaripples, granule ripples) are not included. Not every name for every type of dune is represented in the geomorphology tree. In a perusal of recent literature, we identified more than 50 different terms for types of dunes (Table 1). Many of these terms were duplicative, or specific to niche environments or localities. To combat some of the confusion that arises from so many terms, in Fig. 2 we note some equivalent terms in grey below the dune identification in yellow. In the future, we encourage the community to converge on the use of a single term for a given dune type, but here we include the duplicative names in this work for reference. Because dune type recognition can be aimed to infer wind regimes and environmental constraints, we avoided using dynamical properties or we included them at the end of the classification. For example, we did not include the commonly used term *reversing dunes*. This term can be added to further define a dune. A dune undergoing and integrating successive reversals generally does not have a fully developed avalanche face on one side only, unless the dune is small enough to reverse entirely within one sequence of consistent sand flux direction (Appendix A.1).

Although the geomorphic dune-identification tree was developed with terrestrial aeolian dunes in mind, the tree can be applied to dunes in any system or on any planet. Aeolian bedforms are known to develop on many planetary bodies in our solar system, including Venus, Earth, Mars, Titan, Pluto, Io, and Comet 67P (Bourke et al., 2010; Lorenz and Zimbelman, 2014; Diniega et al., 2017; Jia et al., 2017; Telfer et al., 2018; McDonald et al., 2022). In most cases the morphologies of dunes observed on other planetary bodies are similar to those observed on Earth (Radebaugh et al., 2010; Hayward et al., 2014; Day and Kocurek, 2018; Telfer et al., 2018) and the tree in Fig. 2 can be easily applied to these systems. Some planetary aeolian bedforms have debatable analogs on Earth. For example, transverse aeolian ridges (Balme et al., 2008; Berman et al., 2011) and large ripples (Lapôtre et al., 2016; Sullivan et al., 2020) are both abundant on Mars, but bedforms of similar scales and morphologies are comparatively uncommon on Earth. Large martian 'ripples' have no known direct analog among the many kinds of aeolian ripples on Earth, none of which are included in this geomorphology-based classification tree. However, transverse aeolian ridges (TARs) on Mars can be several meters high and would be considered by this classification to be transverse dunes, though dynamically the processes forming each might be quite different. The application of the geomorphology tree to planetary systems must be done with appropriate caution and context. Together with the other two trees, the tree based on dune morphology will facilitate interplanetary comparison in future research and limit terminological confusion in the literature.

#### 2.3.2. Wind direction and variability inferred from morphology

The classification based on dune morphology does not require prior knowledge of the local wind direction, except in some cases when it is needed to disambiguate between sub-types. However, decades of research studying the relationship between dune morphology and local winds has allowed us to make inferences about the local wind direction when a given morphology is observed (*e.g.*, Bagnold, 1941; Rubin and Hunter, 1987; Rubin and Ikeda, 1990; Zhang et al., 2012; Courrech du Pont et al., 2014; Gao et al., 2015). As noted above, slipfaces develop on the net downwind side of dunes, providing a morphological indicator of the leeward side of dunes with slip faces that are fully developed on one side only.

Asymmetry in planform or cross-section in the morphology of a dune can also provide some information about the local wind variability. For example, barchan dunes with dissimilar horn lengths form when two winds with an obtuse divergence angle have differing strengths (Taniguchi et al., 2012; Parteli et al., 2014; Gao et al., 2015; Rubin et al., 2016; Tsoar and Parteli, 2016). In barchanoid ridges, lee-side spurs that are asymmetric in plan form (skewed rather than transverse to the main dune) indicate the main dune is asymmetrically oriented relative to the winds (*i.e.*, not entirely transverse). Similarly, lee-side spurs that are perpendicular to the main crests but are asymmetric in cross-section (having a steep lee side and gentle stoss side) indicate net transport parallel to the lengths of the main dunes, thereby demonstrating that the main dunes are not perfectly transverse. Net transport parallel to the crests of the main dunes can also be inferred from orientation of asymmetric peaks, saddles, or superimposed dunes enabling significant complexity to be disentangled from observed dune morphologies (Rubin and Hunter, 1983, 1985, 1987; Rubin and Carter, 2005; Courrech du Pont et al., 2014). Superimposed dunes are common on linear dunes that can form with kilometer-scale wavelengths and large enough widths to host subordinate dunes on their surfaces (Dong et al., 2010). Specifically for long-crested dunes, the transverse and longitudinal symmetry/asymmetry indicate whether the transverse and longitudinal net transport, respectively, are zero or greater than zero.

This general approach has been applied to identification of deposits of transverse, oblique, and longitudinal dunes in the stratigraphic record (Rubin and Hunter, 1983, 1985; Rubin and Carter, 2006; Bristow et al., 2007). Stratigraphically, the approach is applied by determining whether the main dunes migrated laterally or aggraded in place and whether or not the superimposed topographic features such as dunes, spurs, peaks, and saddles migrated in a preferred direction along the lengths of the main dunes. Deposits of a perfectly transverse dune preserve migration of the main dune without a preferred along-crest migration direction of superimposed features; perfectly longitudinal dunes aggrade in place with superimposed features migrating with a net along-crest direction; and deposits of oblique dunes preserve both lateral migration of the main dune and net along-crest migration of superimposed features.

Here we suggest that the same general approach can be used to distinguish transverse, oblique, and longitudinal dunes using asymmetry rather than stratification to infer migration of the main dune and superimposed features (Table 2). This approach comes with three limitations. First, it can only be applied where the main dune has superimposed topography. Second, both the main dune and the superimposed bedform must integrate the wind regime. Although some dunes are small enough to re-form seasonally, here we are restricted to dunes that coexist and persist through complete cycles of flow (Rubin and McCulloch, 1980). Third, the determination of dune type may not necessarily match the definition of Hunter et al. (1983). Specifically, dunes that meet the geomorphic criteria of oblique dunes (Table 2) might have orientations outside the defined range of 15° to 75° relative to the net transport direction. Nevertheless, this approach can identify dunes that are qualitatively neither transverse nor longitudinal, and it can do so using only morphologic criteria as shown in Section 5.3. The same information required to classify dunes as transverse, oblique, and longitudinal can be used to infer the net sand transport direction relative to the main dunes. Where dunes meet the geomorphic criteria of transverse or longitudinal dunes, the net sand transport direction is perpendicular or parallel to the dune crests, respectively. Where dunes are oblique, the net transport direction is constrained to the quadrant bounded by the migration direction of the main dunes and the direction of migration of superimposed features along the crests of the main dunes. These directions of migration are derived from the dip direction of the slipfaces. Note that these two migration directions are only used to constrain the net transport direction; the two migration directions do not necessarily correspond to two formative winds.

When considering multiple related dune morphologies, perhaps occurring at different scales, it is important to consider the timescales of formation and how they compare to the time period of the wind regime (Appendix A.1). Smaller dunes migrate faster than larger dunes,

**Table 2**
Identification of transverse, oblique, and longitudinal dunes based on symmetry/asymmetry of main dune and superimposed features.

| Across-crest (transverse) symmetry or asymmetry (identified by cross-section profile) | Along-crest (longitudinal) symmetry or asymmetry (identified by symmetry or asymmetry of superimposed topographic features such as peaks, saddles, crest sinuosities, spurs, or superimposed dunes) | |
|---|---|---|
| | Along-crest symmetrical | Along-crest asymmetrical |
| Across-crest symmetrical | Zero net transport in both the across-crest and along-crest directions suggests formation by opposed equal winds; singular conditions with zero net transport (analogous to some wave ripples) | Longitudinal dunes (net along-crest transport with no net across-crest transport) |
| Across-crest asymmetrical | Transverse dunes (net across-crest transport but no net along-crest transport) | Oblique dunes (net across-crest and along-crest transport) |

and change morphology in response to a change in wind regime faster than larger dunes (Bagnold, 1941; Durán et al., 2009). The most recent winds are reflected by the smallest bedforms (all the way down to wind impact ripples), and larger and larger dunes reflect wind regimes as integrated over longer and longer timescales. Different scales also frequently differ in orientation or morphology for reasons other than changes through time in wind regime. The larger dunes may modify the apparent winds for smaller superimposed or adjacent dunes, or the different scales may interact (Rubin and McCulloch, 1980; Gadal et al., 2022). Often, the different scales experience different boundary conditions. For example, the main dune may extend on bedrock while the superimposed ones develop on the underlying main dune, *i.e.*, a sand bed. Orientation and morphology of both the main dune and the superimposed ones then provide information about winds and potentially help differentiate between longitudinal and oblique dune types (Courrech du Pont et al., 2014; Lapôtre et al., 2018). Additional discussion of the relationship between morphology and process is provided in Section 3.

#### 2.3.3. Dunefield patterns and changes in dune type

The geomorphological identification tree deals with individual dunes and their morphology, but dunes in nature are rarely found in isolation. More commonly, many dunes form a field, and that field may vary spatially in the morphology and size of individual dunes. Boundary conditions that change spatially (*e.g.*, sediment supply, antecedent topography, water table, vegetation) can cause variability in the morphology of the dunes (Derickson et al., 2008; Ewing et al., 2015; Hesp and Walker, 2021). Similarly, dunefield patterns mature spatially and in time, with dunes becoming larger and more widely spaced as they develop and migrate downwind (Gadal et al., 2020a). With time, almost all dunefields and dune systems can be fully stabilized and many other dune forms can develop as a result of vegetative stabilization (Hugenholtz and Wolfe, 2005; Beveridge et al., 2006; Hesp, 2013; Xu et al., 2015). Dunefield patterns are fundamentally constrained by these local boundary conditions, but changes in that pattern are also driven by time and interactions between the bedforms (Kocurek et al., 2010; Eastwood et al., 2011; Marvin et al., 2023). These interactions can act at different scales and be of different kinds, *e.g.*, aerodynamic in nature, a dune modifying the flow in its vicinity, or concern directly the mass exchange (sand loss and capture or collisions) (Endo et al., 2004; Hersen and Douady, 2005; Durán et al., 2009; Worman et al., 2013). For example, in barchan dune fields, smaller dunes migrate faster than larger dunes, resulting in small upwind dunes colliding with slower downwind dunes. When colliding, dunes may split or merge leading to size regulation and spatial organization within the field as in dune corridors (Endo et al., 2004; Hersen and Douady, 2005; Elbelrhiti et al., 2008; Durán et al., 2009; Génois et al., 2013a,b, 2016). Barchan dunes may also link together to form barchanoid ridge dunes, which is an overall change in the morphology of dunes in the field. It is rare to find a dune field composed of a single dune morphology in deserts, although it does occur more frequently in coastal dunefields (*e.g.*, on Earth there are multiple examples of foredune plains, and parabolic dunefields), and just as the morphology of a single dune can help determine information about the local winds and sediment state, interpreting the dune morphologies of a field in aggregate, the spatial succession of forms and types, can yield important information about the larger system (Werner and Kocurek, 1997; Baas, 2007), as exemplified by the case studies in Section 5.1.

## 3. Classification of aeolian dunes based on dune dynamics

### 3.1. Purpose and approach

Aeolian dunes exhibit a wide variety of forms, and geomorphologists have wondered for more than a century what processes control this variability. The goal of this classification is to link the various dune types (right column in Fig. 6) with the formative processes in a dune field (left columns in Fig. 6). Specifically, we propose a tree structure to identify the dynamical processes by which dunes are built and aligned according to wind regime, sand availability, and other boundary conditions that control dune type. This dynamics-based tree diagram thus links dune type to the sediment and wind conditions, allowing for both forward modeling of dune morphologies in specified conditions (left-to-right) or inverse interpretation of observed dune morphologies (right-to-left). The case studies in Section 5.2 complete and illustrate this classification based on dune dynamics and link it to the classification based on morphology (Fig. 2).

The dynamics-based classification reflects the state of the art of the physical understanding of dune morphodynamics derived from field observations, laboratory experiments, numerical simulations, and theoretical studies. Based on these physical insights, environmental conditions are intentionally simplified or conceptualized, and cannot cover the whole range of complexity observed in nature. In such a process-based approach to dune classification, we consider that dune types and general morphologies are in dynamic equilibrium with environmental conditions. Other factors such as interactions between dunes, *e.g.*, collisions, modify these general morphologies. Such morphological properties, which are usually local and transient, are beyond the scope of this classification. As a first step, we focus on free dunes composed of loose sand. Cohesion between grains and vegetation are not taken into account. We expect that this diagram will evolve as the understanding of the formative conditions and processes progresses.

### 3.2. Tree description — Selection of dune shape and orientation from formative processes

The tree in Fig. 6 classifies dunes depending on the dominant dynamics. The dune morphodynamics are controlled by spatial variations of the sand flux. The bed is eroded where sand flux increases and aggrades where sand flux decreases. Those spatial variations can make a dune (i) grow in height, (ii) migrate (propagation perpendicular to crest), and (iii) elongate (dune growth in a direction parallel to the crest

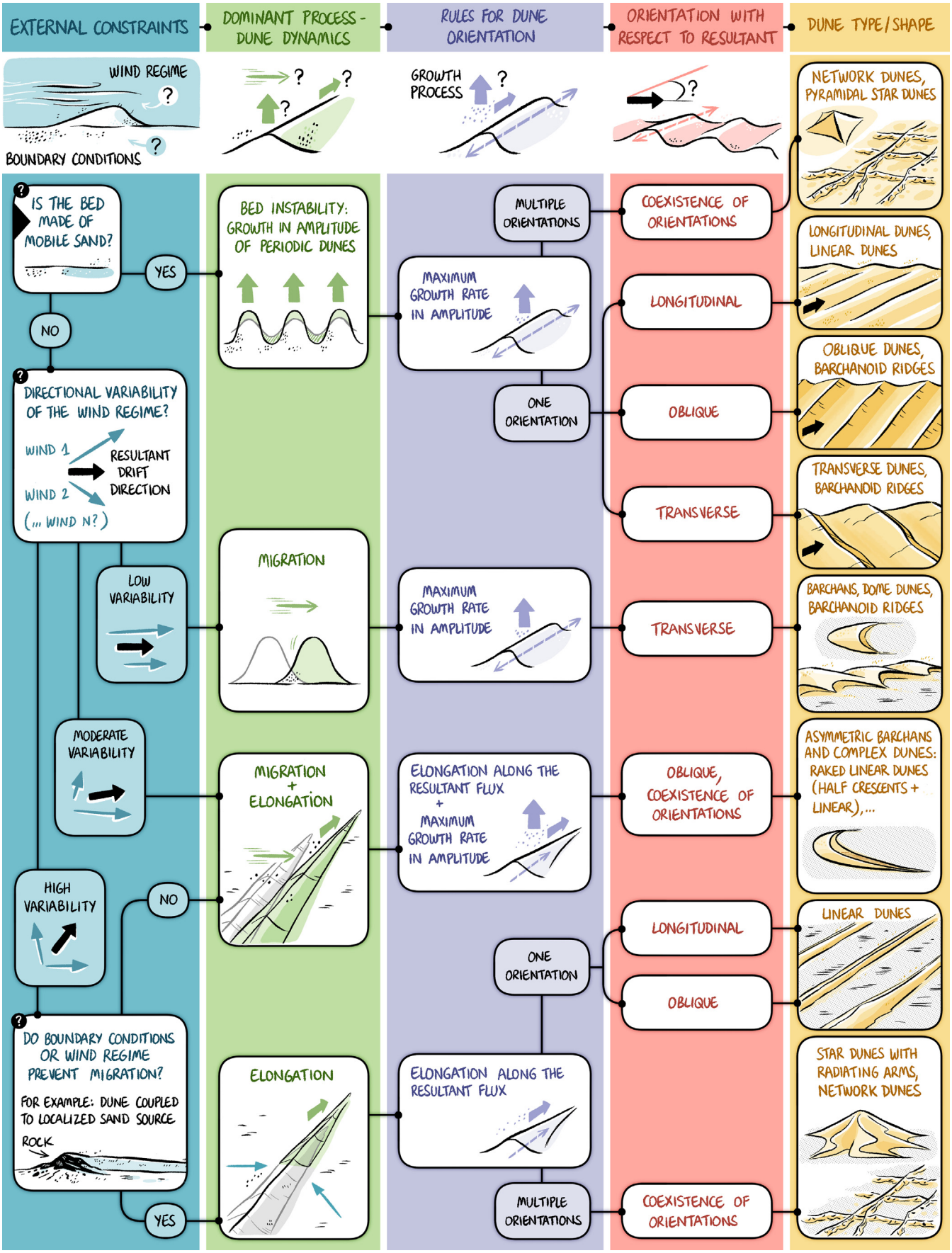


**Fig. 6.** Identification tree for dune classification based on dune dynamics.

line). Growth in height, migration, and elongation correspond to dune dynamics in the three dimensions: vertical, horizontal across-crest, and horizontal along-crest, respectively. Growth in height generally corresponds to an overall increase in dune cross-sectional area so that the dune transverse length increases accordingly. In a multidirectional wind regime, these three dynamics are present to different degrees. Depending on boundary conditions and wind regimes, one of these dynamical processes may prevail and drive the overall dune shape and orientation. The orientation of the dune with respect to the different sand fluxes further determines the secondary dune dynamics, which ultimately set the dune type.

To apply this classification, one first has to choose the dune's length scale or time period to address, the two being linked (Appendix A.1). The tree describes dunes of a given length scale. When different scales are present, each scale can be described by going down the tree separately for each scale. The first decision relates to a boundary condition through the question: Is the bed made of mobile sand? A dune may strongly interact with the surrounding sand bed, *e.g.*, growing from the erosion of the interdune. Conversely, the interaction may be limited, like for a barchan, which evolves on a starved floor. Bed mobility has a strong influence on dune dynamics and shapes. We recognize the floor as a mobile sand bed when the granular medium that composes the dune and the bed surface are similar.

#### 3.2.1. *Mobilized sand bed — Growth in height prevails*

Where the bed is made of loose sand, dunes develop from the destabilization of the bed by the wind (Section 4). We call this growth mechanism the *bed instability*, and growth in height is the dominant dynamic. The resulting dunes are long ridges generally organized periodically. In accordance with an instability mechanism, the observed pattern, and in particular its orientation, is such that the growth rate in height is maximum (Rubin and Hunter, 1987; Courrech du Pont et al., 2014; Gadal et al., 2019). Dunes are built up by normal-to-crest sand fluxes. In a multidirectional wind regime, sand fluxes of opposite directions both contribute to build the dune, so that dune orientation maximizes the *gross bedform-normal transport*, and, depending on the wind regime, can be transverse, oblique, or longitudinal with respect to the resultant drift direction, *i.e.*, the direction of the net transport on a flat bed. For some specific wind regimes, multiple orientations can coexist, resulting in intricate patterns that may be defined as network or star dunes.

The shape of dunes is then modulated by the two other processes, migration and elongation, and by migration in particular. Migration tends to promote the development of sinuous crestlines. In contrast, along-crest sand flux promotes dune straightness (Rubin, 2012).

#### 3.2.2. *Non-mobilized bed — Migration and elongation prevail*

When large areas of the bed cannot be mobilized by the winds, the growth in height of a periodic pattern is inhibited by limited sand supply. Consequently, *migration* and/or *elongation* prevail in determining the dune type and orientation (Courrech du Pont et al., 2014). Although dunes may be arranged periodically, dunes can be isolated objects unlike in the case of a sand-covered bed. They persist because capture of free sand flux and losses balance out, or slowly evolve such that their shape and size are quasi-static.

What controls the relative dominance of migration and elongation remains largely unknown to date. Elongation can be promoted over migration by some boundary conditions that 'pin' part of the dune. Generally, the dune would grow from a localized sand source, behind an obstacle that acts as a sand trap for example. A part of the dune may also be so large that it barely moves during the time it takes to develop extensions, such as the core of a star dune (Zhang et al., 2012). If part of the dune is pinned, the dune cannot propagate but only elongate in the direction of the sediment net transport (Courrech du Pont et al., 2014; Gao et al., 2015). We recognize elongation as another growth mechanism. For most wind regimes, a dune would migrate and elongate if not pinned. The boundary condition can force elongation and prevent migration, but only if such dunes are stable. An elongating dune cannot form in a unidirectional transport regime (Reffet et al., 2010); a multidirectional transport regime is required. Although the dune extends in the direction of transport, its growth in height and sustainability requires that it is subjected to components of wind perpendicular to its crest line; an elongating dune is a reversing dune. Because the direction of elongation is generally different from that of the bed instability (Courrech du Pont et al., 2014; Gao et al., 2015), secondary superimposed patterns in the bed instability mode are likely to develop on an elongating dune (Courrech du Pont et al., 2014). An isolated dune parallel to the direction of the net transport, therefore, eventually destabilizes into migrating dunes if its growth rate in height is not sufficiently large relative to that of the superimposed patterns in the bed instability mode (Reffet et al., 2010; Gao et al., 2015).

*Elongation prevails.* If elongation prevails, dunes have a ratio of length (along crest) to width (across crest) much larger than unity and extend in the direction of the net transport if they do not migrate (Parteli et al., 2009; Reffet et al., 2010; Courrech du Pont et al., 2014; Gao et al., 2015). The orientation of such elongating dunes can be longitudinal or oblique to the resultant drift direction (RDD) because the dune topography modifies the transport (Appendix A.2.3, Courrech du Pont et al., 2014). In a multidirectional wind regime, the topography may change the relative magnitudes between the different transport directions, so that the dune experiences a direction of net transport different from that over a flat sand bed, the RDD. Some specific wind regimes allow multiple elongation directions, which may produce star dunes with radiating arms (Zhang et al., 2012). Arms of adjacent dunes may connect to form network dunes. Although we expect elongation to dominate over migration in the formation of linear dunes and star dunes with radiating arms, unless they are perfectly aligned with the net transport vector(s), they will migrate laterally as well as elongate, which makes their recognition in the rock record difficult (Rubin and Hunter, 1983, 1985; Bristow et al., 2007; Rubin and Hunter, 2008; Bristow and Duller, 2024).

*Migration prevails.* Migration does not directly select dune orientation because only dune growth mechanisms do, *i.e.*, growth in height (cross-section) and growth in crest line length, or elongation. However, migration mutes elongation, so when migration prevails, we expect dune crest orientations to maximize growth rate in height, as in the bed instability mode. The archetypical migrating dune is the barchan dune, which is observed on starved beds under unidirectional wind regimes. As variability in wind directions around the resultant direction increases, the width of the slipface decreases from the full width of the dune (barchan) to a restricted region (Reffet et al., 2010), and then finally disappears completely (dome dune) (Gao et al., 2018). Although they may correspond to transitional regimes, we also classify isolated barchanoid ridges in this branch. Experiments under water (Reffet et al., 2010) and numerical simulations (Parteli et al., 2011; Guignier et al., 2013) have shown that an isolated straight-crested transverse dune subjected to a unidirectional flow is unstable when migrating on a non mobile sand bed and without being fed by an incoming free flux. A perturbation in height or in length in the direction of wind leads to a perturbation in the migration velocity and to the redistribution of sand towards where the avalanche face is concave, which amplifies the perturbation. The transverse dune transforms into a barchanoid ridge and eventually breaks into a row of barchans. In light of those studies, barchanoid ridges on beds of non-mobile sand correspond to transient dynamics. Because they might be stable in different conditions and because this instability is driven by migration, we recognize these dunes as being shaped by migration.

*Concurrent migration and elongation.* If boundary conditions and/or sand supply do not force the development of an elongating dune from a point source, a dune is likely to migrate except in some specific symmetric wind regimes, *e.g.*, two transport directions with an obtuse divergence angle and equal magnitudes (Parteli et al., 2009; Reffet et al., 2010). Most multidirectional transport regimes should involve both dynamics (Rubin and Hunter, 1985). Simulations with tri-directional wind regimes on sand-covered and partially starved beds have shown that in most cases gradual changes in wind regimes produce gradual changes in dune morphology, with many of the familiar dune forms being transitional with others rather than discrete classes (Rubin et al., 2024). The transition between elongation and migration is not sharp but a continuum. As such, when neither migration nor elongation fully dominates, the orientations and morphologies associated with these two dynamics coexist, leading for example to asymmetric barchans, nail dunes, or raked linear dunes (Taniguchi et al., 2012; Parteli et al., 2014; Gao et al., 2015; Lü et al., 2017).

### 3.3. Future improvements

Here, we classify dunes in broad classes and determine their orientation according to the dominant formative dynamical processes. The ideal classification would not only address the dune orientation but also the detailed dune morphology in a quantitative way, *e.g.*, the straightness of linear dunes or the sinuosity of their crest line, the curvature of the avalanche face of barchans, or their asymmetry like the relative size of their horns. Many of those properties should depend on the competition between the three processes, which are all at work at different degrees in multidirectional flow regimes. How much a morphologically long dune migrates relative to its growth in height or elongation should for example control the dune straightness as conceptually proposed in Rubin (2012). Growth in height and elongation should favor the spatial coherence of the dune, while migration destabilizes it (Reffet et al., 2010; Parteli et al., 2011; Guignier et al., 2013). Periodic transverse dunes in the bed instability mode being subject to migration are often barchanoid ridges. However, all these morphological properties not only lack unified predictive models but also quantitative measurements. The quantitative prediction of dune orientation is an important step to the quantitative prediction of dune types as it is a prerequisite to evaluate the components of sand flux associated to the different dynamics.

Other boundary conditions associated with obstacles or confining factors that affect dune shape and dynamics could be added to the tree, *e.g.*, a dune may interact with a cliff to form an echo dune. Finally, the role of cohesion and vegetation is another challenge that would provide additional understanding if incorporated in a dynamics-based classification. Considerable progress has been made in the last two decades in modeling dune interactions with vegetation, successfully reproducing many characteristic shapes (Durán and Herrmann, 2006; Baas and Nield, 2007; Nield and Baas, 2008; Luna et al., 2011; Yan and Baas, 2017). Whereas modeling of wind flow and sediment transport can be based on strong theoretical background, the modeling of vegetation growth and interaction with sediment transport is largely phenomenological. Relating phenomenological model parameters to quantities measurable in the field is currently one of the biggest barriers to quantitative and predictive modeling of dune dynamics in interaction with vegetation.

In Section 5.2, we apply this dynamics-based classification to various characteristic dune types on Earth, using observed wind regimes to evaluate the dynamical processes in a simple way, and give rules to select the prevailing dynamics and to calculate crest orientations.

## 4. Classification of aeolian dunes based on fluid mechanics and sediment transport

### 4.1. Purpose and approach

Dunes are observed at a variety of scales that differ from one environment to another. The purpose of the following classification, based on fluid and sediment-transport mechanics, is to define the different dune-formation regimes, which determine the range of possible dune sizes, from the minimum size at which they form to the maximum size at which dune growth may saturate for reasons dictated by fluid flow and sediment transport. As environmental and boundary conditions vary from one planetary body to another, Earth and extraterrestrial dunes sample these different formation regimes, such that predictions from theory can be compared with observations returned by planetary exploration missions (Section 5.4).

For simplicity, we consider the case of a steady, unidirectional wind blowing over a cohesionless granular bed with unlimited sediment supply, at wind velocity above the threshold of transport. Given that we are interested first in incipient dunes and minimum dune size, the flow can be considered unconfined (*i.e.*, the flow is much thicker than the minimum dune size). Under these conditions, a flat bed may become unstable, leading to the growth of a periodic dune pattern with a characteristic wavelength, $\lambda_{\min}$. Specifically, dunes form from a positive feedback between fluid flow, sediment transport, and bed topography as sketched in Fig. 7. Spatial variations of sand flux drive erosion and deposition through conservation of mass (Exner equation; Exner, 1920, 1925; Paola and Voller, 2005). A dune grows with time if sand is, on average, deposited at its top, *i.e.*, if the sand flux peaks upwind of the dune top and decreases further downwind from the top. Conversely, a peak in flux downwind of the dune top leads to dune flattening. The minimum possible dune wavelength corresponds to the size at the threshold between a negative and a positive feedback of the instability, *i.e.*, when loci of maximum sand flux and maximum topography coincide. This minimum wavelength is very close to the wavelength of incipient dunes that would form from an initially flat sand bed, which formally is the wavelength for which the feedback is maximum.

The response of the fluid flow to a positive topographic perturbation is characterized by an increase of the fluid velocity (speed-up) above the bump and a space shift between the fluid velocity close to the ground (the shear velocity) and the bed elevation profile. For a sinusoidal elevation profile, the space shift corresponds to a phase shift, $\phi = \arctan(\mathscr{B}/\mathscr{A})$ (Appendix A.4.1). In turn, the maximum possible sand flux, called saturated sand flux, increases with shear velocity, or equivalently, with wind shear stress on the bed. However, the flux itself lags spatially as it responds to a change in shear stress. It peaks at some distance downwind of the locus of maximum shear stress. This relaxation distance is called the saturation length, $L_{\text{sat}}$, and is defined as the characteristic length over which sediment flux adapts to a change in transport conditions. The spatial shifts between the basal shear stress and the topography, and between the sand flux and the shear stress are the two key parameters that determine the formation of dunes from a flat sand bed. If the shear stress is maximum downwind of the peak in topography, dunes cannot develop. If the shear stress is maximum upwind of the topography, so could be the sand flux. If the saturation length is short enough for the flux to peak upwind of the crest, a dune grows. Conversely, if the saturation length is so long that the flux would still increase at the dune top, a dune cannot form.

The sign of the phase shift between shear stress and bed topography (positive if shear stress peaks upwind of the topography, negative otherwise) is controlled by the aerodynamic roughness of the bed. In turn, saturation length for wind saltation has been measured on Earth in the field (Andreotti et al., 2010; Lü et al., 2021) and in wind tunnels (Selmani et al., 2018) but still lacks a robust mechanistic model with predictive capabilities. Current empiricism suggests that it

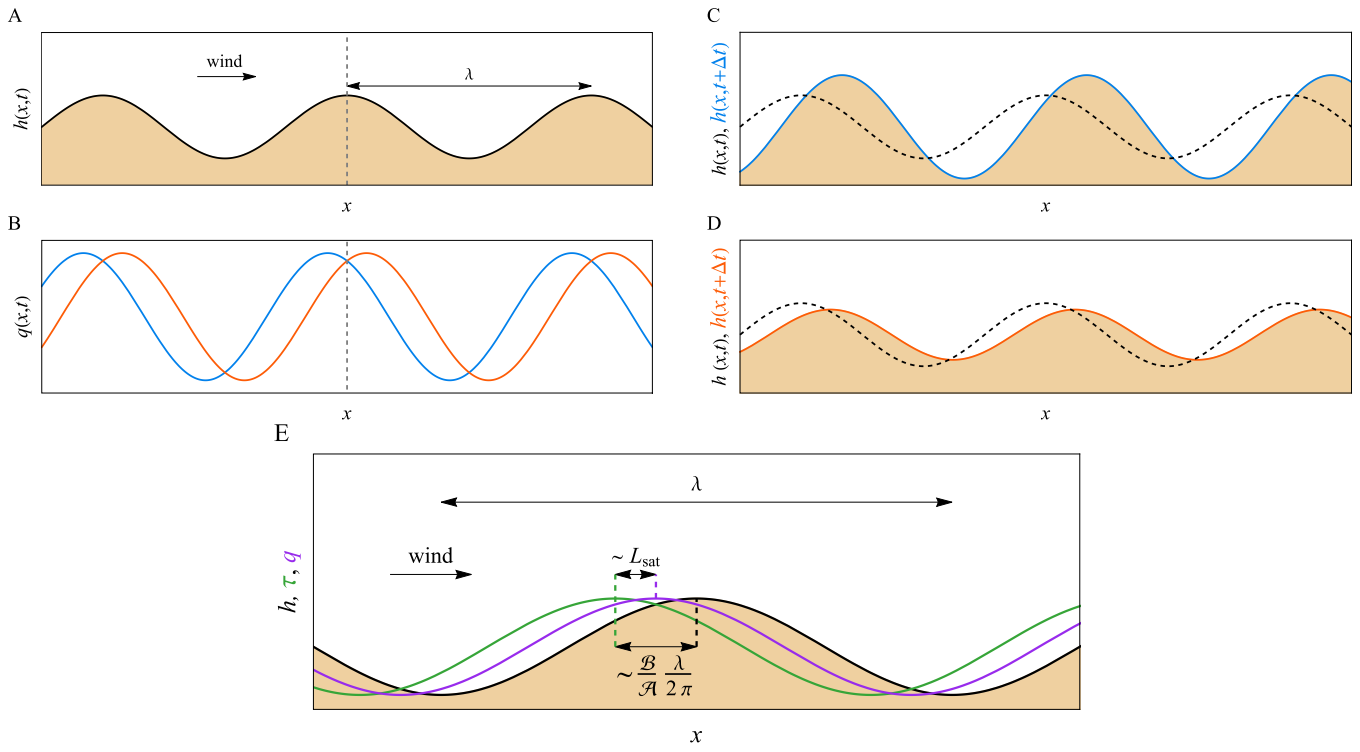


**Fig. 7.** Formation of periodic dunes. A: Sand bed with a sinusoidal elevation profile $h(x)$ of wavelength $\lambda$ at time $t$. B: Sand flux $q$ along the bed profile. The sand flux peaks upwind (blue) or downwind (orange) of the maximum of topography. C & D: Evolution of the sand bed depending on how the sand flux is shifted with respect to the bedform. E: Basal shear stress is shifted - here upwind (positive) shift - with respect to bedform by a distance $(\mathscr{B}/\mathscr{A})\lambda/(2\pi)$. Sand flux lags with respect to shear stress by a distance $L_{\text{sat}}$.

depends on three dimensionless numbers, which compare the density of sand grains with that of the fluid ($s$), the fluid force to the apparent weight of grains (the Shields number $\Theta$), and gravitational to viscous effects (the Galileo number $\mathscr{G}$). The mechanics of a turbulent flow over a corrugated bed and sand transport are further discussed in Appendices A.4.1 and A.2.1, respectively.

Dunes migrate as they develop. This migration forces interactions (such as collisions) between dunes, which leads to the coarsening of the dune pattern, *i.e.*, an increase in dune wavelength. The mechanism by which this coarsening process stops, limiting the size of giant dunes, is debated, possibly involving a limit in sand availability of the bed, flow confinement, or a change in flow regime (Appendix A.5).

In Fig. 8, we describe how the minimum and maximum dune wavelengths are determined depending on fluid and transport conditions, and discuss the different scenarios below. Dunes have been observed on a variety of planetary bodies, which we discuss in Section 5.4. Several parameters that control dune wavelength are currently unknown, and theoretical knowledge gaps still exist, offering exciting avenues for future research and investigation.

### *4.2. Tree description — Selection of dune size from flow regime and sediment transport*

#### *4.2.1. Turbulent flow above the bed - Aerodynamic roughness*

The response of the flow to a topographic perturbation is sensitive to the bed's *aerodynamic roughness*, which affects the turbulent mixing and the surface drag (Fig. 2 in Claudin et al., 2017; Kadivar et al., 2021). The roughness length scale, $r$, is a property of the bed surface at a much shorter length scale than the bedform wavelength, $\lambda$. Depending on the specific bed, flow, and transport conditions, $r$ can be controlled by grain size, $d$, the thickness of the transport layer (Fig. 23 in Durán et al., 2011), or by the height of smaller bedforms like ripples. How this length scale compares with the viscous length scale, $\nu/u_*$ (where $u_*$ is wind shear velocity and $\nu$ the kinematic viscosity of the fluid), has a critical impact on dune formation. Two regimes can be distinguished based on a roughness Reynolds number, $\mathscr{R}_r = ru_*/\nu$ (see Appendix A.4.1).

Above $\mathscr{R}_r \simeq 100$, shear stress peaks upwind of maximum topography regardless of dune wavelength. This is the *aerodynamically rough regime*, favorable to the onset of the dune instability.

For $\mathscr{R}_r$ values lower than ~10, the spatial shift between shear stress and topography strongly depends on the wavelength, $\lambda$, of the bedform perturbation. This regime is called the *aerodynamically smooth regime* and allows for shear stress to peak downwind of the topography maximum for a range of $\lambda$, preventing the formation of dunes at these scales, *i.e.*, a *dune gap* exists (Claudin et al., 2017; Durán Vinent et al., 2019; Bordiec et al., 2020). We refer to this particular response of the flow to the bedform perturbation as the *Hanratty anomaly* (Hanratty, 1981). This peculiar flow regime is predicted from extrapolation of a model built on a few measurements (Appendix A.4.1) and is supported by observations of bedforms on Mars (Rubanenko et al., 2022) as well as dissolution and melting patterns in nature (Appendix A.4.2).

For intermediate $\mathscr{R}_r$ values (~10 – 100), some effects of the Hanratty anomaly are detected but the physics essentially remains that of the rough limit (Claudin et al., 2017).

#### *4.2.2. Minimum wavelength selection*

*Rough flow.* The first branch of Fig. 8 we consider is that of aerodynamically rough conditions. In this case, assuming that the flow is virtually unconfined in the vertical direction, the minimum wavelength, $\lambda_{\text{min}}$, is found, to a first approximation, to scale with the saturation length, $L_{\text{sat}}$, multiplied by a prefactor that is controlled by fluid mechanics, *i.e.*, the spatial shift between the topography and the shear stress, which is roughly constant in this regime, *i.e.*, $\lambda_{\text{min}} \propto (\mathscr{A}/\mathscr{B})L_{\text{sat}}$ (Claudin and Andreotti, 2006; Charru et al., 2013; Gadal et al., 2020a; Appendix A.4.1).

*Smooth flow.* In the aerodynamically smooth regime, shear stress peaks downwind of the topography for a range of wavelengths that is determined by the viscous length. Dunes with those wavelengths cannot

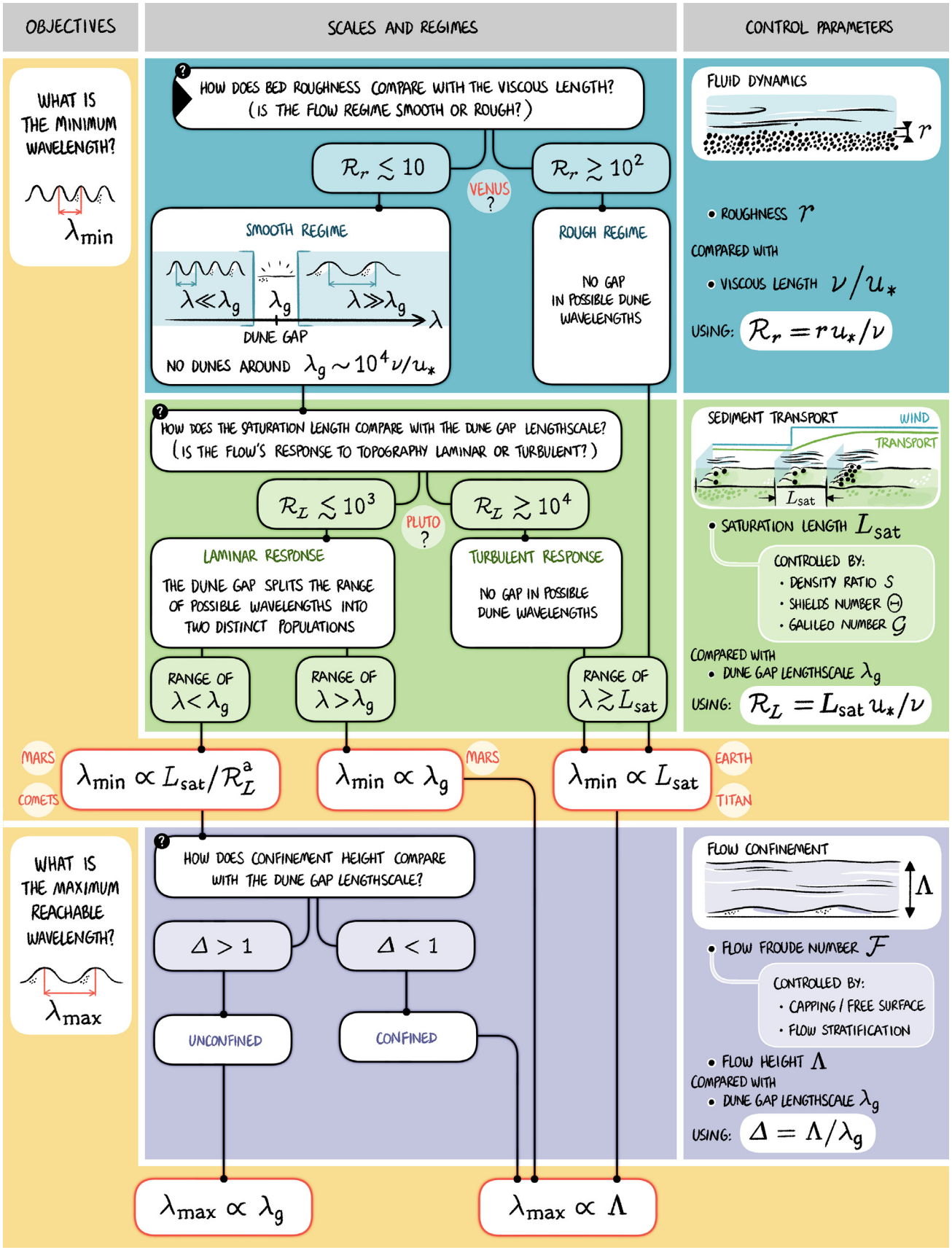


**Fig. 8.** Identification tree for dune classification based on fluid mechanics and sediment transport. Notations: roughness length scale, $r$; shear velocity, $u_*$; fluid kinematic viscosity, $\nu$; particle-to-fluid density ratio, $s = \rho_s/\rho_f$; Shields number, $\Theta = u_*^2/[(s-1)gd]$, where $g$ is the gravitational acceleration and $d$ is the grain size; Galileo number, $\mathcal{G} = \sqrt{(s-1)gd^3}/\nu$. Several Froude numbers can be associated with flow confinement or stratification, *e.g.*, $\mathcal{F} = U/\sqrt{g\Lambda\Delta\rho_f/\rho_f}$ where $U$ is the flow velocity and $\Delta\rho_f$ is the fluid density jump, both evaluated at altitude $\Lambda$. We also show the regimes and scales expected in the different environments of planetary bodies and comets (*e.g.*, 67P/Churyumov-Gerasimenko).

develop, creating a dune gap that extends over an order of magnitude around $\lambda_g \simeq 10^4 \nu/u_*$. As a result, the minimum wavelength for dunes can either be set by the viscous length, as for $\lambda_g$, or by the saturation length. A saturation length-based Reynolds number $\mathscr{R}_L = L_{sat} u_* / \nu$, allows for comparisons of these two length scales.

When $\mathscr{R}_L$ is large enough (*i.e.*, $L_{sat} > \lambda_g$, $\mathscr{R}_L \gtrsim 10^4$), saturation length is the limiting factor like in the rough regime and the most unstable wavelength scales as $\lambda_{min} \propto (\mathscr{A}/\mathscr{B}) L_{sat}$ (Durán Vinent et al., 2019).

For $\mathscr{R}_L \lesssim 10^3$, *i.e.*, $L_{sat} < \lambda_g$, bedforms with two distinct populations of wavelengths can coexist, either independently or as a superimposed pattern. They are scale-separated by the dune gap around $\lambda_g$. The minimum wavelength is thus either $\lambda_g$ for dunes above the gap, or is controlled by $L_{sat}$ for dunes under the gap. In the latter case, the minimum wavelength scales with $\lambda_{min} \propto L_{sat}/\mathscr{R}_L^a$, where $a \simeq 0.4$ (Jia et al., 2017; Durán Vinent et al., 2019).

#### 4.2.3. Maximum wavelength selection

Once initiated, dunes migrate, interact, and coarsen leading to an increase in wavelength. The size of giant dunes in the solar system, however, appears to be limited, with a maximum wavelength, $\lambda_{max}$. The upper limit on dune wavelength could be set either by the boundary conditions, introducing another characteristic length scale, or by the lower bound of the gap (*i.e.*, $\lambda_g$) for dunes initiated below the gap in the aerodynamically smooth regime. The smallest of those scales sets the maximum wavelength for dunes.

A first potential size limitation comes from the sediment supply and availability, which can lead to stalling dune growth (Werner and Kocurek, 1999). Another possible limitation arises from flow confinement. In the case of a non-confined flow, *i.e.*, a deep flow, a dune perturbs the flow above it over a characteristic height proportional to the dune's wavelength. An upper wall or a free surface confining the flow to a comparable or thinner height than dune wavelength would affect the flow above the dune and the sediment transport. Whereas the influence of a free surface is clear in rivers, it remains debated for planetary atmospheres, which are density stratified and do not exhibit a sharp interface. It was proposed that the thickness, $\Lambda$, of the atmospheric boundary layer (ABL) could act as a confinement scale, stalling dune coarsening at $\lambda_{max} \simeq \Lambda$ (Andreotti et al., 2009; Appendix A.5). This hypothesis, showing a correlation between the size of giant dunes on Earth and calculations of $\Lambda$, was challenged by another data set, in which the size of giant dunes on Earth were compared with satellite measurements of $\Lambda$ (Gunn et al., 2022). The question of the confining role of the ABL remains debated to date and may lack a good estimate or proxy of the characteristic thickness, $\Lambda$, which depends on time and space.

## 5. Case studies

Here we analyze different dune fields in light of the three classifications, demonstrating their complementarity and practical utility to describe and understand the observed patterns and untangle their complexity. We provide keys and methods for approaching pattern interpretation and their evolution through space and time. These also emphasize remaining open questions in fully predictive classifications and models.

### 5.1. Spatial and temporal changes in dune morphology as markers of evolution in external forcing and boundary conditions

#### 5.1.1. Framework

Although dunes are dynamical patterns that interact with each other and continuously grow or shrink, migrate, elongate, or reorganize within the field, equilibrium dune types are entirely determined by external forcing and boundary conditions, which include bed mobility, sand and vegetation coverage. Some changes in equilibrium dune type occur as discontinuous jumps when a factor varies. Perhaps the best known example is the change associated with the abrupt switch in dune orientation of periodic pattern on a mobile bed from transverse to longitudinal that occurs where the divergence angle between equal bimodal winds changes from less than to more than approximately 90°, as has been studied with experiments, simulations, and theory (Rubin and Hunter, 1987; Parteli et al., 2009; Reffet et al., 2010). Other changes in dune morphology vary along a continuum, such as where increasing dispersion of wind directions produces dome dunes rather than barchans (Gao et al., 2018).

Just as external forcing and bed conditions can cause differing equilibrium dune morphologies – either abrupt or along a continuum – dune type and morphology can also vary spatially or evolve temporally as forcing or bed conditions change through space or time. Typical changes in external forcing include environmental, climatic, and tectonic (*e.g.*, Kocurek and Ewing, 2016). These manifest as changes in wind regime (speed and direction), sediment supply, substrate type or geology, topography, vegetation cover, or moisture (*e.g.*, water table). In today's vast active sand seas on Earth, dune types are, in most cases, in approximate equilibrium with current conditions (Courrech du Pont et al., 2014; Figs. 12–20). However, shifts in winds on millennial scales change dune morphology (Gunn, 2023) and can create generations of superimposed dune morphologies (Lancaster et al., 2002; Baas and Delobel, 2022). Larger dunes incorporate so much sand and inherit so much environmental history that to rearrange their morphology could indeed require millennia (*e.g.*, Werner and Kocurek, 1997; Lancaster et al., 2002). In a multidirectional wind regime, dune type can also vary with dune size at the same location because they respond with different time scales to a change in wind direction. On the other hand, dunes formed in drier, windier climates may now be fully vegetated because of a climate shift. One example is the Nebraska Sand Hills, which were once characterized by active megabarchans and large barchanoid ridges during the Pleistocene but are now fully vegetated relict dunes (Mason et al., 2011).

Environmental factors and bed conditions typically vary over 100's km length scales across vast sand seas, or across a few kilometers' length scales, as with small dune fields that develop from beaches and extend inland. Migrating dunes can experience varying conditions, and the larger dunes may then inherit morphology from upwind, thereby lagging the local conditions in which they are observed.

As far as equilibrium dune types are concerned, changes in space or time are interchangeable. In transitional zones or periods, however, dunes are likely out of equilibrium. In case of migrating dunes, spatial morphologic and size changes in a dune field could still reveal what would be an autogenic temporal evolution. Ageing and coarsening of dune pattern, the arrangement of dunes within a field and response to changes in external forcing or boundary conditions are generally driven by the autogenic process of dune interactions such as dune collision, linking or repulsion, which may result in recognizable dune patterns that are inherently transitional. In the simplest case, merging and linking of barchan dunes results in transient barchanoid ridges (*e.g.*, Elbelrhiti et al., 2008). Blowouts and, to a lesser extent, migrating parabolic dunes may be other examples. Some dune types also correspond to specific boundary conditions, *i.e.*, to a transitional zone. This is the case for foredunes or lunettes, for example.

These examples paint a complex picture of dune equilibrium, where understanding the morphologic and dynamic richness of such dune fields relies first and foremost on recognizing changes in dune type and size along with potential external factors that influence these changes (Ewing and Kocurek, 2010).

#### 5.1.2. Field examples

Here we first discuss two examples of spatial evolution of dune type within fields where sediment enters the system from an upwind source, *e.g.*, a beach (Ewing and Kocurek, 2010). These examples illustrate the interplay between spatially varying external drivers and

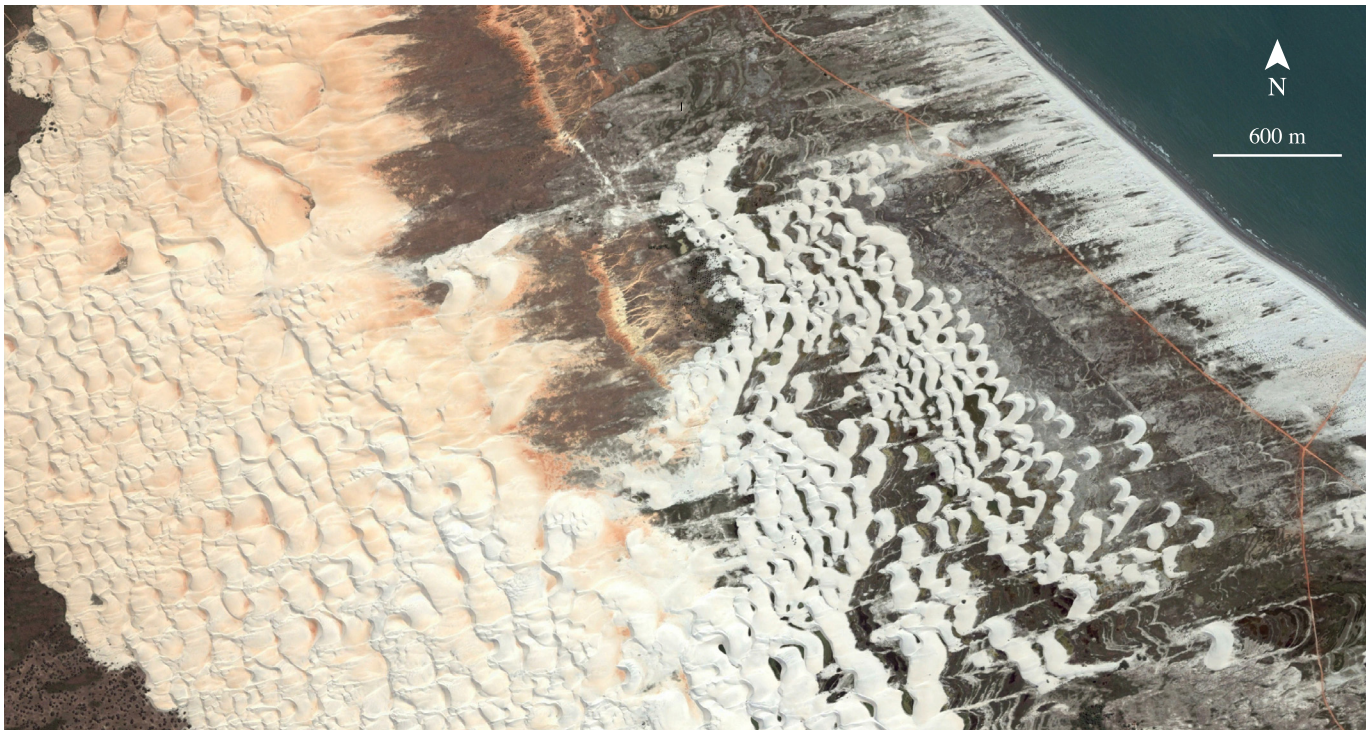


**Fig. 9.** The Porto do Mangue, Northeast Brazil coastal transgressive dunefield illustrating downwind development as the areal coverage of sand increases. The middle of the image lies at (5.05°S, 36.83°W), date: 07/2006. Credit: Maxar Technologies.

autogenic processes occurring at different stages of dune development. Then, we show how the observation of dunes in continuously varying environments can be extrapolated to the time evolution of dunes. We use examples that show evolutionary sequences that result in parabolic dunes, but the trajectory to the parabolic state differs due to varying boundary conditions within the fields.

Where sediment enters a dune system from a margin (*i.e.*, not from excavation of substrate alone) such as a beach or a playa, dune morphological evolution generally follows a characteristic morphologic evolutionary sequence that largely reflects a decrease in flux that drives an increase in sand cover and dune growth through dune–dune interactions. Boundary conditions including water table and feedbacks from vegetation growth can also play a role.

Fig. 9 illustrates a coastal example from NE Brazil where sand sheets and stringers evolve downwind across a deflation plain into barchans and barchanoids, and then sinuous transverse dunes. This change in dune types is correlated to a change in bed surface cover, which suggests that the wind is weakening inland.

It is also common to observe active mobile dunes such as barchans, barchanoids, and transverse dunes evolve into parabolic dunes downwind in both continental and coastal environments (Hack, 1941; Cooper, 1967; Hesp and Smyth, 2019; Benjumea-Lopez and Hesp, 2023) as observed in the White Sands dunefield shown in Fig. 10. White Sands is a gypsum dune system in New Mexico, which formed in the late Pleistocene to early Holocene (~9–12 kyr), and which provides a type-example of spatial changes in dune morphology from an upwind sediment source (McKee, 1966; Fryberger, 2000; Kocurek et al., 2007; Ewing, 2020; Holliday et al., 2023). Sand sheets and proto dunes emerging from the playa margin (Fig. 10A; Phillips et al., 2019; Gadal et al., 2020a) develop into sinuous transverse dunes (also termed crescentic dunes), then more complex barchanoids (Fig. 10B), to sub-parabolic and then parabolic dunes (Figs. 10C and D) as vegetation takes root and expands (Durán and Herrmann, 2006; Ewing and Kocurek, 2010; Reitz et al., 2010; Jerolmack et al., 2012). The evolution from incipient dunes at the playa margin to stagnant parabolic dunes downwind occurs over a distance of approximately 10 km. This transition has been explained by changes in field-scale aerodynamics and a reduction in groundwater salinity (Langford et al., 2009; Jerolmack et al., 2012). In the aerodynamic model, vegetation growth becomes more favorable downwind as the dune roughness relative to the playa reduces near-bed wind speed and therefore sediment transport (Jerolmack et al., 2012; Gunn et al., 2020). The barchan–parabolic transition occurs 8 km downwind of the field margin over a characteristic distance of 2 km and is correlated with an increase in plant density (number per dune) and a drop in the groundwater table (Jerolmack et al., 2012). The change in morphology begins with vegetation stabilizing the margins and horns of the mobile barchan dunes. The edges being held while the central and larger volumetric portion of dunes continue to advance, the dunes switch to a parabolic morphology (Durán and Herrmann, 2006; Reitz et al., 2010).

Different from the transition described above, parabolic dunes may instead develop directly from blowouts forming above the backshore of beaches or within continental dune fields where vigorous vegetation growth is supported (Carter et al., 1990; Luna et al., 2011; Barchyn and Hugenholtz, 2013; Durán and Moore, 2013; Hesp et al., 2021). The driving external factors affecting the transition are sediment transport rate and supply, and climate (*e.g.*, rainfall) (Hesp and Smyth, 2017; Hesp and Walker, 2021). Fig. 11 shows dunes at different stages of interaction with vegetation, suggesting what might be the typical evolution of a dune from its initiation on a foredune to its complete stabilization by vegetation as it migrates inland. This scenario may apply to the coastal dunefield in South Australia shown in Fig. 4I, for example. In Fig. 11A, a 50-m long blowout is beginning to develop incipient trailing ridges (note the vegetation stabilizing the edges of the depositional lobe), and if the depositional lobe continues to migrate downwind will evolve into a parabolic dune. Fig. 11B shows a large 750-m long parabolic dune with a well vegetated deflation basin. In semi-arid environments, nebkha often form on the depositional-lobe margins as shown in this photograph. Fig. 11C illustrates an older, long-walled (2.3-km long) parabolic dune with pronounced nebkha development around the lobe and trailing ridges. Trailing ridges are eventually stabilized by nebkha development and vegetation cover of the inside trailing ridges. Deflation basins and plains are colonized by

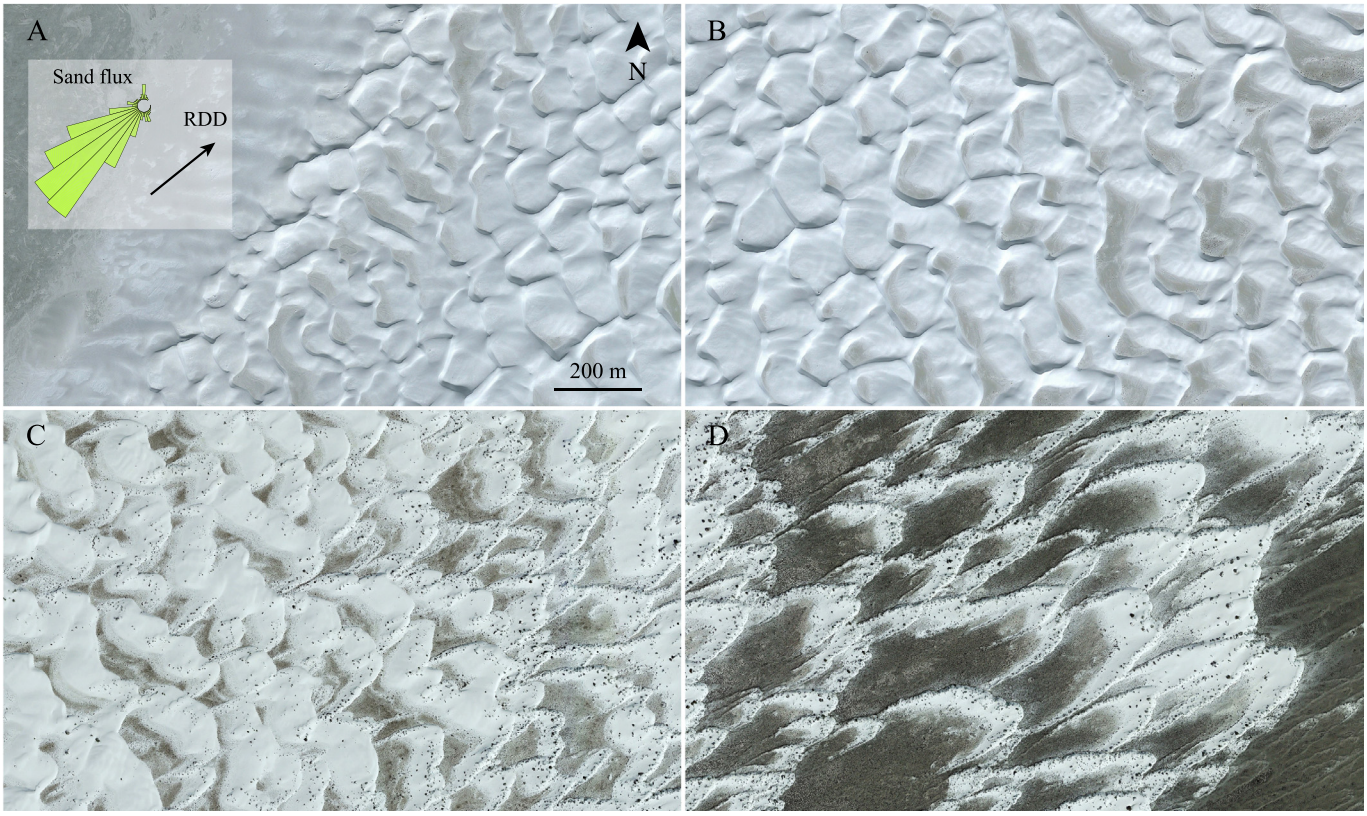


**Fig. 10.** A west-to-east along-RDD (30°N of East) evolutionary sequence across the White Sands dunefield starting at (32.802°N, 106.302°W) and ending at (32.848°N, 106.204°W), which corresponds to a distance of approximately 11 km. Sand sheets and proto dunes (A) evolve into transverse barchanoid ridges (B) and downwind into parabolic dunes (D). Panel (C) shows an area of morphological transition from barchanoid ridges to parabolic dunes. Date: 10/2013. Scale is the same for all snapshots. Sand flux rose points upwind. See Appendix for details of calculations. As in Gadal et al. (2020a), we used a density $\rho_s = 2300\,\mathrm{kg.m^{-3}}$ and a grain diameter $d = 670$ μm in the calculations for this particular case. Grain diameter decreases in the downwind direction from 670 μm (panel A) to 350 μm (panel D) (Jerolmack et al., 2011). Credit: Maxar Technologies.

vegetation once the deflation has occurred down to a base level fixed by the water table (*e.g.*, Fig. 11B), or hard surfaces (*e.g.*, Pleistocene calcrete in Fig. 11C). Parabolic dunes eventually stabilize due to running out of sediment or due to climate changes (*e.g.*, higher rainfall, lower wind speeds). Fig. 11D illustrates an example where a later parabolic dune phase has created a nested parabolic dune system.

The changes in dune morphology described herein present a basis for interpreting environmental conditions and processes through space and time. The characteristic spatial changes in morphology from an upwind source reveal the direction of the source area, sediment flux gradient, bed conditions, and the presence, absence, and feedbacks of vegetation in the system. The trajectory of the morphologies towards vegetated parabolic dunes from differing initial states highlights the strong control vegetation has on dune morphology. These systems also show the time-varying characteristics of dune morphological evolution that has only been revealed through long-term observations, numerical simulations, field-scale experiments, and scaled laboratory experiments (Durán and Herrmann, 2006; Nield and Baas, 2008; Reffet et al., 2010; Eastwood et al., 2011; Luna et al., 2011; Génois et al., 2013a,b; Ping et al., 2014; Moore et al., 2016; Yan and Baas, 2017; Phillips et al., 2019). Understanding these as time-varying morphological characteristics provides a foundation to interpret the recent and future climatic changes that could affect dune morphology (Baas and Delobel, 2022).

### 5.2. Revealing dune patterns on Earth from dynamical processes

The dynamic-based classification aims to quantify dune morphodynamics according to environmental forcing. Dune type and orientation result from the competition between three dynamical processes, which are growth in height, elongation, and migration. The prevailing dynamics and the balance between the three depend on boundary conditions and on the regime of sand transport the dune experiences, *e.g.*, the distribution of sand flux orientations, the magnitude and the sequence of transport events. In order to quantify this concept, three different sand flux components are defined in the reference frame of the dune crest. (i) The crest-normal component of sand flux, $Q_\perp$, is associated with dune migration. (ii) The crest-parallel component of sand flux, $Q_\parallel$, is associated with dune elongation. (iii) The growth in height is quantified through the gross bedform-normal transport, *i.e.*, the absolute value of crest-normal component of sand flux, $|Q_\perp|$. Following the mass conservation principle, the rates of growth in height, of migration, and of elongation correspond to the divergences of $|Q_\perp|$, $Q_\perp$, and $Q_\parallel$, respectively. Growth in height depends on gross transport (absolute value) rather than net transport, because transports in both directions across the crest contribute to dune growth (Rubin and Hunter, 1987; Courrech du Pont et al., 2014). Before presenting analysis for various common dune types on Earth, we review the different parameters that allow us to evaluate the dynamical processes and calculate their relative importance from wind data.

#### 5.2.1. Parameters for the characterization of the sand transport regime and dune dynamics

*Sand transport regime.* Using wind data from the last decade (Hersbach et al., 2019; Muñoz-Sabater et al., 2021), we calculate the instantaneous shear velocities, $u_*$, with Eq. (6), and saturated sand flux vectors on a flat sand bed, $\vec{Q}_0$, with transport law Eq. (2) using a transport threshold velocity, $u_t$ (Appendix). We then characterize the sand transport regime at a given location using the time-averaged $\langle u_* \rangle$, $\langle \vec{Q}_0 \rangle$, and $\langle \|\vec{Q}_0\| \rangle$. The mean shear velocity, $\langle u_* \rangle$, is averaged over the duration of active transport, *i.e.*, when $u_* > u_t$, so that the ratio $\langle u_* \rangle / u_t$ is a proxy for the average intensity of transport when it occurs. Because norms of individual sand flux vectors, $\vec{Q}_0$, correspond to the

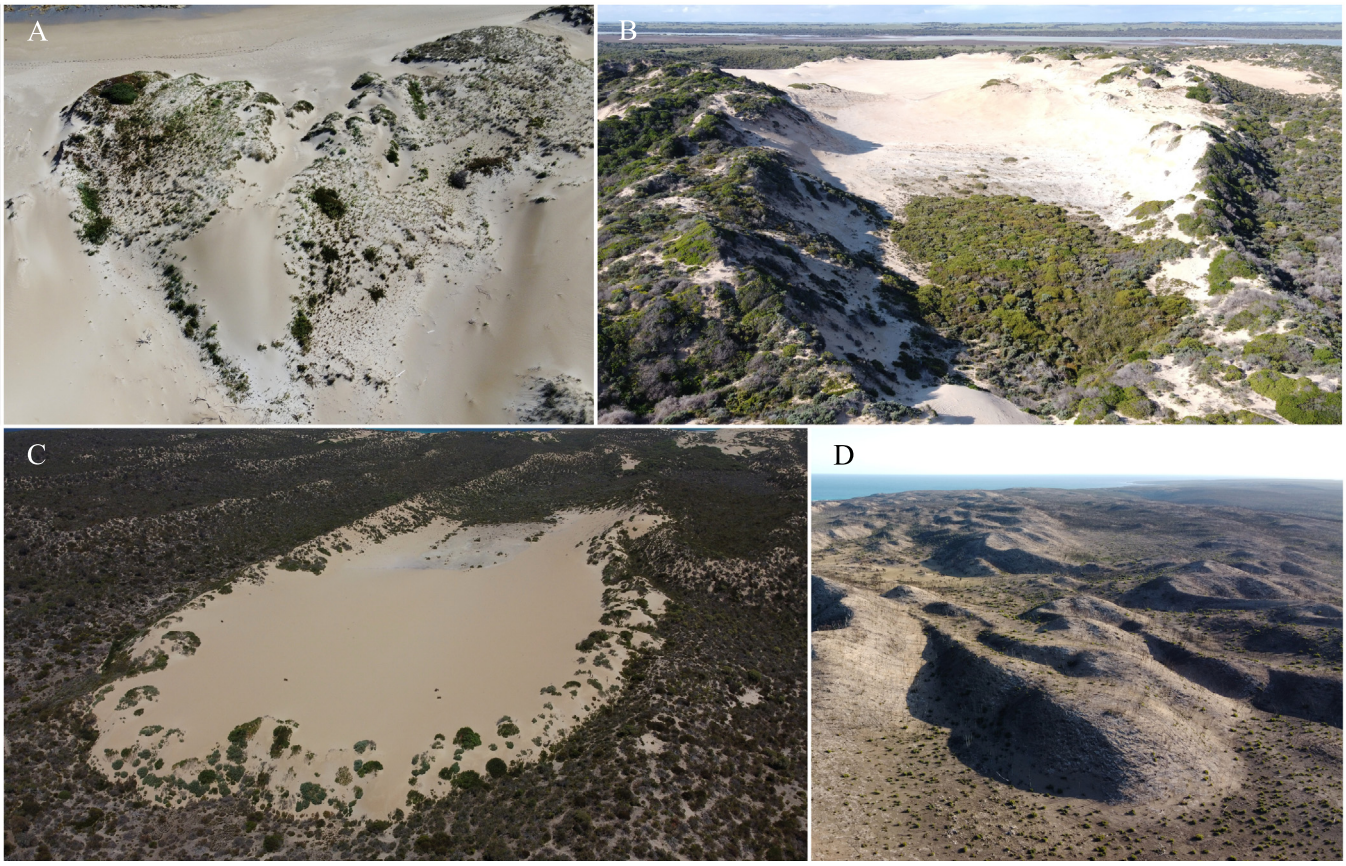


**Fig. 11.** A: Blowout at Maurpetuis Bay, Kangaroo Island, South Australia. B: Parabolic dune near Cantara, Younghusband Peninsula, South Australia. C: Long-walled parabolic dune near Port Lincoln, South Australia. D: Nested, long-walled parabolic dunes at Snake Lagoon, Kangaroo Island, South Australia. Credits: P. Hesp.

saturated values of sand fluxes, the norm of the time averaged sand flux is equivalent to the resultant drift potential, $\|\langle\vec{Q}_0\rangle\|$ = RDP, and its direction is the resultant drift direction, RDD. The time average of the norms of instantaneous sand fluxes is equivalent to the drift potential, $\langle\|\vec{Q}_0\|\rangle$ = DP, so that the ratio RDP/DP is a measure of the directional variability of sand transport (Fryberger and Dean, 1979; Pearce and Walker, 2005). RDP/DP → 1 where sand transport tends to be unidirectional; RDP/DP → 0 indicates high directional variability resulting in a small net transport compared with what it would be if all transport events were in the same direction.

*Sand transport over dunes.* Dune dynamics are evaluated with the time-averaged components of the characteristic sand flux over dunes, $\langle\vec{Q}_c\rangle$, in the reference frame of dune crest: $\langle Q_\perp\rangle$, $\langle Q_\parallel\rangle$, and $\langle|Q_\perp|\rangle$, which we calculate using the same transport law as for $Q_0$, but including the effect of *wind speed-up*, *i.e.*, the increase in wind shear velocity induced by dune topography. For this purpose, we reduce dunes to straight and symmetrical ridges of constant orientation and cross-section, *i.e.*, the cross section is constant along the dune and neither the size nor the slopes of the dune change over time. This simplification is valid within the limit of large dunes that fully integrate the wind regime (Appendix A.1). Following the approach of Jackson and Hunt (1975), we assume that the relative increase in wind velocity is proportional to the dune slope (increase in elevation with distance) along a wind streamline. It is maximum when the wind is perpendicular to the dune crest. Wind speed-up modulates the norm of each instantaneous sand flux, $\|\vec{Q}_c\|$, as a function of the angle between the wind and the dune crest. Therefore, the direction and magnitude of the time averaged sand flux the dune experiences, $\langle\vec{Q}_c\rangle$, depend on dune orientation in a multidirectional transport regime (see Appendix A.3 for details and Fig. 23 for a sketch of the different components of sand flux). $\langle Q_\perp\rangle$, $\langle Q_\parallel\rangle$, and $\langle|Q_\perp|\rangle$ can be evaluated for any potential dune orientation, $\alpha$. The functions $\langle Q_\perp\rangle(\alpha)$, $\langle Q_\parallel\rangle(\alpha)$, and $\langle|Q_\perp|\rangle(\alpha)$ allow us to predict the orientation of dunes according to the prevailing dynamical process.

*Evaluating dune orientation.* When growth in height prevails, as in the bed instability mode where dunes develop from a loose sand bed, the selected orientation of dunes, $\alpha_H$, maximizes the growth rate in height, $\sigma$, or equivalently the gross bedform-normal transport, $\langle|Q_\perp|\rangle$ (Appendix A.3.3). In a multidirectional wind regime, this orientation can be transverse, oblique or parallel to the RDD. $\alpha_H$ is also the expected crest orientation when migration prevails. When elongation prevails, and when dunes elongate without migrating, dune crest orientation, $\alpha_E$, corresponds to the direction of elongation, which in this case is also the direction of the mean sand flux on the dune, $\langle\vec{Q}_c\rangle$, such that $\langle Q_\perp\rangle(\alpha_E) = 0$ (no migration), and $\langle Q_\parallel\rangle(\alpha_E) > 0$ (elongation).

*Sand flux depending on dune orientation.* We use these predicted dune orientations to determine the averaged characteristic sand flux experienced by dunes in the two modes of orientation: $\langle\vec{Q}_H\rangle = \langle\vec{Q}_c(\alpha_H)\rangle$ of direction $\theta_H$ for dunes whose orientation maximizes growth in height, and $\langle\vec{Q}_E\rangle = \langle\vec{Q}_c(\alpha_E)\rangle$ of direction $\theta_E = \alpha_E$ for dunes that elongate without migrating. Except in singular situations, dunes whose orientation maximizes growth in height migrate according to the resultant crest-normal component of sand flux of norm $\|\langle\vec{Q}_M\rangle\| = |\langle Q_\perp(\alpha_H)\rangle| = \|\langle\vec{Q}_H\rangle\|\,|\sin(\theta_H - \alpha_H)|$ and direction $\theta_M$, which is perpendicular to the dune orientation, $\alpha_H$. The characteristic migration velocity equals $\|\langle\vec{Q}_M\rangle\|/H$, where $H$ is dune height. Similarly, the elongation rate of a non-migrating dune can be evaluated with $\|\langle\vec{Q}_E\rangle\|/H$ (Lucas et al., 2015; Lü et al., 2017).

*Competition between dynamics.* We argue that the orientation of dunes depends on the prevailing growth mechanism and that dune type depends on the competition (relative balance) between the three dynamical processes. The main factor selecting the prevailing growth

mechanism for dune orientation appears to be the mobility of the sand bed and the boundary conditions. The variety of shapes within a given regime of orientation, as the balance between migration and elongation on a starved bed, must depend on the wind regime alone when all boundary conditions are fixed. Aiming at a fully predictive phase diagram of dune type and equilibrium shape, we propose and review from previous studies several dimensionless ratios built from the different sand fluxes just discussed to assess the competition between the three dynamics. For each of the two dune orientations, the three sand fluxes, $\left|\langle Q_{\parallel}\rangle\right|$, $|\langle Q_{\perp}\rangle|$, and $\langle|Q_{\perp}|\rangle$, associated with the three dynamics, elongation, migration, and growth in height, can be calculated. Because dunes in the elongation mode do not migrate ($\langle Q_{\perp}\rangle(\alpha_E) = 0$), this makes 5 different fluxes ($2 \times 3 - 1$), with which we can build 4 independent dimensionless ratios, *i.e.*, that cannot be built as a combination of the others. We chose 3 ratios that allow us to compare dynamics of dunes in a given mode of orientation: $\left|\langle Q_{\parallel}(\alpha_H)\rangle/\langle Q_{\perp}(\alpha_H)\rangle\right| = \hat{Q}_{\parallel/\perp,H}$ and $\left|\langle|Q_{\perp}(\alpha_H)|\rangle/\langle Q_{\perp}(\alpha_H)\rangle\right| = \hat{Q}_{|\perp|/\perp,H}$ for dunes whose orientation maximizes growth in height, and $\left|\langle|Q_{\perp}(\alpha_E)|\rangle/\langle Q_{\parallel}(\alpha_E)\rangle\right| = \hat{Q}_{|\perp|/\parallel,E}$ for dunes in the elongation mode of orientation. In addition, we select one ratio that compares the two different modes of orientation: $\langle|Q_{\perp}|(\alpha_E)\rangle/\langle|Q_{\perp}|(\alpha_H)\rangle = \sigma_E/\sigma_H$, the ratio between growth rates in height of dunes under the two modes of orientation. In the simplified framework we developed, these 4 ratios fully define the parameter space associated with wind forcing.

$\sigma_E/\sigma_H$ varies between 0 and 1, and has been proposed to evaluate the stability of elongating dunes when they develop from a point source (Gao et al., 2015). The stability of dunes elongating on a starved bed from a sand source in bimodal wind regimes was numerically studied in Gao et al. (2015). Depending on the divergence angle and transport ratio between the two alternate wind directions, an elongating linear dune or a train of propagating asymmetric barchans is observed. The ratio $\sigma_E/\sigma_H$ was found to discriminate between the two morphologies in the simulations and in a dune field around the Tibesti Massif (east central Sahara); elongating dunes are observed when $\sigma_E/\sigma_H$ is larger than 0.6. This result reflects the fact that perpendicular flows are required to build a dune, regardless of its mode of orientation. Note that in experiments under water with a bimodal flow regime, a linear dune elongating from a point source on a starved bed turns into a highly asymmetric barchan with an oblique arm if the sand source shuts off so that the dune is free to migrate (Rubin et al., 2016). The sand source helps to mute dune migration. As such, the ratio $\sigma_E/\sigma_H$ cannot be used to distinguish the prevailing dynamics for dune orientation under different boundary conditions, including bed mobility. This could be the case if the boundary conditions were specifically taken into account in the calculations, which is not the case here.

When dunes develop on a sand covered bed, growth in height prevails and the orientation of the dune crest is $\alpha_H$. Within given boundary conditions, the variety of shapes should then depend on the two dimensionless ratios $\hat{Q}_{\parallel/\perp,H}$, and $\hat{Q}_{|\perp|/\perp,H}$. The ratio between the crest-parallel and the crest-normal components of sand flux, $\hat{Q}_{\parallel/\perp,H}$, was conceptually proposed to quantify the impact of a wind regime on straightness and sinuosity of morphologically long dunes (Rubin, 2012). The crest-parallel component should favor straightness whereas the crest-normal component, causing migration, should favor sinuosity. We note, however, that crest-straightness could be favored by the gross crest-parallel component instead of the crest-parallel component of resultant, so that the ratio $\left|\langle|Q_{\parallel}(\alpha_H)|\rangle/\langle Q_{\perp}(\alpha_H)\rangle\right| = \hat{Q}_{|/|/\perp,H}$ could be more appropriate. As growth in height also builds the spatial coherence of a dune, the ratio $\hat{Q}_{|\perp|/\perp,H}$ may also be relevant for assessing dunes straightness, as well as to evaluate the relative balance between growth in height and migration dynamics.

For dunes migrating on a starved bed, which also have an orientation that maximizes growth in height, the migrating direction, $\theta_M$, does not necessarily correspond to the resultant transport direction, $\theta_H$. This asymmetry in sand fluxes must drive an asymmetry in dune morphology, which in turn may be evaluated through the ratio $\hat{Q}_{\parallel/\perp,H}$.

For dunes that elongate without migrating, the crest-normal component of sand flux is zero, so that the ratio $\hat{Q}_{|\perp|/\parallel,E}$ alone should allow us to distinguish between morphologies.

Finally, since the very existence of a dune relies on the ability of winds to raise it in height, the ability of migration and elongation to select dune shape and orientation on a starved bed could be assessed through the ratios $\hat{Q}_{|\perp|/\perp,H}$ and $\hat{Q}_{|\perp|/\parallel,E}$, respectively. A dynamic should be promoted if it favors the growth in height over migration or elongation. The relative balance between migration and elongation dynamics in dune pattern selection could be evaluated by comparing the two ratios.

Although only a few of these parameters have been tested in previous studies, and that their calculations are based on numerous simplifications, they formalize a framework for studying dune morphology based on dune dynamics. We already remarked that fully predictive parameters should take into account boundary conditions, which affect sand supply and the divergence of sand flux at the dune scale. Some parameters, such as free flux, may be difficult to infer remotely. For example, the migration velocity of an isolated dune like a barchan decreases and its size may increase when it captures an incoming free flux. More importantly, useful predictive parameters should involve the temporal sequence of transport directions and the relative size of dune to transport capacity of individual wind events. For example, experiments in water and simulations have shown that a dune will completely reverse before migrating if subjected to an abrupt change in flow direction (Hersen, 2005; Courrech du Pont et al., 2014; Rozier et al., 2019; Sandoungout, 2019; Gao et al., 2021). Furthermore, in bidirectional wind regime, numerical simulations show that the ratio between the time period of wind reversal and the characteristic turnover time of dune controls the crest sinuosity (Parteli et al., 2009; Nakao-Kusune et al., 2020).

#### 5.2.2. Example analyses for various characteristic free dune types on Earth

Different types of free dunes from the geomorphological classification 2 are shown in Figs. 12–20. The sand transport parameters for characterization of their formative processes and orientation according to the dynamics-based classification are gathered in Table 3. Transport parameters are calculated from wind data provided by the ECMWF ERA5-Land reanalysis (Hersbach et al., 2019; Muñoz-Sabater et al., 2021) from January 1, 2000 to December 31, 2020. Using these twenty years of wind data, we derive a characteristic dune cross-sectional length, $L_{20\,yr} = \sqrt{2\,\langle|Q_{\perp}(\alpha_H)|\rangle \times 20\,\mathrm{yr}/0.1}$, that integrates the winds over the entire period considered (Sections A.1, A.3.3). Here we assume a dune aspect ratio (height to length) of 0.1. Many of the dunes shown in Figs. 12–20 are much larger than this characteristic length. We therefore test the hypothesis that dune types and orientations are in equilibrium with modern winds. This hypothesis was found to be reasonable in many examples (Courrech du Pont et al., 2014), however there are others where it is known not to be the case (Gunn, 2023). More importantly, we derive the characteristic length, $L_{1\,yr} = \sqrt{2\,\langle|Q_{\perp}(\alpha_H)|\rangle \times 1\,\mathrm{yr}/0.1}$, that integrates winds over one year, the typical time duration of a wind cycle on Earth. Although it would be more accurate to consider each individual wind sequence between two significant changes in direction separately, *e.g.*, for reversing dunes, this characteristic length is an estimate of the minimum cross-sectional length of dunes that integrate the wind regime.

*Periodic long-crested dunes on sand covered beds.* Periodic long-crested dunes on sand covered beds can form with orientations that are transverse (Fig. 12), oblique (Fig. 13), or longitudinal (Fig. 14) with respect to the RDD. The expected prevailing process on a sand bed is the growth in height of a periodic pattern (bed instability) with dunes forming in the orientation that maximizes the gross bedform-normal transport, *i.e.*, $\langle|Q_{\perp}|\rangle$, which is well verified in these three examples. Where the wind regime tends to be unidirectional, long transverse dune patterns develop with an asymmetric shape showing a clear difference between gentle stoss side and steep lee face (Fig. 12). Under bimodal

**Table 3**
Dune type, wind velocity, sand flux, and dune orientation calculated from wind data at the different locations shown in Figs. 12–20. Bed surface: CB, SB, and PSB stand for sand covered bed, starved bed, and partially starved bed, respectively. Shape: Long-C., Barch., and Asym. stand for Long-crested, Barchan, and Asymmetric, respectively. Dune orientations are with respect with the RDD. T, O, and L stand for Transverse, Oblique, and Longitudinal, respectively. The value of the threshold velocity used in the calculation is $u_t = 0.153\,\mathrm{m/s}$. Calculated orientations are with respect to the east, counter-clockwise. $\alpha_H$ is the dune orientation that maximizes growth rate in height. $\alpha_E$ is the dune orientation in the elongation mode. $\Delta\alpha$ is between 0 and 90 degrees. $\theta_H$ is the direction of mean sand flux at dune crest for dunes whose orientation is $\alpha_H$. The definitions of dimensionless numbers are: $\sigma_E/\sigma_H = \langle|Q_\perp(\alpha_E)|\rangle/\langle|Q_\perp(\alpha_H)|\rangle$, $\hat{Q}_{\parallel/\perp,H} = \left|\langle Q_\parallel(\alpha_H)\rangle/\langle Q_\perp(\alpha_H)\rangle\right|$, $\hat{Q}_{|\perp|/\perp,H} = |\langle|Q_\perp(\alpha_H)|\rangle/\langle Q_\perp(\alpha_H)\rangle|$, and $\hat{Q}_{|\perp|/\parallel,E} = \langle|Q_\perp(\alpha_E)|\rangle/\langle Q_\parallel(\alpha_E)\rangle$.

| **Figure** | 12 | 13 | 14 | 15 | 16 | 17 | 17inset | 18 | 19 | 20 | | |
|---|---|---|---|---|---|---|---|---|---|---|---|---|
| **Location** | 16.6°S 11.9°E | 37.7°N 105.1°E | 30.8°N 33.1°E | 18.8°N 12.5°E | 24.3°N 4.3°W | 27.5°N 13.1°W | 27°N 12.9°W | 20.1°S 13.3°E | 40.2°N 92.2°E | 26°S 15.9°E | | |
| **Dunes** | | | | | | | | | | | | |
| Bed surface | CB | CB | CB | SB | SB | SB | SB | SB | SB | PSB | | |
| Shape | Long-C. | Long-C. | Long-C. | Linear (Lee) | Linear | Barch. | Barch. | Barch. (Asym.) | Linear (Raked) | Star | | |
| Periodic/Isolated | Per. | Per. | Per. | Iso. | Per. | Non Per. | Non Per. | Non Per. | | | | |
| Orientation | T | O | L | O | L | T | T | T/O | L/O | T/L/O | | |
| **Shear velocity** | | | | | | | | | | | | |
| $\langle u_* \rangle$ (m/s) | 0.241 | 0.24 | 0.229 | 0.217 | 0.227 | 0.289 | 0.268 | 0.238 | 0.237 | 0.226 | | |
| $\langle u_* \rangle / u_t$ | 1.58 | 1.57 | 1.5 | 1.42 | 1.48 | 1.89 | 1.75 | 1.56 | 1.55 | 1.48 | | |
| **Flux on a flat sand bed** | | | | | | | | | | | | |
| DP = $\langle\|\vec{Q}_0\|\rangle$ ($m^2$/yr) | 38.1 | 37.8 | 31.5 | 24.5 | 44 | 120.1 | 89.5 | 39 | 30.1 | 29.3 | | |
| RDP = $\|\langle\vec{Q}_0\rangle\|$ ($m^2$/yr) | 32.6 | 9.7 | 15 | 14.5 | 19.6 | 100.9 | 72.3 | 27.7 | 15.8 | 2 | | |
| RDP/DP | 0.86 | 0.26 | 0.48 | 0.59 | 0.45 | 0.84 | 0.81 | 0.71 | 0.52 | 0.07 | | |
| RDD (deg.) | 49 | 300 | 337 | 216 | 223 | 252 | 256 | 90 | 219 | 61 | | |
| **Prediction of dune orientations** (deg.), **fluxes at the crest** ($m^2$/yr), **and characteristic cross-sectional lengths** (m) | | | | | | | | | | | | |
| $\alpha_H$ | 136 | 51 | 150 | 144 | 110 | 163 | 169 | 168 | 111 | 128 | | |
| $\alpha_E$ | 45 | 281 | 329 | 205 | 233 | 251 | 251 | 92 | 222 | 29 | 127 | 252 |
| $\Delta\alpha = \|\alpha_H - \alpha_E\|$ | 89 | 49 | 1.4 | 61 | 57 | 88 | 82 | 77 | 68 | 81 | 0.4 | 56 |
| $\|\langle\vec{Q}_H\rangle\| = \|\langle\vec{Q}_c(\alpha_H)\rangle\|$ | 146 | 35 | 44 | 70 | 90 | 394 | 299 | 138 | 69 | 8 | | |
| $\theta_H$ | 48 | 299 | 328 | 225 | 217 | 253 | 257 | 87 | 212 | 127 | | |
| $\Delta\theta = \theta_H - \alpha_E$ | 2.8 | 18 | −1.2 | 20 | −16 | 2.4 | 6 | −5 | −10 | 98 | −0.5 | −125 |
| $\|\langle\vec{Q}_M\rangle\| = \|\langle Q_\perp(\alpha_H)\rangle\|$ | 146 | 32 | 2 | 69 | 85.6 | 394 | 298 | 136 | 68 | 0.1 | | |
| $\|\langle\vec{Q}_E\rangle\| = \|\langle\vec{Q}_c(\alpha_E)\rangle\|$ | 55 | 19 | 44 | 40 | 43 | 145 | 109 | 45 | 38 | 11 | 8 | 5 |
| $\langle\|Q_\perp(\alpha_H)\|\rangle$ | 160 | 154 | 98 | 103 | 160 | 424 | 320 | 164 | 121 | 132 | | |
| $L_{1y}$ | 57 | 55 | 44 | 45 | 57 | 92 | 80 | 57 | 49 | 51 | | |
| $L_{20y}$ | 253 | 248 | 198 | 203 | 253 | 412 | 358 | 256 | 220 | 230 | | |
| **Competition between dynamics** | | | | | | | | | | | | |
| $\sigma_E/\sigma_H$ | 0.19 | 0.58 | 1 | 0.57 | 0.62 | 0.18 | 0.24 | 0.25 | 0.41 | 0.25 | 1 | 0.47 |
| $\hat{Q}_{\parallel/\perp,H}$ | 0.03 | 0.42 | 22 | 0.16 | 0.31 | 0.004 | 0.02 | 0.15 | 0.21 | 66 | | |
| $\hat{Q}_{\|\perp\|/\perp,H}$ | 1.1 | 4.8 | 49 | 1.5 | 1.9 | 1.1 | 1.1 | 1.2 | 1.8 | 1111 | | |
| $\hat{Q}_{\|\perp\|/\parallel,E}$ | 0.55 | 4.6 | 2.2 | 1.5 | 2.3 | 0.54 | 0.72 | 0.9 | 1.3 | 2.8 | 16.3 | 12.2 |

| **Parameter** | **For assessing** |
|---|---|
| $\sigma_E/\sigma_H$ | Stability of elongating dunes on starved beds |
| $\hat{Q}_{\parallel/\perp,H}$ | Straightness vs. sinuosity of periodic long-crested dunes on covered bed (bed instability mode, growth in height dominates)<br>Asymmetry of migrating dunes |
| $\hat{Q}_{\|\perp\|/\perp,H}$ | Relative balance between growth in height and migration dynamics<br>Straightness vs. sinuosity of periodic long-crested dunes on covered bed (bed instability mode, growth in height dominates) |
| $\hat{Q}_{\|\perp\|/\parallel,E}$ | Morphology of elongating dunes |
| $\hat{Q}_{\|\perp\|/\perp,H}$ vs. $\hat{Q}_{\|\perp\|/\parallel,E}$ | Relative balance between migration and elongation dynamics on starved beds |

wind regimes, long-crested dune patterns with more symmetric slopes are observed. As predicted from theory, they are usually oblique in orientation (Fig. 13), and only tend to be longitudinal where the transport ratio between the two main wind directions is close to one (Fig. 14; Rubin, 2012; Courrech du Pont et al., 2014). Transverse dune patterns in Fig. 12 show a range of sizes with smaller dunes either being superimposed on larger ones or spatially separated. Subjected to an almost unidirectional flux regime, they must migrate as predicted by the net sand flux associated with migration, $\langle Q_M \rangle$. In these examples, the ratios $\hat{Q}_{\parallel/\perp,H}$ and $\hat{Q}_{|\perp|/\perp,H}$ increase by two orders of magnitude as the predicted dune orientation goes from transverse, to oblique, to longitudinal. This may explain why transverse dunes in Fig. 12 resemble barchanoid ridges, whereas oblique dunes in Fig. 13 are straighter. Crests of oblique dunes in Fig. 13 still display some sinuosity, suggesting that they are subject to migration. We note that the sizes of these reversing dunes are barely of the order of $L_{1yr}$, so that they may undergo non-negligible back and forth migration during a single wind cycle (Parteli et al., 2009; Nakao-Kusune et al., 2020). The temporal sequence of transport directions is not taken into account by the parameters used here, which may lead to an underestimate in migration relative to growth in height. Although ratios $\hat{Q}_{\parallel/\perp,H}$ and $\hat{Q}_{|\perp|/\perp,H}$ are even larger for longitudinal dunes in Fig. 14, crests are not straight. However, we observe that in this region, sand transport directions are much more widely distributed. Here, the amplitude of gross bedform-normal transport as a function of crest orientation, $\langle|Q_\perp|\rangle(\alpha)$, varies by 30%, compared to 400% and 300% for transport regimes in Figs. 12 and 13, respectively. This smaller value may lead to a weaker selection of a well defined orientation, especially at small scale, explaining the greater variability in crest alignment observed for the longitudinal dunes in Fig. 14.

*Dunes on starved beds.* Starved interdunes should promote elongation or migration. In multidirectional wind regimes, elongation without migration can be favored by boundary conditions such as a localized sand source, which inhibits migration. Extended lee dunes are good candidates, like the isolated linear oblique dune extending downwind

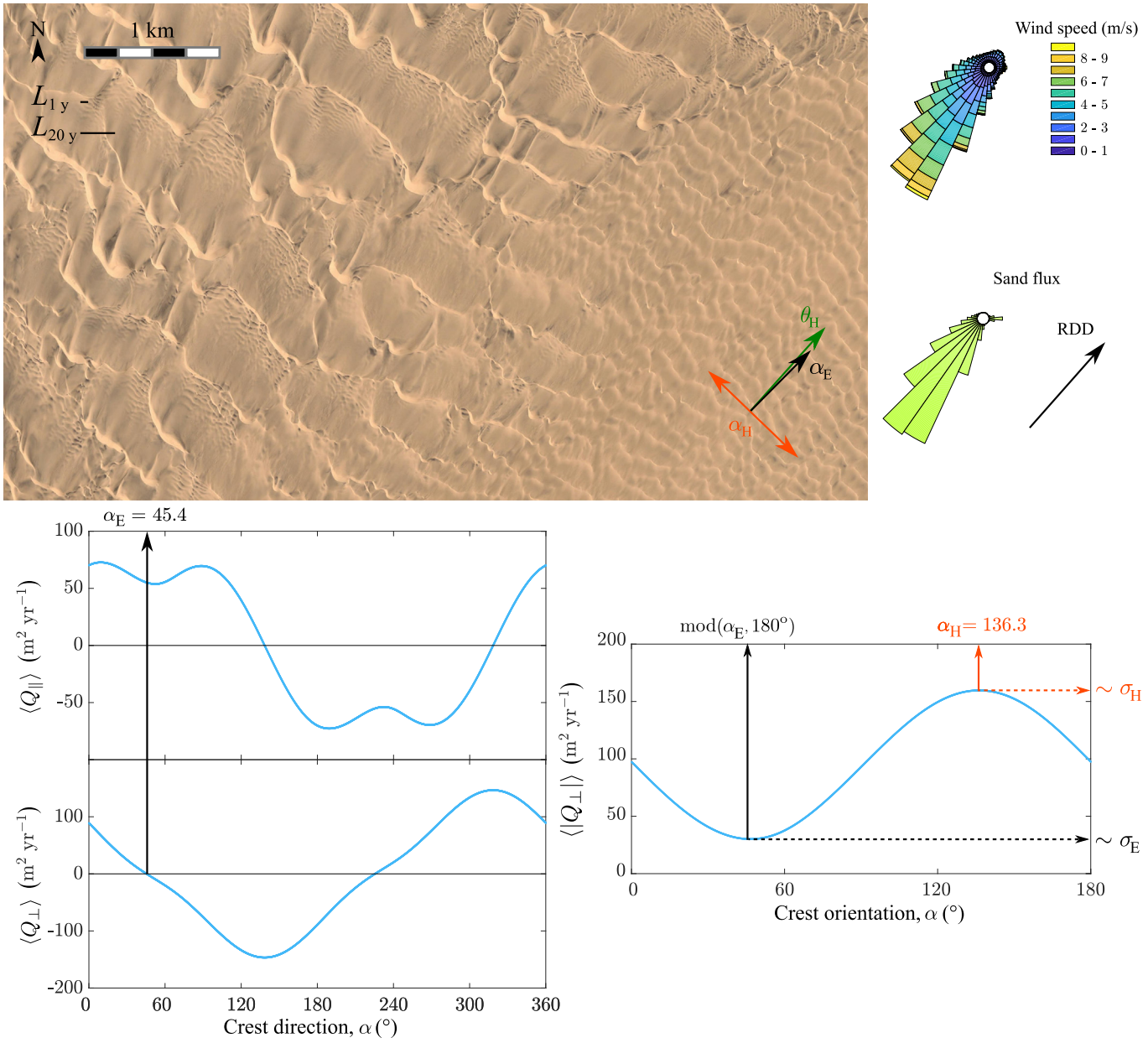


**Fig. 12.** Transverse long-crested dunes on sand-covered bed in the Moçâmedes Desert in Angola (16.6°S, 11.9°E), date: 03/2004, credit: Maxar Technologies. Roses, which point upwind, show the wind regime at 10 m above ground level and the corresponding sand flux regime from 2000 to 2020. See Section 5.2 and Appendix for an explanation of parameters and details of calculations. Graphics show the calculated characteristic sand flux components $\langle Q_\perp \rangle$, $\langle Q_\parallel \rangle$, and $\langle |Q_\perp| \rangle$ over a dune with direction $\alpha$. Angles are measured relatively to east direction. $\alpha_H$, the dune orientation that maximizes $\langle |Q_\perp| \rangle$, $\alpha_E$, the dune direction for elongation ($\langle Q_\parallel \rangle > 0$) without migration ($\langle Q_\perp \rangle = 0$), and $\theta_H$, the direction of the sand flux over a dune of orientation $\alpha_H$, are shown by arrows in the image. The characteristic lengths $L_{1\,yr}$ and $L_{20\,yr}$ are shown to scale for comparison with cross-sectional lengths of dunes.

from a large obstacle shown in Fig. 15. The predicted orientation for elongation without migration, $\alpha_E$, corresponds to the observed orientation of this dune and is significantly different from the oblique alignment predicted for dunes whose orientation maximizes growth in height, $\alpha_H$. In a different bimodal wind regime, the larger periodic linear longitudinal dunes shown in Fig. 16 also exhibit an orientation that corresponds to the elongation mode. Because longitudinal linear dunes can elongate along the sand flow paths, they are the most likely to extend over long distances. These massive dunes follow a major sand flow path that extends from southwestern Algeria to Mauritania. Unlike the bed instability, experiments and numerical simulations have shown that the elongation process does not directly determine dune size or wavelength (Courrech du Pont et al., 2014; Gadal et al., 2020b). The periodicity and sizes are instead imposed by boundary and initial conditions, which, with self-organization, are possible explanations for the periodic pattern in the elongation mode observed in this field. We note that, in this dune field and for the isolated linear dune shown in Fig. 15, the ratio $\sigma_E/\sigma_H$ is close to 0.6 – the threshold value for stable elongation from a point source as found in numerical simulations (Gao et al., 2015).

Barchan dunes, such as those observed in the Western Sahara (Fig. 17), are the archetype of migrating dunes. Here, and most often for symmetric barchans, the sand flux regime is unidirectional. Barchan slip faces are oriented perpendicular to the transport direction, which, for a unidirectional transport regime, is also the predicted orientation when growth in height prevails. Many boundary and initial conditions

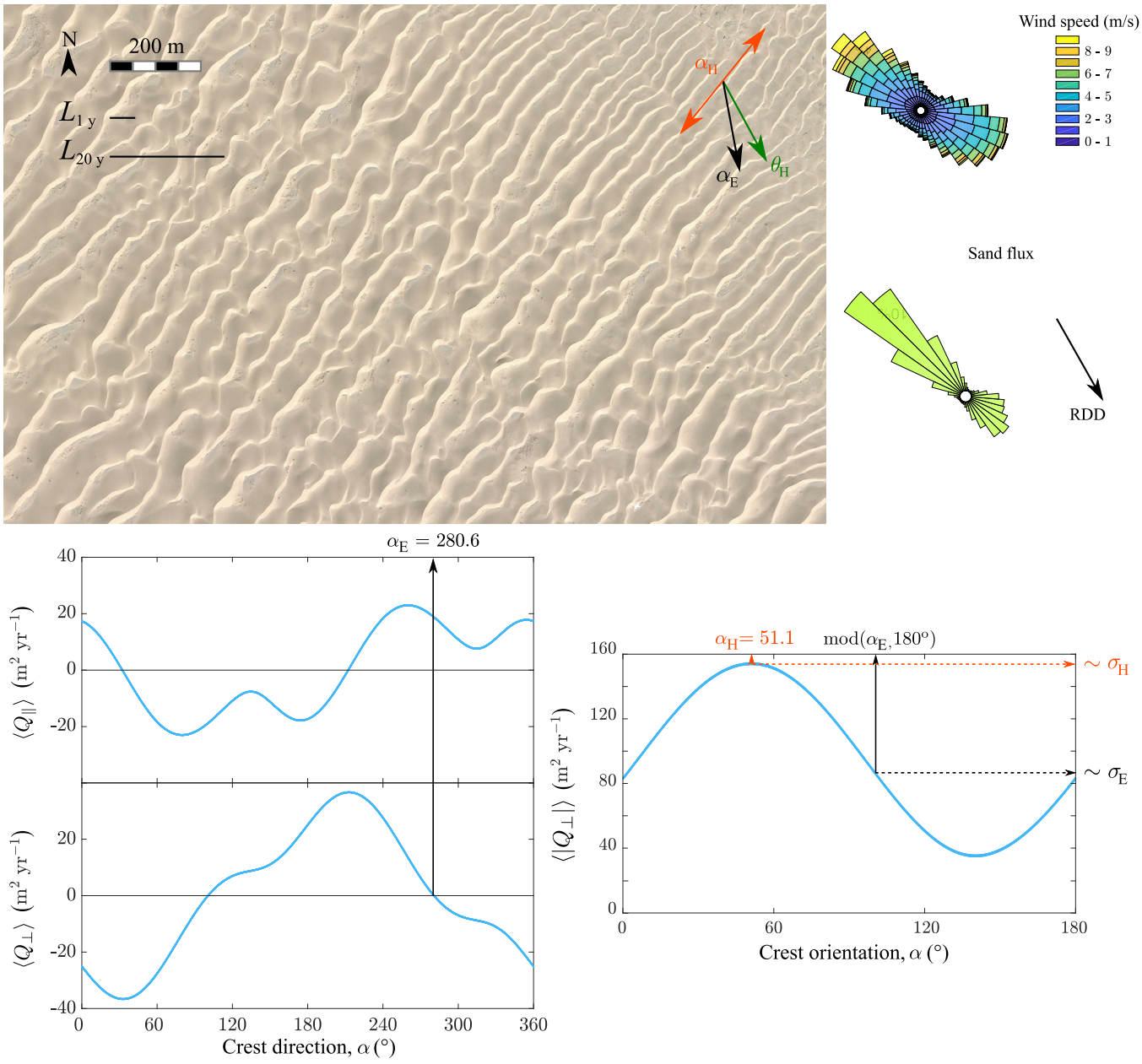


**Fig. 13.** Oblique long-crested dunes in the Tengger Desert in China (37.7°N, 105.1°E), date: 03/2009, credit: Maxar Technologies. See caption of Fig. 12 for an explanation of parameters and plots.

can generate barchan dunes. For example, barchans can be emitted from the tip of a lee dune as shown in Fig. 17. Here, in contrast to the isolated longitudinal dune shown in Fig. 15, the lee dune does not extend far behind the cliff and has a much smaller aspect ratio (length to width). In this region the wind is unidirectional ($\sigma_E/\sigma_H = 0.24$), such that dunes cannot elongate and a localized source of sand generates a train of barchans (Gao et al., 2015). The lee dune is a localized sand source for the formation of barchans, but here, unlike for the isolated longitudinal dune shown in Fig. 15 where the dune is coupled to the localized sand source, this boundary condition neither controls dune type, nor does it affect the shape and dynamics of the barchan dunes (other than their spatial organization).

*Towards complex patterns.* The recognizable shape and ubiquity of barchan dunes on Earth and Mars have made them a popular subject of study, so much so that models have been developed to explain 'seif dunes', *i.e.*, isolated longitudinal (or oblique) linear dunes on a starved bed, as morphological evolutions of this elemental dune (Bagnold, 1941; Tsoar, 1984; Tsoar and Parteli, 2016; Lv et al., 2016). This approach is certainly partly motivated by the widespread observation of asymmetric barchans with an elongated arm. Four causes for barchan asymmetry have been identified (Bourke, 2010; Parteli et al., 2014; Zhang et al., 2018): dune collision, asymmetry of influx, inclined topography, and bidirectional winds. The autogenic processes of dune collision and asymmetry of influx are very common in barchan dune fields (Elbelrhiti et al., 2008; Génois et al., 2013a) but only cause transitional dune asymmetry, localized in space and time. Along the Skeleton coast of Namibia, asymmetric barchans always have an elongated arm on the same side, which is ascribed to the bidirectional sand flux regime (Fig. 18). All the dunes above a certain size display an elongated arm, which is not the case for the smaller barchans. This might be because smaller dunes are not large enough to integrate the entire period of

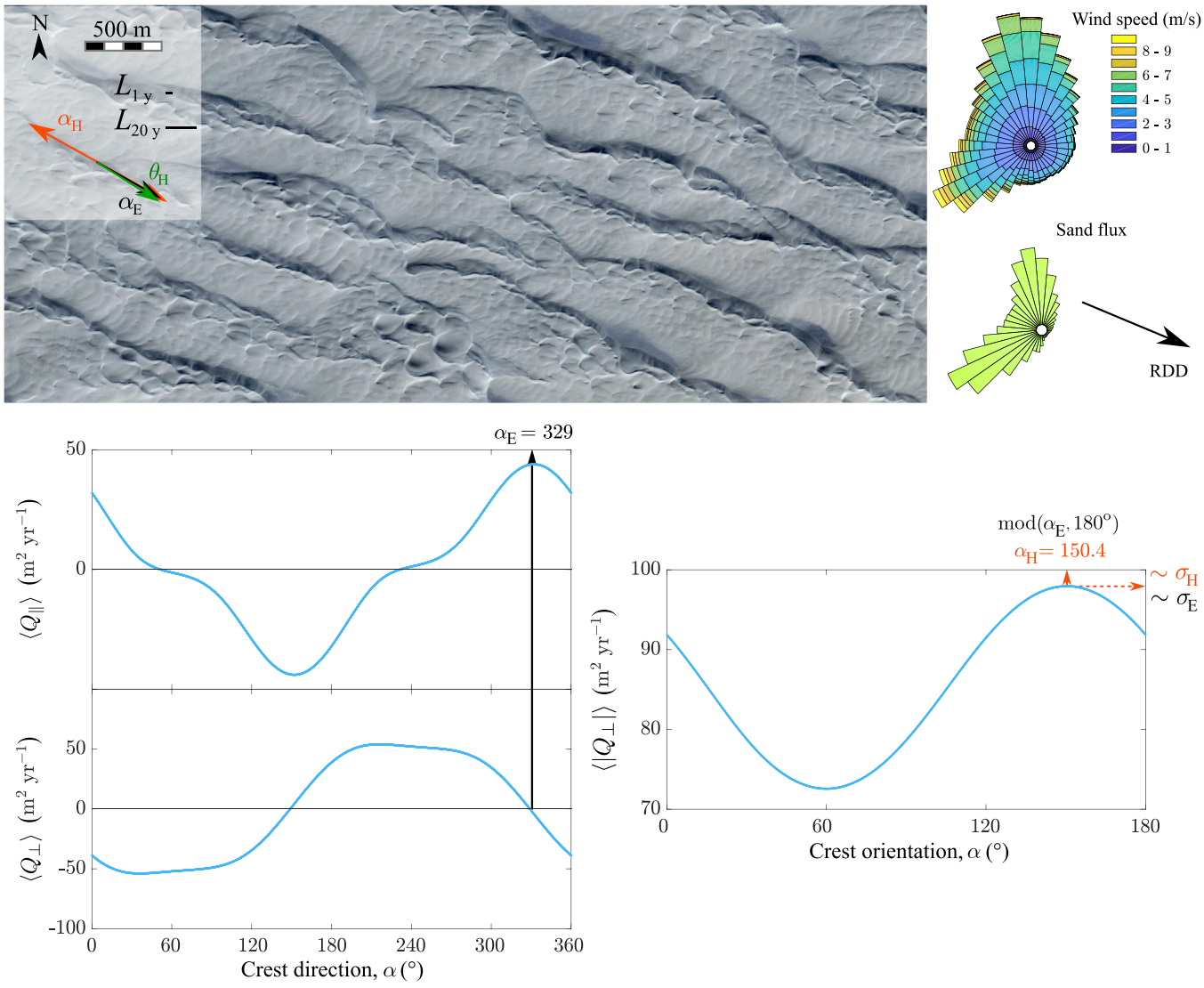


**Fig. 14.** Longitudinal long-crested dunes on sand-covered bed in the northern Sinai in Egypt (30.8°N, 33.1°E), date: 12/2010, credit: Maxar Technologies. See caption of Fig. 12 for an explanation of parameters and plots.

wind reorientation, as observed in a field experiment reported in Lü et al. (2022). Note that the characteristic length $L_{1\,yr}$ is a good estimate of dunes size at the transition. In this bidirectional regime of sand flux, the direction of sand flux for a dune that maximizes growth in height, $\theta_H$, does not correspond to the direction of migration, $\theta_M$. Here, the two directions differ by 9°, compared to 0.2° in the symmetric barchans example (Fig. 17). We believe this small difference drives an asymmetric sand redistribution between the two arms, which in this case leads to the elongation of the arm that is fed by the crest-parallel component of sand flux. In this example, the ratio $\hat{Q}_{\parallel/\perp,H}$ equals 0.15, which is significantly larger than the value for the symmetric barchans example (0.004, Fig. 17). Such asymmetric barchans with an elongated arm can also be seen as combinations of a migrating dune and an elongating dune at different scales. The barchan dune (large scale) has little sediment supply but is a source of sand for the elongated arm (smaller scale). As a result of dune migration, the orientation of the elongated arm is further away from the direction of migration than would be the case for elongation without migration (here the "source" is mobile). Conversely, an elongating dune can be seen as an extremely asymmetric barchan, whose crescentic base is prevented from migrating. This picture is supported for example by the dune termination of one of the large linear longitudinal dunes on a partially starved bed observed in the bottom right corner of Fig. 16. The ratio $\hat{Q}_{\parallel/\perp,H}$ increases consistently with dune asymmetry in the three examples of symmetric barchans, asymmetric barchans, and large longitudinal linear dunes.

Asymmetric barchans are isolated structures, which clearly exemplify a coexistence of the different formative processes. Meanwhile, most sand seas exhibit complex dune patterns that may also result from such a coexistence. 'Raked linear dunes', such as those shown in Fig. 19, are another example of this coexistence. These dunes, which lie on an armored bed composed of coarse grains, have a constant orientation for considerable distances and a marked asymmetry between a periodic pattern of semi-crescentic structures on one side and a continuous slope on the other. This semi-crescentic periodic pattern has been described as resulting from the development of superimposed dunes that grow in height and migrate in the bed instability mode on a linear dune that elongates (Lü et al., 2017). The coexistence of these processes produces coupled primary and secondary patterns with similar height but with different shapes and orientations, which are oblique to each other. The orientation of primary linear ridges corresponds to the predicted orientation for dunes in the elongating mode, albeit $\sigma_E/\sigma_H$ has an intermediate value. The tri-directional transport regime also enables the

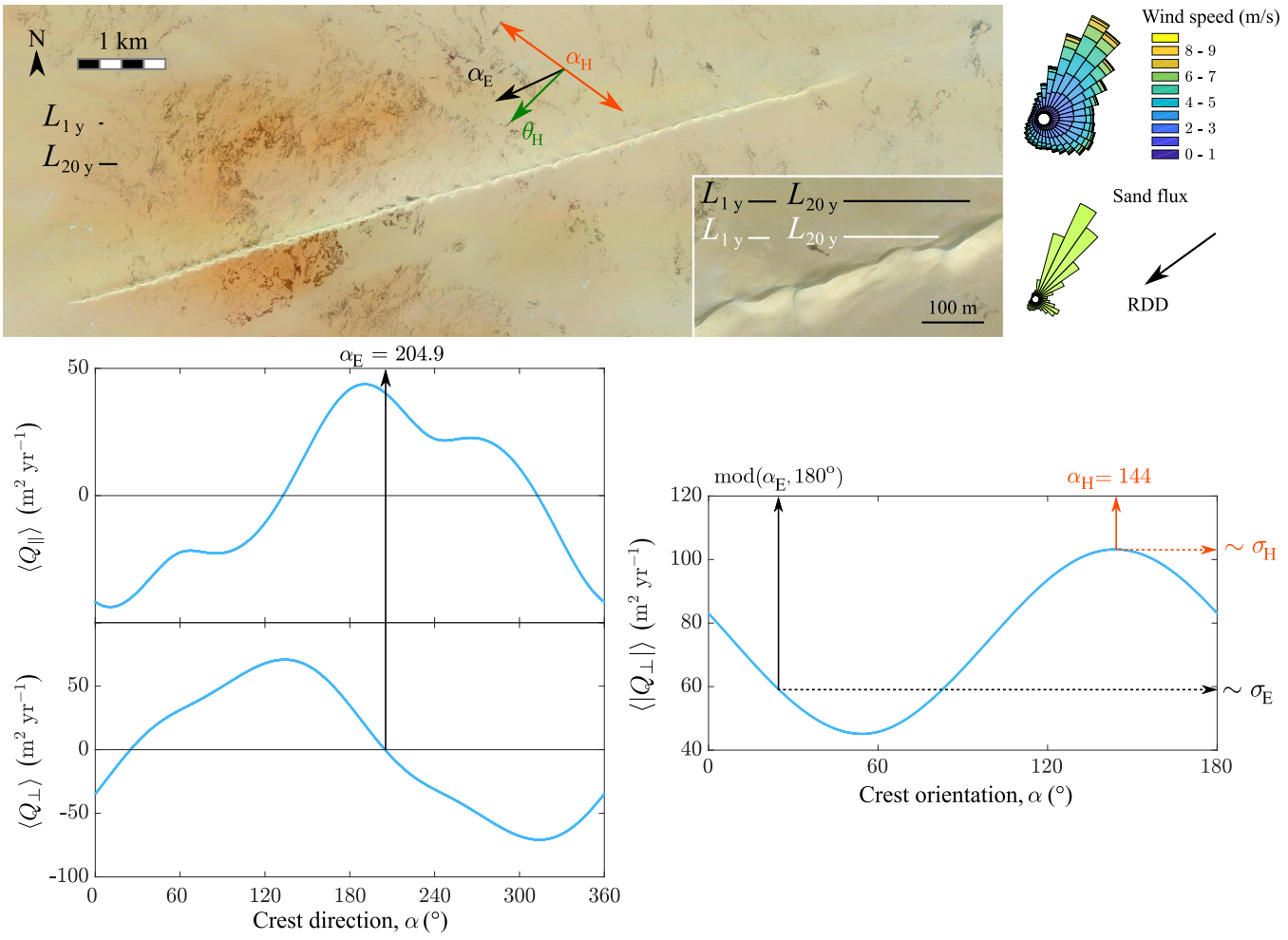


**Fig. 15.** Isolated oblique linear dune on a starved bed in the Ténéré in Niger (18.8°N, 12.5°E), date: 09/2013, credit: Maxar Technologies. It extends downwind from an obstacle. See caption of Fig. 12 for an explanation of parameters and plots. It is worth noting that the direction of elongation, $\alpha_E$, does not generally correspond to the direction for which sand flux along crest is maximum but to the one for which crest-normal component of sand flux vanishes (no migration) and crest-parallel component is positive. There, the derivative of the crest-normal component is negative, which makes the elongation direction a stable equilibrium (sand transport tends to rebalance the direction of the dune if it deviates from $\alpha_E$). Since the dune here is oriented in the direction of elongation, we also show (in white) the two characteristic lengths $L_{1\,yr} = \sqrt{2\,\langle |Q_{\perp}(\alpha_E)| \rangle \times 1\,yr/0.1}$ and $L_{20\,yr} = \sqrt{2\,\langle |Q_{\perp}(\alpha_E)| \rangle \times 20\,yr/0.1}$, which are calculated for a dune of orientation $\alpha_E$.

secondary raked pattern to develop on the leeward side of the primary linear ridges, in consistency with the predicted migration direction for dunes in the bed instability mode. Quantitatively predicting the occurrence of this pattern still remains challenging.

Finally, we examine an example of star dunes (Fig. 20), one of the most emblematic intricate dune patterns. In this example in the Namib Desert, the bed is partially starved and, starting from dune summits, we observe three main directions for the arms: (i) towards the northeast, (ii) the northwest, and (iii) the southeast. Star dunes should be observed in zones where the migration process is muted and where elongation and/or growth in height may be promoted in multiple directions. In this specific area, the ratio RDP/DP is close to zero so that dunes should barely migrate. The model shows three directions for elongation, which is made possible by taking into account the wind speed-up: towards the northeast ($\alpha_{E,1}$), the northwest ($\alpha_{E,2}$), and the southwest ($\alpha_{E,3}$). The predicted orientation for dunes that maximizes growth in height is close to the northwest direction of elongation, $\alpha_{E,2}$. For this direction of elongation, the ratio $\sigma_E/\sigma_H$ is close to one. This is clearly the prevalent crest orientation in the field. However, an orientation close to $\alpha_{E,1}$ is observed, although the ratio $\sigma_E/\sigma_H = 0.25$ is significantly smaller than the theoretical threshold value of 0.6. On the other hand, the predicted orientation $\alpha_{E,3}$ is not observed, whereas the ratio $\sigma_E/\sigma_H$ is larger (but still below the theoretical threshold value). Instead, we observe a direction towards the southeast, opposite to the other prevailing direction, which is towards the northwest. Both orientations could therefore correspond to the orientation that maximizes growth in height, which would be promoted by migration. We note that $\hat{Q}_{|\perp|/\perp,H}$ is much larger than any of the values of $\hat{Q}_{|\perp|/\|,E}$. Such a pattern with several orientations is still difficult to predict correctly. On the one hand, this could be partly due to the fact that this complex pattern is significantly different from the symmetric linear ridges assumed in calculations. On the other hand, for these massive dunes much larger than $L_{20\,yr}$, and especially at these latitudes close to horse latitudes, we cannot rule out the possibility that the winds that shaped them were significantly different from the modern winds we have considered (Gunn, 2023).

As demonstrated in the examples above, the proposed framework for dynamics-based dune classification appears promising. In most cases, it correctly predicts dune orientation. However, the definitive phase diagram of dune morphodynamics is still far from being developed, and the relevant parameters are only very partially determined. Such a comprehensive phase diagram requires a more exhaustive study than the few examples discussed here, for which we note that the values of the various dimensionless parameters are correlated. The

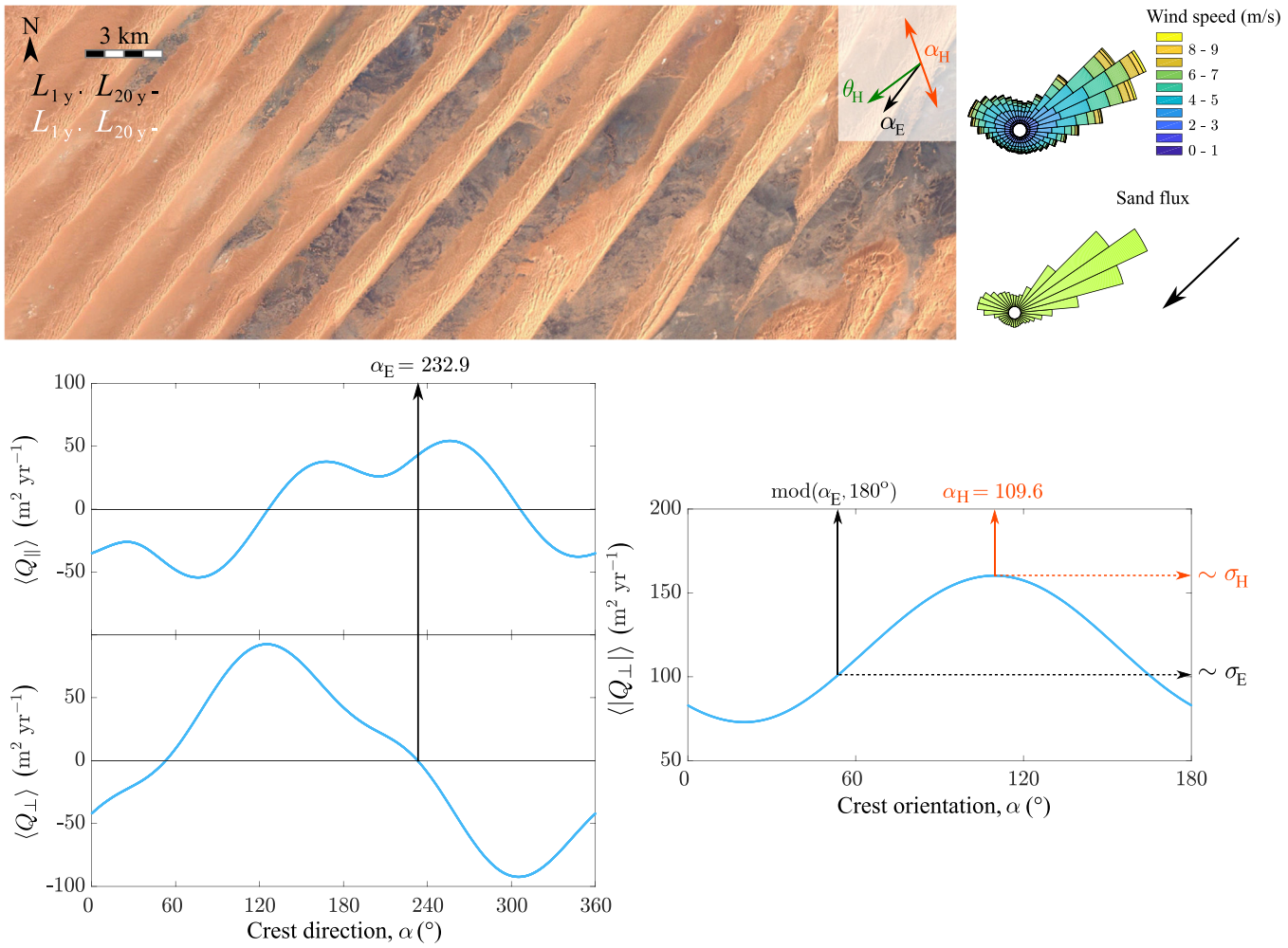


**Fig. 16.** Periodic longitudinal linear dunes with partially starved interdune area in the Chech Desert in Mali (24.3°N, 4.3°W), date: 12/2015, credit: Landsat/Copernicus. See caption of Figs. 12 and 15 for an explanation of parameters and plots.

model may also gain predictive power by further taking into account the coupling between dune morphology and sand transport. A first step could be to include the larger sand flux that occurs during crest reversals, as observed over the entire height of the elongated arm of the asymmetric barchan in the inset of Fig. 18. Such a refinement of sand flux calculations requires consideration of the variation of the upwind slope with the time series of wind directions.

### *5.3. Determining dune orientation relative to sand transport direction from morphology*

The preceding discussion considers classification of dunes and characterization of formative mechanisms where wind measurements or sand transport measurements are available. As discussed in Section 2.3.2, however, some dynamic properties can be inferred from dune observations without such measurements. The long-crested examples in Figs. 12–16, 19, and 21 can be used to test the approach of inferring dune orientation relative to the net transport direction based solely on morphology, as proposed in Table 2. In some of these examples dune morphology/asymmetry is unclear unless the image is rotated, so that the illumination comes from the top of the image. Except for Fig. 16 – in which the resolution is insufficient to determine the cross-sectional asymmetry of the main dunes and superimposed dunes – the examples are consistent with Table 2.

The dunes in Figs. 12 and 21 are known from wind measurements to be transverse dunes, and in both cases this interpretation is demonstrable from morphology alone. The main dunes are asymmetrical, and the superimposed lee-side spurs are approximately symmetrical in cross-section (the spurs lack a steep lee side and gentle stoss side), demonstrating a lack of systematic migration and net transport parallel to the crests of the main dunes.

The dunes in Fig. 13 are oblique to the resultant transport direction, and this can also be demonstrated from morphology. The main dunes have cross-sectional asymmetry indicating across-crest transport towards the southeast. Most of the dunes in the figure lack sufficient superimposed features to determine their migration direction, but the superimposed leeside spurs in the lower right corner of the image have slipfaces that preferentially dip in a direction parallel to the crests of the main dunes. This combination of across-crest transport and along-crest transport demonstrates obliquity of the main dunes, at least in this corner of the image.

Wind data show that the dunes in Figs. 14, 15, and 19 are longitudinal dunes, which also can be demonstrated from morphology alone. The main dunes are relatively symmetrical in cross-section, and the superimposed dunes (Figs. 14 and 19) or sinuosities (Fig. 15), have consistent asymmetric cross-sections, thereby demonstrating systematic transport in an along-crest direction over the main dunes. The steeper lee sides of the superimposed features indicate net transport parallel to the crests of the main dunes towards the east southeast in Fig. 14, and

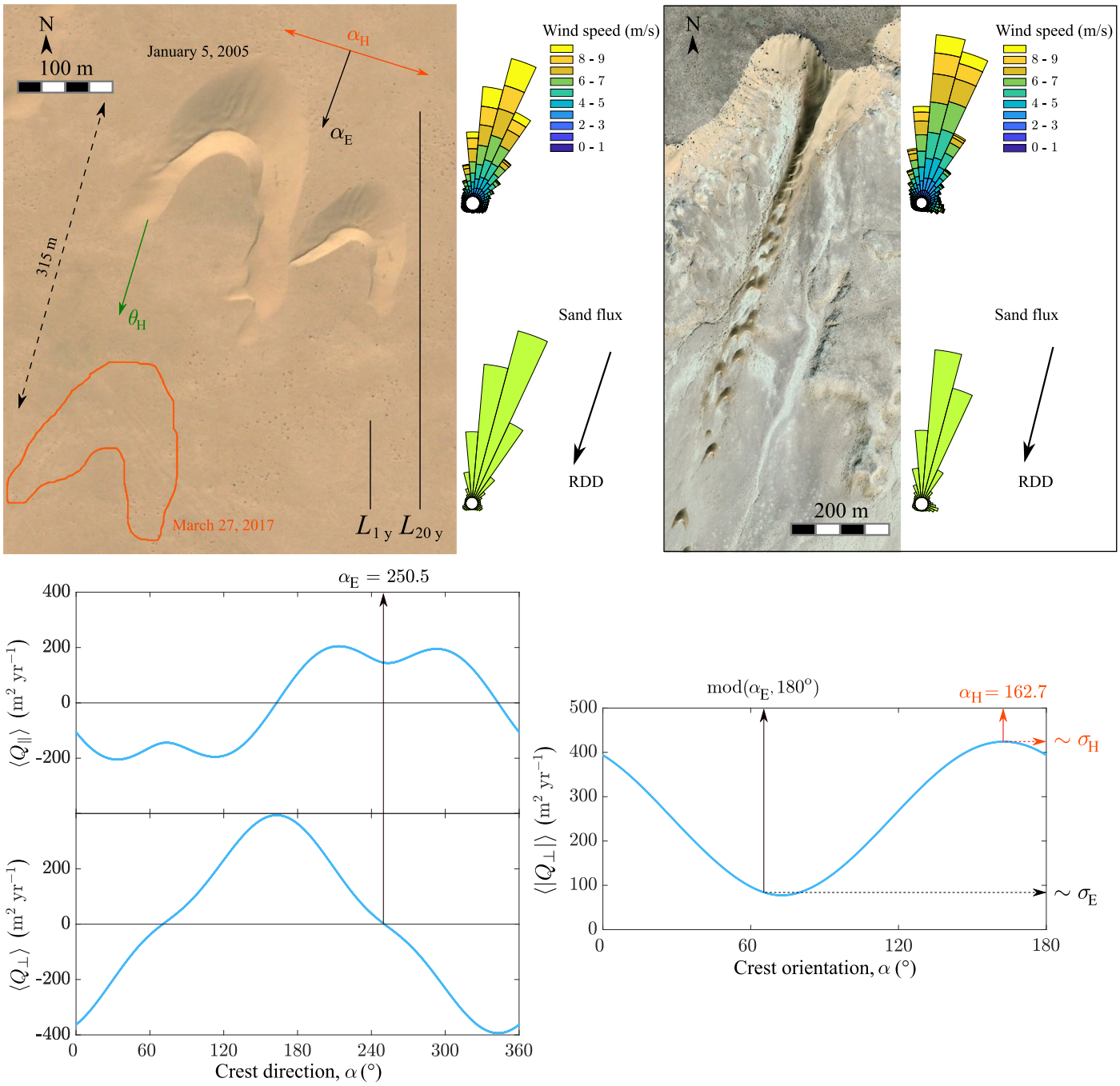


**Fig. 17.** Barchan dunes on a starved bed in Western Sahara in Morocco (27.5°N, 13.1°W), date: 01/2005, credit: Maxar Technologies. The red contour shows location of the main barchan 12 years after the snapshot was taken. Inset: Train of barchan dunes downwind of a lee dune attached to a cliff further south in Western Sahara (27°N, 12.9°W), date: 11/2018, credit: CNES/Airbus. See caption of Fig. 12 for an explanation of parameters and plots.

towards the west southwest in Fig. 15. In Fig. 19, the superimposed features resemble half-barchans migrating southwest along the lengths of the main dunes (Lü et al., 2017).

In summary, the migration directions superimposed topographic features relative to the main dunes can be used to determine whether the main dunes are transverse, oblique, or longitudinal and similarly to constrain the direction of net sand transport relative to the dunes. These inferences are qualitative and do not necessarily match the quantitative definition of Hunter et al. (1983). Nevertheless, this approach may be useful in interpretations of dunes where wind data or measurements of sand transport or dune migration are not available. This is often the case for other planets and is always the case for interpreting deposits of dunes in the stratigraphic record, the purpose for which this approach was initially developed (as discussed in Section 2.3.2).

### *5.4. Expected dune sizes in the solar system from fluid and sediment-transport mechanics*

As environmental and boundary conditions significantly vary from one planetary body to another, dunes on their surfaces sample the different formation regimes.

On Earth, typical grain sizes are about 200 μm, such that the thickness of the saltation layer is of the order of $20\,d \simeq 4$ mm (Valance

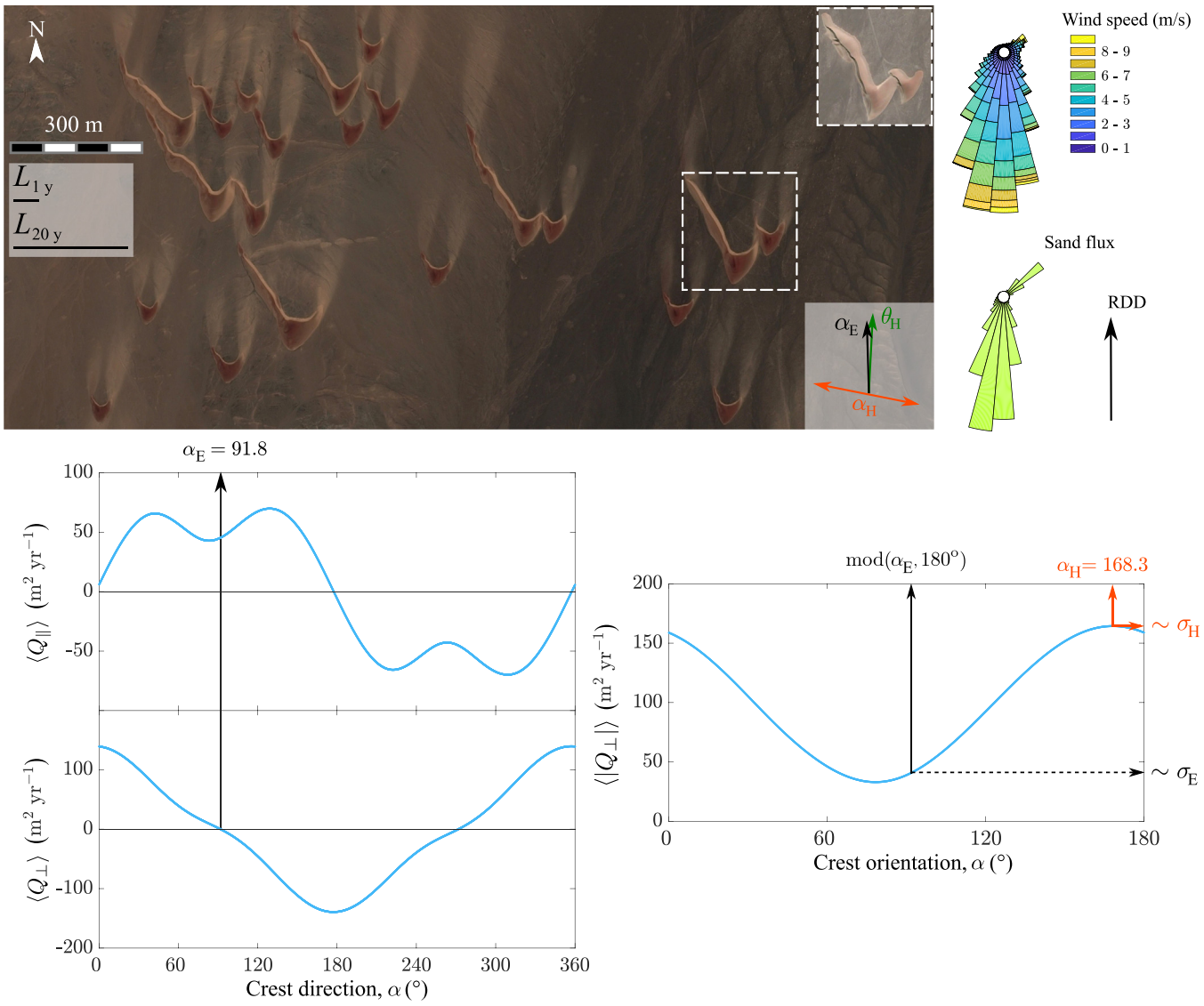


**Fig. 18.** Asymmetric barchan dunes with an elongated horn on a starved bed on the Skeleton Coast in Namibia (20.1°S, 13.3°E), date: 03/2013, credit: CNES/Airbus. The inset shows the dunes in the white dashed box after a secondary wind event (date: 06/2003). See caption of Fig. 12 for an explanation of parameters and plots.

et al., 2015). The height of aeolian impact ripples that mantle the surface of sand dunes is of similar, millimeter-scale. For an aerodynamic roughness, $r$, of that scale, and a typical shear velocity of the order of 0.4 m/s, one finds $\mathcal{R}_r \simeq 100$ (with $\nu = 1.5 \times 10^{-5}$ m$^2$/s), indicating that terrestrial saltation occurs in the rough regime. A smooth regime could possibly be observed for smaller grains and weak winds just above the transport threshold, for example. The typical value of the density ratio on Earth is $s \simeq 2200$ for quartz grains ($\rho_s \simeq 2650\,\mathrm{kg/m^3}$) and air ($\rho_f \simeq 1.2\,\mathrm{kg/m^3}$), which justifies the use of the transport law given in Eq. (2). The typical saturation length measured on Earth is of the order of 1 m, which yields a minimum dune wavelength in the order of 10 m, consistent with observations in nature (Gadal et al., 2020a; Delorme et al., 2020) and in a landscape-scale field experiment (Lü et al., 2021).

Fig. 21 illustrates dunes forming in the aerodynamically rough regime, showing a coastal dune field in southwest Angola. The environment there closely matches the assumptions behind our classification, with a fairly unidirectional wind blowing over a loose sand bed. Incipient dunes form with a scale $\lambda_{min} \simeq 20$ m. Then, dunes coarsen as evidenced by a range of dune sizes, and display a consistent large-scale wavelength of the dune pattern, $\lambda_{max} \simeq 850$ m. There, using ERA5-Land reanalysis data based on global atmospheric models (Muñoz-Sabater et al., 2021), the thickness of ABL, $\Lambda$, is directly calculated as 300 m, or as 2 km using the same proxy as in Andreotti et al. (2009).

For the low-pressure (*i.e.*, low-density, $\rho_f \simeq 0.02\,\mathrm{kg/m^3}$) atmosphere of Mars, atmospheric kinematic viscosity is larger than on Earth, $\nu \simeq 10^{-3}$ m$^2$/s and although uncertain, typical shear velocities are thought to be of the order of $u_* \simeq 1$ m/s (Lapôtre et al., 2016; Durán Vinent et al., 2019; Andreotti et al., 2021) so that $\mathcal{R}_r \sim 1$ for a millimeter-scale aerodynamic roughness. As a result, saltation occurs under an aerodynamically smooth regime on Mars, and two distinct ranges of dune sizes are expected if the ratio between the saturation length and the viscous length is smaller than about 1000. Saturation length has not been measured on Mars to date. With a larger density ratio than on Earth ($s \simeq 1.5{\times}10^5$ for basalt grains, $\rho_s \simeq 3000\,\mathrm{kg/m^3}$), some models also predict a larger saturation length on Mars than on Earth (Pähtz et al., 2013). Two distinct scales of bedforms larger than impact ripples are observed in monodisperse sand on Mars, as shown in Fig. 22. Meter-scale ripples (distinct from smaller, decimeter-scale impact ripples) migrate on top of large hundred-meter-scale dunes (Lapôtre et al., 2016; Ewing et al., 2017; Lapôtre et al., 2018; Lapôtre et al., 2021). In that sense, large martian ripples and dunes are analogous to ripples superimposed on dunes in a subaqueous environment (Lapôtre et al., 2016, 2017; Durán Vinent et al., 2019), where a smooth regime

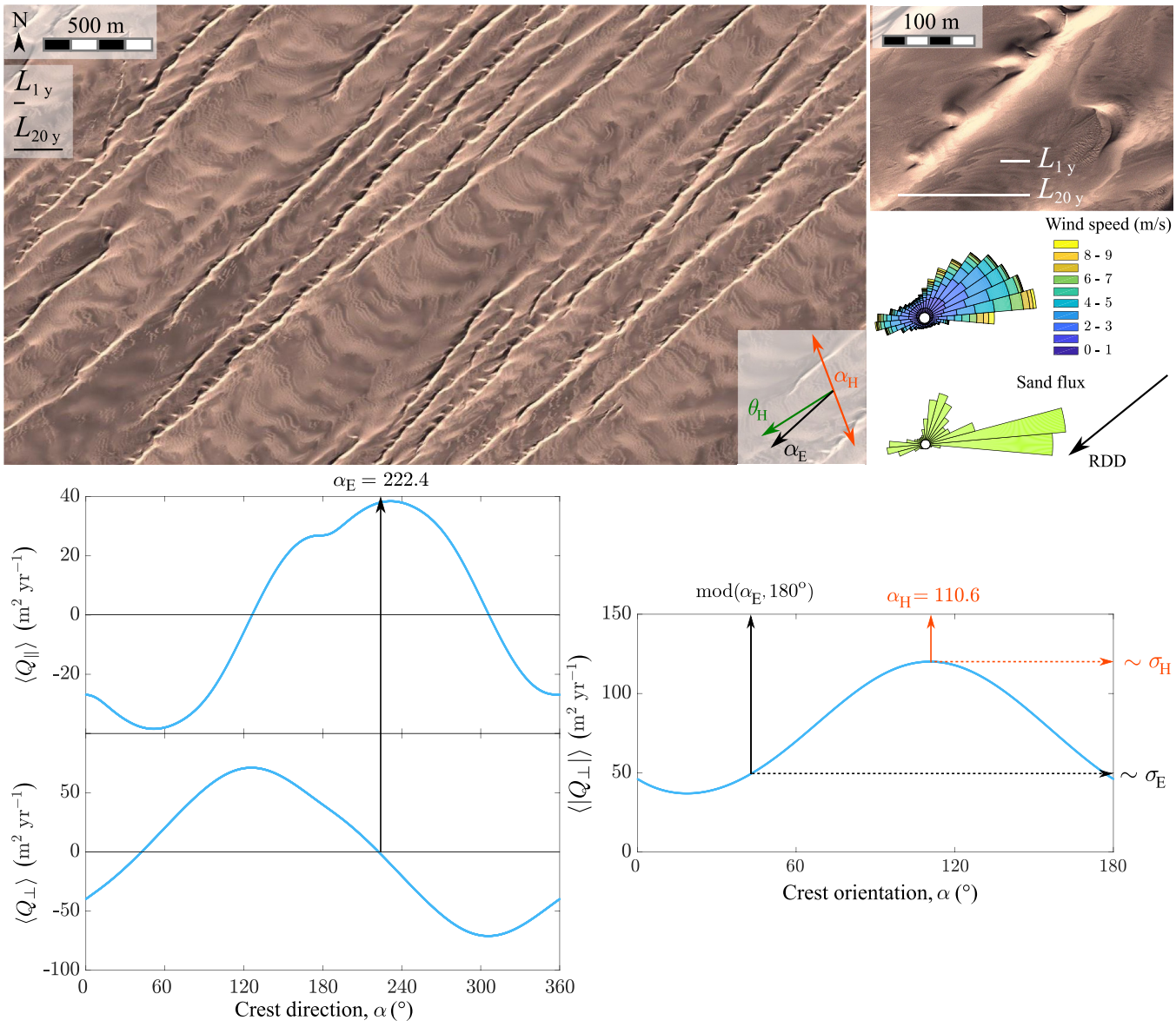


**Fig. 19.** Raked linear dunes on an armored bed of coarse grains in Kumtagh Desert in China (40.2°N, 92.2°E), date: 01/2014, credit: Maxar Technologies. See caption of Figs. 12 and 15 for an explanation of parameters and plots.

is expected as well. An alternative interpretation was proposed for these meter-scale ripples, under which they would simply be large impact ripples, growing to meter-scale wavelengths from their initial, decimeter-scale wavelengths (Sullivan et al., 2020). However, that model cannot explain the absence of bedforms with wavelengths in the ~20–80 cm range in relatively well sorted sand (Lapôtre et al., 2021). Furthermore, the observed gap in bedform wavelengths between a large ripples and Mars' smallest dunes ($\lambda \sim 80$ m) matches the predictions of the Hanratty anomaly (Rubanenko et al., 2022).

Dune formation regimes, and thus dune scales, on other planetary bodies remain highly uncertain (owing, *e.g.*, to large uncertainties in the materials that make up dune sand). On Titan, grains have been proposed to be made of complex hydrocarbons, water ice, or a combination of both; a density of $\rho_s \simeq 1000\,\mathrm{kg/m^3}$ was proposed for porous organics that would form from a photochemical haze (Yu et al., 2018). Although many uncertainties remain, a value of $s \simeq 200$ seems reasonable given current knowledge. For $u_* \simeq 0.1$ m/s, $\nu \simeq 10^{-6}$ m$^2$/s, and $r \simeq 10^{-3}$ m (Rodriguez et al., 2018), one finds that $\mathscr{R}_r \simeq 100$, indicating that dunes on Titan would form under an aerodynamically rough regime, similar to terrestrial dunes. Linear dunes on Titan are observed around the equatorial region with a kilometer-scale, similar in scale to large linear dunes found on Earth (Lorenz et al., 2006). Finally, on Venus, we consider the case of $u_* \simeq 5 \times 10^{-2}$ m/s, $\nu \simeq 5 \times 10^{-7}$ m$^2$/s, and $r \simeq 10^{-4}$ m (Greeley et al., 1984), such that $\mathscr{R}_r \simeq 10$, *i.e.*, a value near the upper bound of the smooth regime.

## 6. Conclusion

Dunes are common landforms throughout the solar system, and they can teach us about past and current environmental conditions on Earth as well as on a variety of planetary bodies including Venus, Mars, Titan, and Pluto. Building a fundamental understanding of dune morphodynamics as well as predictive capabilities and mitigation strategies will require scientific collaboration across traditional field boundaries, and thus, a common language to describe sand dunes. Here, we synthesized existing terminology and distilled it into three independent but complementary dune classification schemes. First, we proposed a unifying description of dunes based on their morphology. This classification

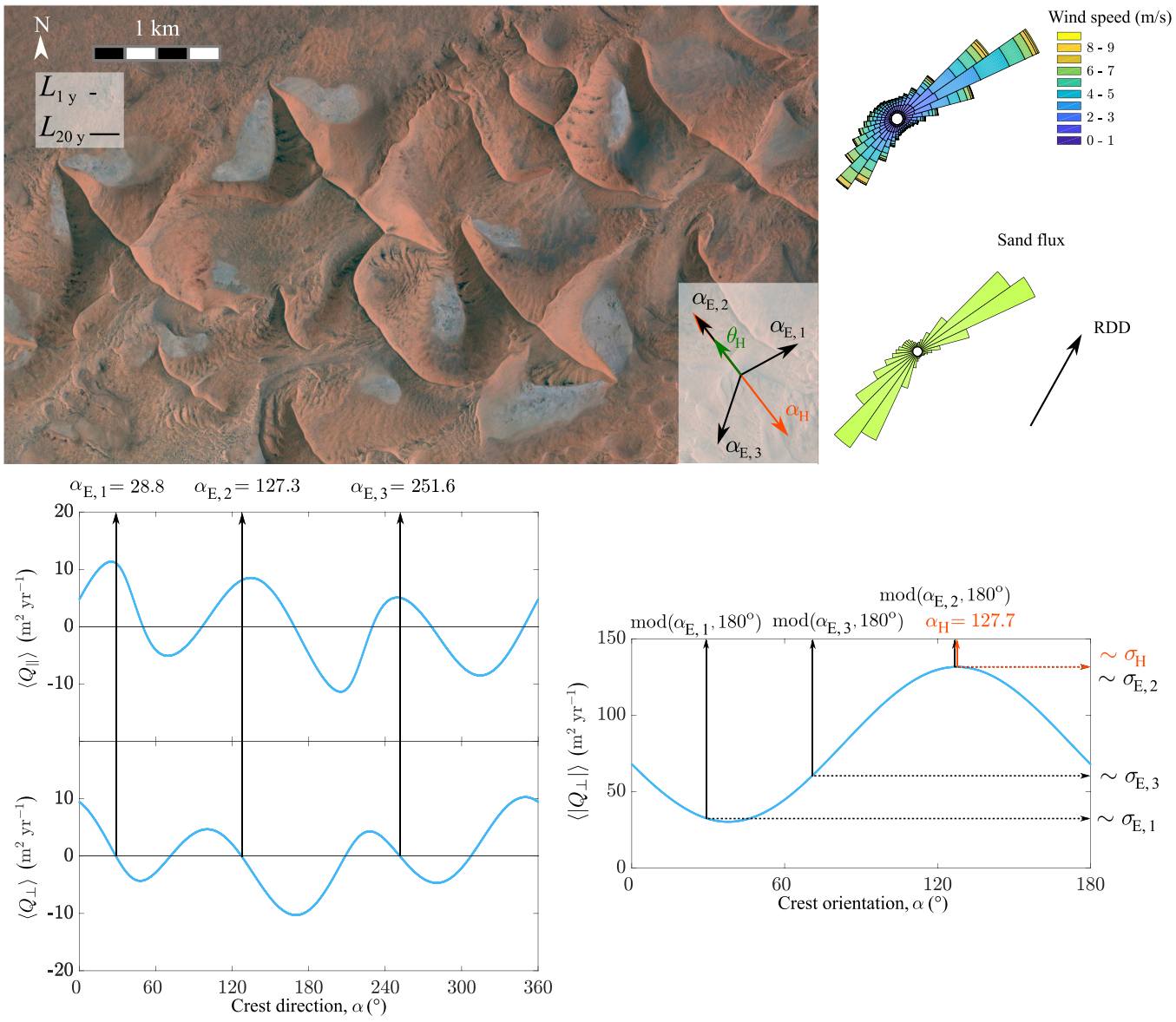


**Fig. 20.** Star dunes on a partially starved bed in the Namib Desert in Namibia (26°S, 15.9°E), date: 12/2010, credit: Maxar Technologies. See caption of Fig. 12 for an explanation of parameters and plots.

builds on a long legacy of existing terminology and solely requires observations of dune shapes as can be gathered from the ground, or from aerial or satellite imagery. Terminology can be further refined within that classification scheme when information about winds and dune migration is available. Second, we synthesized state-of-the-art models for dune morphodynamics, tying specific morphologic types with their formative dynamics as selected by wind regimes and boundary conditions. Third, we presented a classification of the various fluid dynamics regimes under which dunes may form, leading to different controls on initial and equilibrium dune sizes. This last scheme was developed for transverse dunes only, and encapsulates the complexity of variable boundary and environmental conditions that may be found across planetary bodies of the solar system. Together, these three classification schemes allow for variable levels of descriptive detail depending on available data, and encompass dune shape, dynamics, and scale as linked to their environmental conditions. Importantly, they offer a complete and unified framework, anchored in the mechanics of dune formation, for future studies to describe dunes on Earth and other planets.

## Declaration of competing interest

The authors declare that they have no known competing financial interests or personal relationships that could have appeared to influence the work reported in this paper.

## Data availability

Data will be made available on request.

## Acknowledgments

This work began during a funded workshop at the Fondation des Treilles (www.les-treilles.com), a wonderful place in the south of France for scientific exchange, creativity, and reflection. The authors are grateful to their collaborators who have contributed to the work reviewed in this paper over the years. SCdP and CN would like to thank Stéphane Douady, Xin Gao, Mathieu Génois, Ping Lü, Antoine Lucas, Erwan Reffet, Sébastien Rodriguez, Olivier Rozier, and Deguo Zhang.

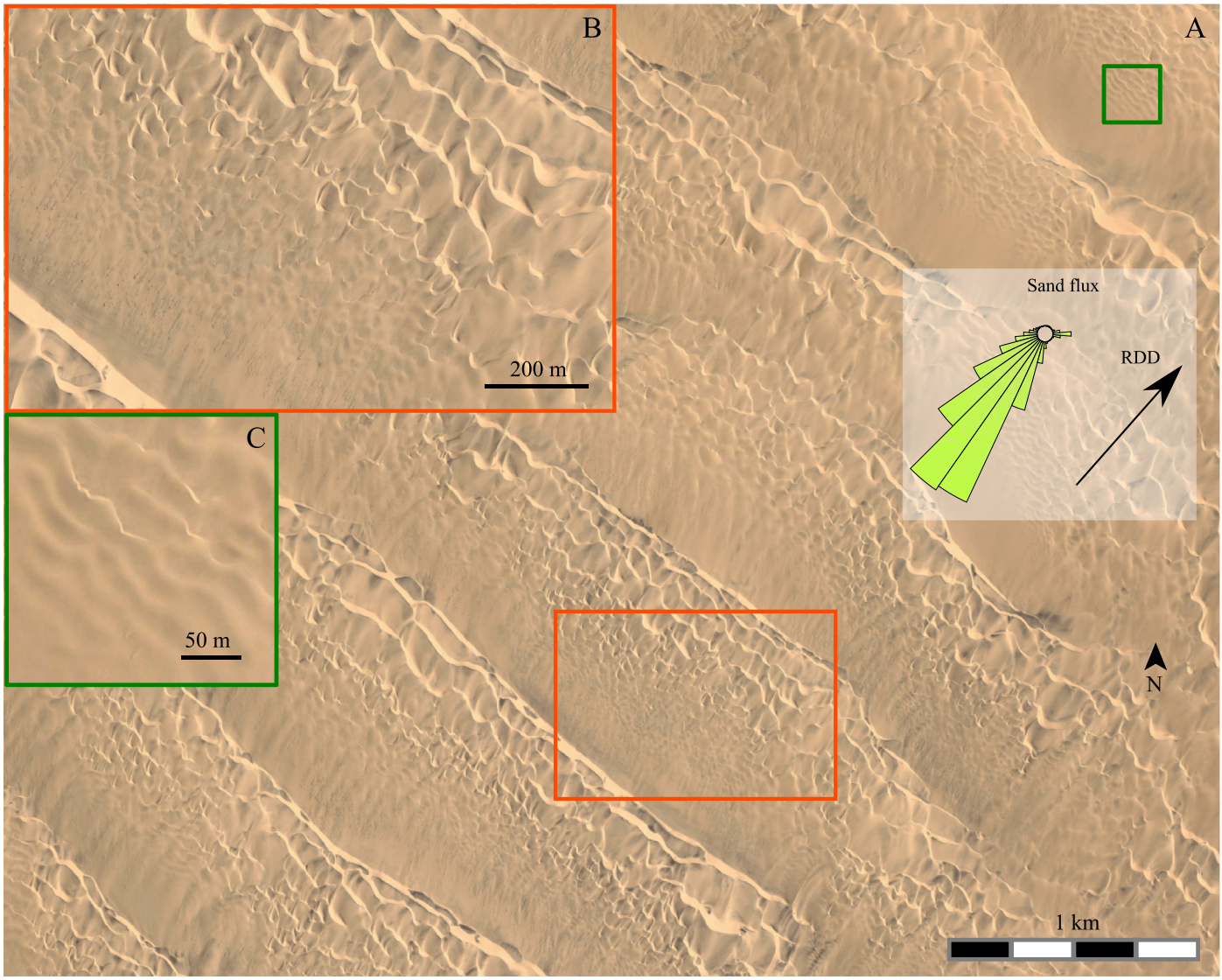


**Fig. 21.** Illustration of the rough case with terrestrial dunes ($\mathscr{R}_r \simeq 100$). Photographs of a coastal dune field in southwest Angola (16.4°S, 11.9°E), date: 03/2004, credit: Maxar Technologies. The parameters for calculating the sand flux distribution from wind data are the same as in Figs. 12–20 (Appendix). The spokes point upwind. Local winds are approximately unidirectional (see flux rose), and the dunes, with fairly straight crests perpendicular to the resultant drift direction (RDD), can be denominated as 'linear transverse'. Sand availability is high (no cohesive interdune). The dunes form at the elementary scale $\lambda_{min} \simeq 20$ m (panel C, green frame), interact and coarsen in the course of their migration downwind (panel B, red frame) and the large-scale dune pattern has a wavelength $\lambda_{max} \simeq 850$ m (panel A).

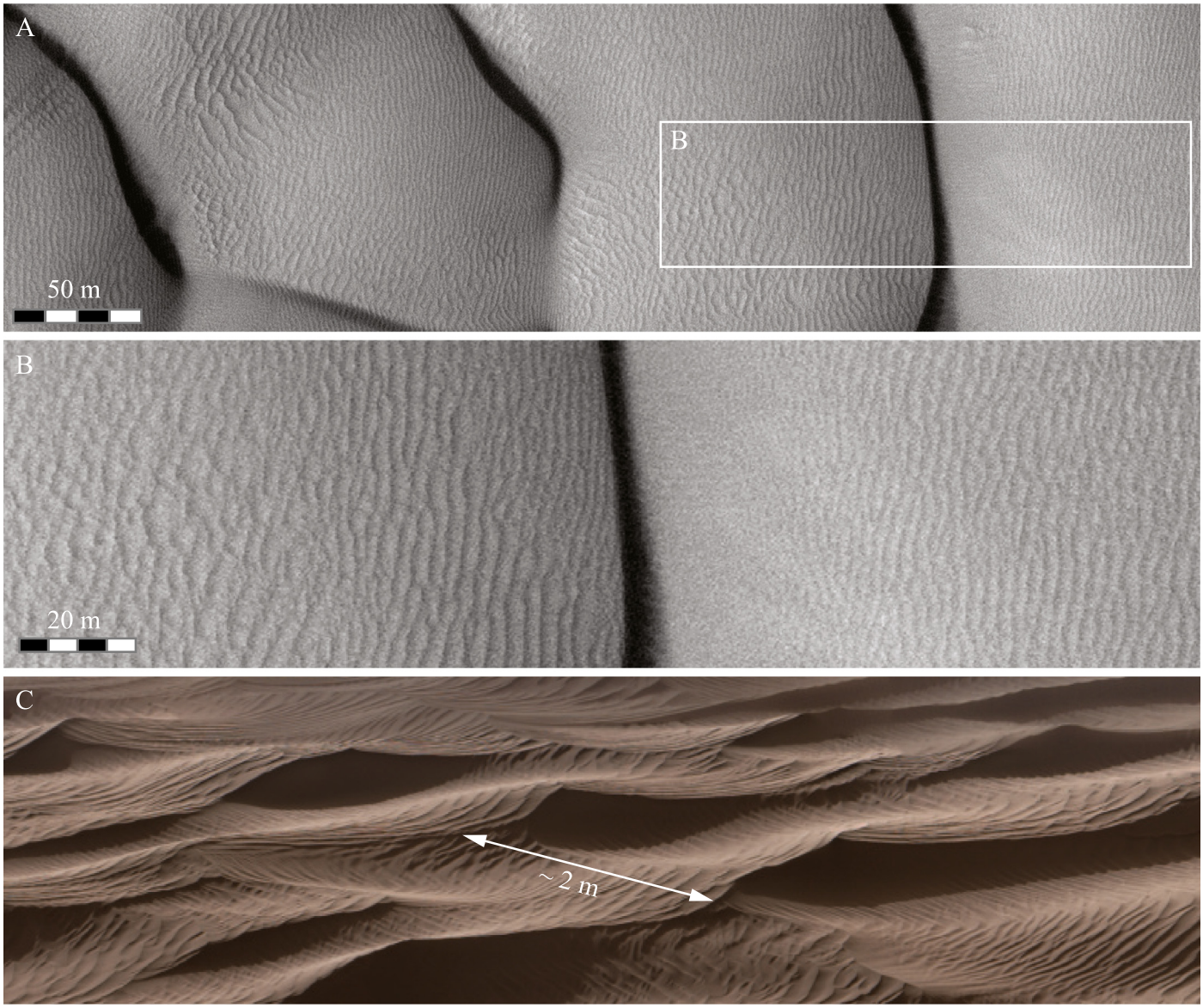


**Fig. 22.** Illustration of dunes forming under aerodynamically smooth conditions, showing large martian ripples and dunes ($\mathscr{R}_r \simeq 1$). Dunes in Lyot (A, B) and Gale (C) craters. Martian bedforms display distinct scales. Dunes with hundred-meter-scale wavelengths (A) are mantled with meter-scale ripples (B). No bedforms with wavelengths between those two scales are observed. A closer look at a dune's surface with the Curiosity rover (here on 'Namib dune' within the Bagnold Dune Field) reveals smaller decimeter-scale bedforms, construed as impact ripples migrating on top of large ripples. Credit: (A–B), HiRISE image ESP_017605_2295; (C), NASA/JPL-Caltech/MSSS/Thomas Appere.

PC would like to thank Bruno Andreotti, François Charru, Orencio Durán, Pan Jia, and Michel Louge. DR acknowledges Ralph Hunter for discussions on the topics in this paper, beginning 40 years ago. Naïs Coq (plectoneme@proton.me) did the graphic design of classification figures. We thank editors Timothy James Horscroft and Christopher Fielding, and two anonymous reviewers, whose comments improved our manuscript. AG acknowledges funding from the Australian Research Council through grant #DE240100552. CN acknowledges funding from Initiative d'Excellence Université Paris Cité through grant ANR-18-IDEX-0001, and the French National Research Agency through grant ANR-23-CE56-0008.

## Appendix. Concepts, models and methods

### *A.1. Dune size and timescale of wind-regime integration*

We define the dune length scale as the square root of the dune cross-section, $\sqrt{HL/2}$, where $H$ and $L$ are the dune height and length, respectively. This assumes a triangular dune profile. To this dune size is associated a time scale $HL/(2Q)$ called the *dune turnover time*, which is the characteristic time to completely reshape the dune with a sand flux of magnitude $Q$ (Bagnold, 1941). $Q$ is a volumetric flux per unit width (*i.e.*, it has the dimension of a length squared per time) and takes into account dune compactness. This timescale sets the time duration over which one should consider the wind regime so that the dune integrates the whole complexity of the wind regime and is in a dynamical equilibrium over the considered period of time. A complex wind regime consists in a succession of wind events with different directions and strengths. We consider a wind sequence of duration $\tau_i$ between two significant changes of sand flux direction. The different wind sequences may repeat periodically, defining a wind regime. On the one hand, the dune integrates the wind regime if none of individual wind sequence completely reshapes the dune (Rubin and Ikeda, 1990). On the other hand, one can expect that the dune has reached a dynamical equilibrium if the full considered period of time, $\tau_{tot}$, is long enough to shape the dune. Thus, the size of the dune sets

the period of time to consider (and vice versa) such that

$$\int_{\tau_i} Q(t)dt \ll HL/2 \leqslant \int_{\tau_{tot}} Q(t)dt. \quad (1)$$

The boundary conditions should also not significantly change over the considered period of time. Note that Eq. (1) does not take into account the direction of the sand flux because two winds with opposite directions contribute to build dunes. In principle, only the component of fluxes in line with the cross-section should be considered. In practice, it is difficult to obtain wind data for longer than the time required to build very large dunes. Shorter periods may be appropriate, but the duration should not be less than one period of the wind regime. Considering a shorter time period also enables to study whether the wind regime has changed (Warren and Allison, 1998; Kocurek and Ewing, 2005; Gunn, 2023). The integral of the sand flux over a period of time $T$, $\int_T Q(t)dt$, where $T$ is the duration of the wind cycle (one year on Earth), also defines the characteristic minimum cross-sectional area of dunes that integrates the wind regime. This concept of turnover time is derived from dimensional analysis and has never been systematically studied. It only sets a time scale as in principle, a dune can be fully reshaped without having to move all the sand it contains (Rubin and McCulloch, 1980).

### A.2. Sediment transport

#### A.2.1. Characterization of aeolian sediment transport

Sediment transport is coupled to fluid flow in the transport layer. It is characterized by a threshold (minimum) shear velocity (or basal shear stress), a saturated (maximum) sediment flux in steady state, the saturated flux, and a saturation length (Kroy et al., 2002). The saturation length corresponds to the spatial lag of the response of flux to a change in transport conditions, *i.e.*, how far downwind from a change in transport conditions (such as an increase of wind velocity) the sediment flux equilibrates with the new conditions. Three main parameters control sediment transport and saltation in particular.

First, the particle-to-fluid density ratio, $s = \rho_s/\rho_f$, encapsulates the reduced weight of particles in the fluid. Second, a commonly used parameter is the Shields number, $\Theta = u_*^2/[(s-1)gd]$ (where $u_*$, $g$, and $d$ are the wind shear velocity, the gravitational acceleration, and the grains diameter, respectively), which allows for comparisons of the basal shear stress on grains ($\rho_f u_*^2$) relative to the grains' apparent weight per unit of surface ($\sim (\rho_s - \rho_f)gd$). Third, the Galileo number, $\mathcal{G} = \sqrt{(s-1)gd^3}/\nu$ (where $\nu$ is the fluid viscosity), can be envisioned as the ratio of gravitational and viscous effects. It is the square root of a Reynolds number in which the length scale is taken as the grain size and the velocity scale as the Stokes limit of the grains' settling velocity. This parameter is useful to compare different environments regardless of flow velocity.

The dynamic threshold for sediment transport is defined by the minimum shear stress exerted by the fluid on the granular bed that can sustain transport in saltation. It is associated to a critical value of the Shields number, $\Theta_t$. $\Theta_t$ varies with grain and flow properties, and is typically expressed as a function of grain size and apparent density or equivalent dimensionless parameters such as $\mathcal{G}$ and $s$ (Chepil, 1945; Greeley et al., 1980; Swann et al., 2020; Pähtz and Durán, 2020; Andreotti et al., 2021).

The saturated sand flux at steady state, $Q_{sat}$, is proportional to the difference between the actual Shields number and its critical value. Such transport laws (*e.g.*, Eq. (2)) are valid for saltation transport over a loose sand bed, when $s \gtrsim 100$. Under such conditions, the velocity of grains in saltation is independent of wind shear velocity, $u_*$, due to coupling between the wind flow and sediment transport (Fig. 13 in Durán et al., 2012). If transport laws are fairly well established and calibrated in steady and homogeneous conditions (Bagnold, 1941; Owen, 1964; Ungar and Haff, 1987; Rasmussen et al., 1996; Creyssels et al., 2009; Ho et al., 2011; Durán et al., 2012; Martin and Kok, 2017; Pähtz and Durán, 2020), threshold Shields numbers are much less constrained under extraterrestrial conditions, including on Mars (Andreotti et al., 2021; Gunn and Jerolmack, 2022).

Some experimental data are available for the saturation length, $L_{sat}$, under terrestrial saltation (with $L_{sat}$ typically between 0.5 and 1 m for sand grains in the range [100, 200 μm], Bagnold, 1941; Shao and Raupach, 1992; Andreotti et al., 2010; Selmani et al., 2018; Lü et al., 2021) as well as under subaqueous suspension (Claudin et al., 2011), but significant knowledge gaps remain (Pähtz et al., 2013, 2014, 2015; Pähtz and Durán, 2017) rendering predictions for saltation on Mars or Titan challenging. These knowledge gaps are particularly significant given that $L_{sat}$ is a key parameter in dune-instability analysis (Kroy et al., 2002; Charru et al., 2013). As the minimum length required to generate an effective coupling between the wind flow and sand transport, $L_{sat}$ sets the characteristic wavelength of incipient dunes in most cases (Fig. 8).

#### A.2.2. Transport law — Saturated sand flux and onset of transport

There are many transport laws, which are more or less phenomenological, each with their own validity regime (Valance et al., 2015). Here, we compute the saturated sand flux, $Q_{sat}$, (*i.e.*, maximum sand flux over a flat sand bed) using the relationship proposed in Durán et al. (2011) and Kok et al. (2012), such that

$$Q_{sat} = \begin{cases} a_q \dfrac{\rho_f}{\rho_s g} u_t \left(u_*^2 - u_t^2\right) \equiv a_q \dfrac{s-1}{s} d u_t \left(\Theta_*^2 - \Theta_t^2\right) & \text{if } u_* > u_t, \\ 0 & \text{otherwise,} \end{cases} \quad (2)$$

where the dimensionless prefactor, $a_q \approx 8.33$, was calibrated in Durán et al. (2011) and takes into account dune compactness (~0.6) so that sand fluxes can be used directly for dunes dynamics. Eq. (2) is a volumetric flux per unit width, *i.e.*, it has the dimension of length squared per time. In this formula, $u_t$ is the threshold shear velocity for transport, which corresponds to the critical value of the Shields number, $\Theta_t$, such that

$$u_t = \sqrt{\Theta_t}\sqrt{\frac{\rho_s - \rho_f}{\rho_f} g d}. \quad (3)$$

We take $\Theta_t^{1/2} = 0.082$ (Iversen and Rasmussen, 1994), so that $u_t$ accounts for the dynamic (or impact) threshold, *i.e.*, the lowest shear velocity that can sustain saltation once it has been initiated (Bagnold, 1941). For calculations, we use a constant threshold velocity of $u_t = 0.153$ m/s, which corresponds to quartz sand grains of diameter $d \simeq 160$ μm in air on Earth.

The transport law Eq. (2) is valid for transport in saltation over a mobile sand bed for moderate wind velocities above transport threshold. In such conditions, sand transport occurs in a few centimeters thick surface layer above the bed (Creyssels et al., 2009; Dong et al., 2012). In this law, first proposed by Ungar and Haff (1987), the amount of transported grains is proportional to the difference between the basal shear stress and its threshold value, and the mean velocity of grains corresponds to the transport threshold wind velocity. Grains in saltation slow the wind in the transport layer, down to the transport threshold value when flux is saturated (Durán et al., 2011; Valance et al., 2015).

#### A.2.3. Wind speed-up over a dune

The first source of complexity in morphodynamics of dunes relies in the coupling between wind flow, sand transport, and dune topography. Positive topography deflects the air flow and the compression of streamlines causes the wind speed close to the ground to be stronger over the obstacle than over a flat bed away from any topography, so that the sand flux over a dune depends on its shape. Usually defined as the *speed-up*, this is a critical ingredient that couples the dune topography and sand transport at all stages of the development of dunes, from the formation of incipient bedforms to the dynamics of major dune systems. It is often described in terms of a *fractional speed-up ratio* (or *relative speed-up ratio*), $\delta$, which is the relative speed-up

between the wind velocity at some elevation above the dune profile ($u$) and the wind velocity at the same elevation above a flat bed away from any topography ($u_0$) (Jackson and Hunt, 1975):

$$\delta = \frac{u - u_0}{u_0}. \tag{4}$$

The value of $\delta$ varies with position along the dune profile, elevation above the bed, dune aspect ratio and aerodynamic roughness (Jackson and Hunt, 1975; Britter et al., 1981). In the field, measurements should be made in the transport layer to be relevant for flux variation and, if possible, under transport conditions because transport affects aerodynamic roughness. When measured close to the bed for different types of dunes on Earth, reported $\delta$-values typically range between 0.4 and 1 for the maximum value, or for the one measured at the top of the dune (Arens and Van der Lee, 1995; Wiggs et al., 1996; Walker and Nickling, 2003; Walker et al., 2009; Claudin et al., 2013). In general, the wind velocity is not expected to be maximum at the top of the dune when measured sufficiently close to the ground, but slightly upwind (Appendix A.4.1). However, on mature dunes the difference between the maximum wind velocity and wind velocity at the dune top should be small.

Jackson and Hunt (1975) analyzed the theoretical response in 2D of a turbulent air flow in aerodynamically rough regime to the perturbation induced by a symmetric hump with small aspect ratio and curvature (Section 4 & Appendix A.4.1). They found that in this case the fractional speed-up, taken at its maximum or at top of the hump, is independent of wind velocity, depends only weakly on aerodynamic roughness, and is almost proportional to the hump aspect ratio (Jackson and Hunt, 1975):

$$\delta \simeq \beta \frac{H}{L}, \tag{5}$$

where $L$ and $H$ are the characteristic length and height of the hump, and $\beta$ a dimensionless coefficient that takes into account the aerodynamic roughness, position along the hump profile, and elevation above the bed. For typical values of aerodynamic roughness encountered in dunes on Earth, $\beta \simeq 6$ when considering the maximum of shear velocity, $u_*$ (Jackson and Hunt, 1975; Charru et al., 2013; Courrech du Pont, 2015; Appendix A.4.1).

The increase in wind shear velocity leads to an increase in saturated sand flux up the dune slope. Equivalently to the relative speed-up ratio, one can define a relative flux-up ratio (Courrech du Pont et al., 2014; Courrech du Pont, 2015), $\gamma = (Q - Q_0)/Q_0$, which can be calculated for saturated flux with Eq. (2) given a value for $\delta$. Because of transport threshold in Eq. (2), $\gamma$ depends on wind velocity even if $\delta$ does not as in Eq. (5), *e.g.*, $\gamma$ goes to infinity if unperturbed wind velocity, $u_0$, is just below $u_t$ (Gao et al., 2015).

The variation of wind shear velocity along the dune profile, which leads to variation of sand flux, is a key parameter to understand dune growth and dynamics (Section 4 & Appendix A.4.1). Its dependency on the dune aspect ratio in the direction of wind, $H/L$, which has been observed in the field for reversing dunes (Neuman et al., 1997), also has a strong impact on dune dynamics in multidirectional wind regimes (Section 5.2 & Appendix A.3.3). The 3D shape of the dune and the orientation of wind relative to the dune (*e.g.*, the wind may not blow perpendicularly to crest line) can also deflect the sand flux direction above the dune (Tsoar, 1983; Tsoar and Yaalon, 1983; Arens and Van der Lee, 1995; Walker and Nickling, 2002; Walker et al., 2009; Walker and Shugar, 2013) by combined effects of wind streamline deflection and of gravity, because the dune topography gradient has components in both parallel and normal to (non-deflected) wind. The sand flux deflection by topography explains the 3D shapes of a barchan (Hersen, 2004; Reffet et al., 2010) or the transverse instability of a migrating ridge (Parteli et al., 2011; Guignier et al., 2013) in a unidirectional flow. Here, we do not take into account the sand flux deflection in calculations but only the wind-speed-up and its dependence on the apparent dune aspect ratio.

### A.3. Sand flux from wind data

#### A.3.1. Sand flux on a flat sand bed from wind data

We compute sand fluxes using the surface wind data from the ECMWF ERA5-Land reanalysis (Hersbach et al., 2019; Muñoz-Sabater et al., 2021). This global weather forecasting model based on data assimilation aims to include all available measurements from weather stations, radiosondes, ships, and satellites. It provides numerical extrapolation of many parameters from the beginning of 1979 up to the time of writing (2023) with a horizontal spatial resolution of $0.1° \times 0.1°$ (about 11 km at the equator) and a time resolution of 1 h. We denote $t_i$, $i \in [1; N]$ the different times, which are regularly spaced. We extract from data the wind direction, $\theta$, relative to the east and wind speed, $u$, at a height $z = 10$ m and calculate the shear velocity, $u_*$, over a flat sand bed using the law of the wall:

$$u_*(t_i) = u(z, t_i)\frac{\kappa}{\ln(z/z_0)}, \tag{6}$$

where $\kappa$ is the von-Kármán constant ($\kappa = 0.41$) and $z_0$ the aerodynamic roughness length scale, which is modified by grains in saltation in transport conditions. We take $z_0 = 1$ mm for all calculations on Earth.

We define the mean shear velocity $\langle u_* \rangle$ as the shear velocity averaged over the time during which transport occurs:

$$\langle u_* \rangle = \frac{1}{\sum_{i=1}^{N} H_u} \sum_{i=1}^{N} H_u u_* \qquad \text{where} \qquad H_u = \begin{cases} 1 & \text{when } u_* > u_t, \\ 0 & \text{else.} \end{cases} \tag{7}$$

Using the calculated shear velocity, $u_*(t_i)$, and extracted wind direction, $\theta(t_i)$, we compute the saturated sand flux over a flat sand bed, $\vec{Q}_0$, using the transport law in Eq. (2):

$$\vec{Q}_0(t_i) = \begin{pmatrix} Q_{\text{sat}}(t_i)\cos\left[\theta(t_i)\right] \\ Q_{\text{sat}}(t_i)\sin\left[\theta(t_i)\right] \end{pmatrix}, \tag{8}$$

where first and second components are eastward and northward components, respectively. We sum the successive sand fluxes, $\vec{Q}_0(t_i)$, over the entire time period to calculate the resultant sand flux:

$$\langle \vec{Q}_0 \rangle = \frac{1}{N} \sum_{i=1}^{N} \vec{Q}_0. \tag{9}$$

#### A.3.2. Sand flux over dunes from wind data

To evaluate the characteristic growth, migration, and elongation rates of dunes in the field, we need to calculate the characteristic wind shear velocity and corresponding sand flux over dunes. This characteristic wind shear velocity takes into account the wind speed-up and is typically the maximum value, or the one at the top of the dune, which we take to be the same. Wind fractional speed-up ratio, $\delta$ (Eq. (4)), depends on dune aspect ratio in the direction of wind (Eq. (5)). Considering a symmetric linear dune of uniform and steady aspect ratio $H/L$ in cross section and orientation $\alpha$, a wind of direction $\theta$ experiences an apparent dune aspect-ratio $H\,|\sin(\theta - \alpha)|\,/L$, so that the characteristic wind shear velocity, $u_c$, depends on the angle between wind direction and dune orientation:

$$u_c(\alpha) = u_*\left(1 + \delta\,|\sin(\theta - \alpha)|\right), \qquad \text{where} \qquad \delta = \beta\frac{H}{L}. \tag{10}$$

In Eq. (10), $u_*$ is the shear velocity over a flat sand bed (Eq. (6)). For the calculations in Section 5.2, we use $\delta = 0.8$. Future improvements could include unsteady aspect ratios, which are probably important to better model reversing dunes, but here we only take into account the effect of dune orientation with respect to winds.

The corresponding characteristic sand flux over the dune, which we assume to be saturated, can be decomposed into crest-parallel and crest-normal components of transport (Fig. 23):

$$\vec{Q}_c(\alpha) = \begin{pmatrix} Q_{\parallel}(\alpha) \\ Q_{\perp}(\alpha) \end{pmatrix} = \begin{pmatrix} Q_{\text{sat}}(u_c)\cos(\theta - \alpha) \\ Q_{\text{sat}}(u_c)\sin(\theta - \alpha) \end{pmatrix}, \tag{11}$$

where $Q_{\text{sat}}$ is calculated with Eq. (2) using $u_c$ (Eq. (10)). The effect of the topography on the saturated sand flux due to the wind speed-up is

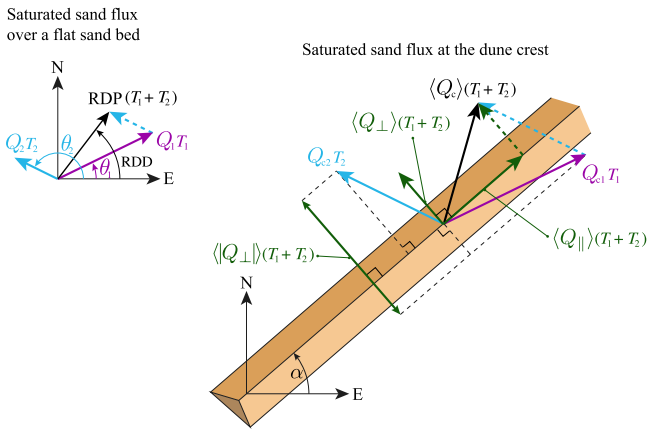


**Fig. 23.** Sand flux over a dune. A dune of orientation $\alpha$ with respect to the east is subjected to a bimodal wind regime, which, over a flat sand bed, would generate a saturated sand flux $Q_1$ during a time $T_1$ in a direction making an angle $\theta_1$ with respect to the east, and a saturated sand flux $Q_2$ during a time $T_2$ in a direction making an angle $\theta_2$ with respect to the east (top left). The combination of these two transport events defines the resultant drift potential, RDP, and direction, RDD. The wind accelerates over the dune and the speed-up increases with the dune aspect ratio experienced by the wind. Near the dune crest, the two transport events have a magnitude of $Q_{c1}$ during $T_1$ and $Q_{c2}$ during $T_2$. The individual transport directions, $\theta_1$ and $\theta_2$, do not change. The combination of the two transport events at the dune crest results in an average sand flux $\langle\vec{Q}_c\rangle$, which can be decomposed into crest-parallel, $\langle Q_\parallel\rangle$, and crest-normal, $\langle Q_\perp\rangle$, components. The gross bedform-normal transport has a magnitude $\langle|Q_\perp|\rangle$. All vectors are in the horizontal plane.

not directly integrated into the sand flux, but into wind shear velocity to better account for the transport threshold. Sand can be transported at the dune top while shear velocity is below the threshold for transport where the bed is flat. However, our analysis assumes that wind velocity is above threshold where the bed is flat. $\vec{Q}_c$, is the characteristic sand flux over the dune, which can be assimilated to the maximum value of the sand flux or the value at the dune top. In our analysis, we assume that the sand flux varies in line with the topography along the dune profile (and wind boundary layer detaches in the lee side), so that the averaged sand flux over a dune section in the direction of wind is assumed to be proportional to $Q_c$, and the characteristic divergence of the sand flux is $Q_c/L$, where $L$ is the length of the dune in the direction of the wind. This is not valid if transport occurs only at the dune top.

Then, the time-averaged components of these fluxes allow us to predict the orientation of dunes according to the prevailing growth mechanism.

#### *A.3.3. Orientation of dunes in multidirectional flow regimes depending on the prevailing growth mechanism*

*Growth rate in height.* The growth rate in height of a dune is directly related to the sand deposition rate at the crest and erosion rate at the trough, which correspond to divergences of the sand flux at the crest and the trough, respectively. For long straight dunes with an avalanche face or large aspect ratio that are much larger than the minimum dune size (Section 4), we assume that the sand flux typically varies over a length proportional to the dune length in the direction of wind, $L$, between a maximum value $Q_{max}$ upwind of the crest and zero downwind of the crest, because the wind boundary layer detaches in the lee side. Thus, the characteristic growth rate is:

$$\sigma = \frac{2\,Q_{max}}{H\,L}, \tag{12}$$

where $H$ is the dune height. As in Eq. (1), the factor 2 comes from the assumption of a triangular dune profile.

Dunes that exhibit smaller lengths in the direction of wind have larger growth rate. When growth in height is the prevailing growth mechanism, like in the bed instability mode, the orientation of the dune crestline is such that the growth rate is maximum. In a multidirectional wind regime, a dune should then have an orientation $\alpha_H$ that minimizes the different lengths in the direction of wind, so that it experiences *Maximum Gross Bedform-Normal Transport* (MGBNT) (Rubin and Hunter, 1987), which we consider to be equivalent to the maximum of $\langle|Q_\perp|\rangle$. The absolute value reflects that transport in both directions across the crest contribute to dune growth (Rubin and Hunter, 1987; Courrech du Pont et al., 2014). Using signed values of transport subtracts transport in opposing directions, even though they both contribute to dune growth.

MGBNT yields good agreement with experiments on wind ripples (Rubin and Hunter, 1987), centimetric and decimetric sand bedforms under water (Rubin and Ikeda, 1990; Reffet et al., 2010; Courrech du Pont et al., 2014), numerical simulations (Werner and Kocurek, 1997; Parteli et al., 2009; Gao et al., 2015), and field measurements for bimodal flow regimes (Ping et al., 2014; Lü et al., 2021) in full mobilized bed conditions.

*Elongation without migration.* The direction of elongation is the direction of sand net transport as experienced by the dune. The direction $\alpha_E$ of an elongating dune corresponds to a null perpendicular to crest net transport ($\langle Q_\perp\rangle = 0$) and a positive along crest net transport ($\langle Q_\parallel\rangle > 0$). This is the predicted orientation for dunes on a starved bed if they do not migrate. Prediction of several directions of elongation within a same wind regime is made possible by taking into account the dependency of wind speed-up on dune orientation.

The predicted orientation for elongating dunes is in good agreement with experiments on centimetric sand bedforms under water (Courrech du Pont et al., 2014), numerical simulations (Gao et al., 2015), and field measurements (Lü et al., 2022) for bimodal flow regimes. This rule also correctly predicts the multiple directions of elongation observed for star dunes on a starved bed in numerical simulations when the flow regime is multidirectional with a null RDP (Zhang et al., 2012).

### *A.4. Wind flow over incipient free dunes*

#### *A.4.1. Turbulent flow model*

Wind flow over a flat bottom or topography with a small aspect ratio can be divided in different regions above the bed (or layers) in which the transfer of fluid momentum is dominated by different processes. Sediment transport takes place in an *inner layer* where the flow is turbulent (high Reynolds number) and is characterized by velocity fluctuations and intermittent flow structures that transport the fluid momentum to the bed, where the flow is slowed by wall friction. In the outer layer, the fluid is comparable to a perfect fluid. In a sublayer, just above the bed, viscous effects are dominant.

Turbulent stress in the inner layer can be described by means of an *eddy viscosity* characterized by a *mixing length*. There is no characteristic length scale intrinsic to turbulence and the mixing length is a local quantity, usually similar to the distance to the obstacle that is causing the momentum transfer. Under this model for a stationary outer flow, the time-averaged velocity profile, $u(z)$, inside the inner layer above a flat wall is known as the law of the wall:

$$u(z) = \frac{u_*}{\kappa}\ln\left(\frac{z}{z_0}\right), \tag{13}$$

where $u_*$ is the shear velocity, $\kappa \simeq 0.41$ the von Kármán constant, $z$ the distance from the wall, and $z_0$ is the distance at which the velocity as given by Eq. (13) goes to zero and relates to *aerodynamic roughness*. The shear velocity is defined from the basal shear stress $\tau$, such that $\tau = \rho_f u_*^2$, where $\rho_f$ is the fluid density. The law of the wall is well supported by experimental data (Schultz and Flack, 2009; Flack and Schultz, 2010; Kadivar et al., 2021). The length $z_0$ is either set by the characteristic roughness length scale of the wall, $r$, or by the thickness of the viscous sublayer when it is larger than roughness. The characteristic thickness of the viscous sublayer is $\nu/u_*$, where $\nu$ is the fluid kinematic viscosity. The roughness Reynolds number,

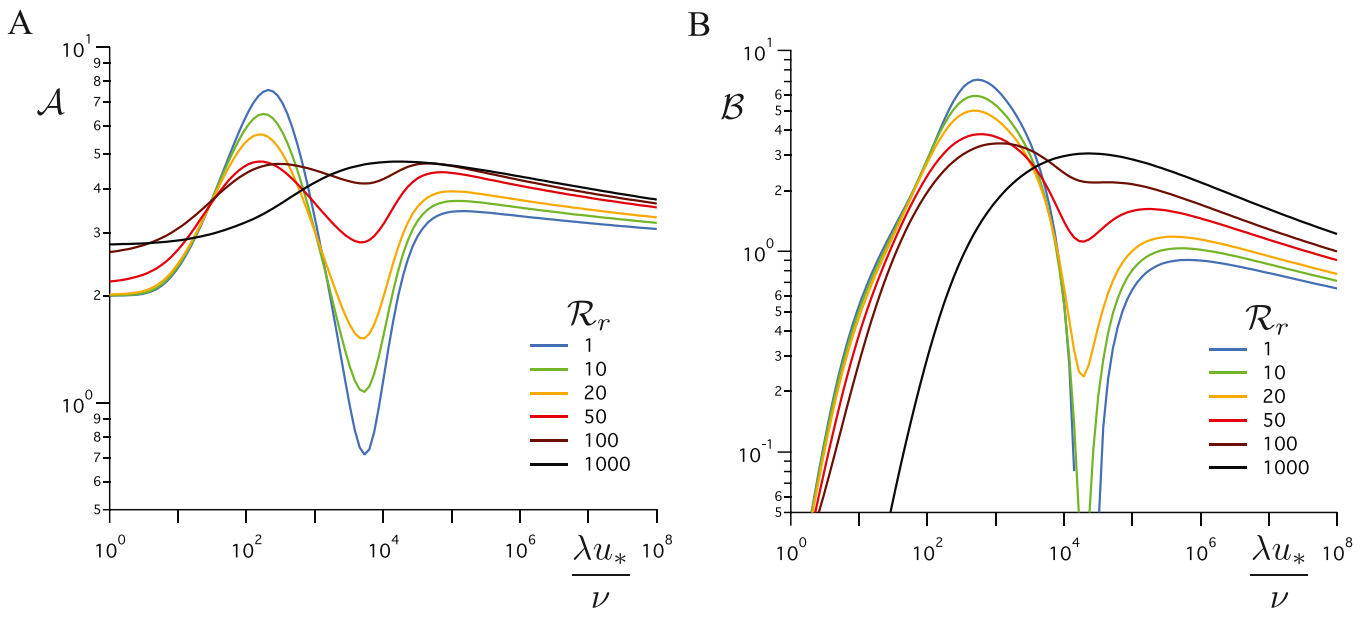


**Fig. 24.** Response of the flow to a sinusoidal perturbation of wavelength $\lambda$ for different boundary Reynolds numbers $\mathscr{R}_r$ (adapted from Claudin et al., 2017). The coefficients $\mathscr{A}$ (A) and $\mathscr{B}$ (B) are the weight coefficients of the perturbation of the basal shear stress for the in-phase and in-phase-quadrature components, respectively. They are plotted as a function of wavelength, normalized by the viscous length, *i.e.*, a bedform-scale Reynolds number.

$\mathscr{R}_r = ru_*/\nu$, compares that two length scales. When $\mathscr{R}_r > 100$, flow is aerodynamically rough ; conversely, when $\mathscr{R}_r$ is smaller than a few units, flow is aerodynamically smooth, and the thickness of the viscous sublayer sets the characteristic length $z_0$ (Kadivar et al., 2021).

For a wavy bed, the thicknesses of the boundary layers are modulated by topography. They are thinner where flow velocity spatially increases, and thicker where flow velocity decreases. In order to study the formation of incipient dunes from a flat sand bed, we consider the linear response of the flow to a small sinusoidal perturbation of the bed topography of wavelength $\lambda$ and low amplitude $h_0$ ($h_0/\lambda \ll 1$), such that

$$h(x) = h_0 \sin(2\pi x/\lambda). \tag{14}$$

In this case, the perturbation of the basal shear stress is proportional to the aspect ratio of the topographic perturbation, and can be expressed as the sum of two components: one that is in phase with topography, with a weight denoted $\mathscr{A}$, and one that is in phase quadrature, with a weight denoted $\mathscr{B}$, *i.e.*,

$$\tau(x) = \tau_0 \left[1 + \frac{2\pi\, h_0}{\lambda} \left(\mathscr{A} \sin(2\pi x/\lambda) + \mathscr{B} \cos(2\pi x/\lambda)\right)\right], \tag{15}$$

where $\tau_0$ is the unperturbed (flat bed) shear stress. In principle, coefficient $\mathscr{A}$ accounts for dune migration, whereas coefficient $\mathscr{B}$ accounts for dune growth (Kroy et al., 2002; Andreotti et al., 2002; Courrech du Pont, 2015). Within this framework, the ratio of the relative increase in shear-stress at the tops of the sinusoidal bed equals $\mathscr{A}(2\pi h_0/\lambda)$. In the limit of small perturbations, the relative speed-up of shear velocity is half of that (because $\tau \propto {u_*}^2$) and the fractional speed-up ratio is $\delta = (\mathscr{A}/2)(2\pi h_0/\lambda)$ at the tops of the bed. However, wind shear velocity and shear stress are not maximum at the top of the bed perturbations but are phase-shifted. The phase shift, $\phi = \arctan(\mathscr{B}/\mathscr{A})$, is positive if $\tau$ is maximum upwind of the top of the bed perturbations. There, the maximum fractional speed-up ratio of shear velocity is $\delta = (\sqrt{\mathscr{A}^2 + \mathscr{B}^2}/2)(2\pi h_0/\lambda)$.

Under the above framework, the flow response to a small perturbation was calculated by Jackson and Hunt (1975) in the rough case (constant $z_0$, $\mathscr{R}_r \to \infty$). In that limit, $\mathscr{A}$ and $\mathscr{B}$ weakly (logarithmically) vary with the wavelength of the bed perturbation (Fig. 24). More importantly, in rough conditions, $\mathscr{B}$ and the phase shift are always positive, favoring the development of the dune instability at all wavelengths (Kroy et al., 2002; Fourrière et al., 2010).

This positive shift can be explained as follows. In the outer region of the flow, well above the bed, the flow behaves as a potential flow, with inertia and pressure gradient balancing each other. Therefore, the flow is in phase with the topography, such that wind velocity is maximum over topographic highs and minimum over troughs. According to Bernoulli's principle, pressure is in turn minimal over topographic highs and maximum over troughs. Thus, along a streamline, the pressure gradient is minimum (and negative) where the velocity increases the most, above the maximum slope. It is in phase quadrature with topography. In contrast, flow velocity is reduced due to friction in the inner turbulent layer, and fluid inertia is therefore reduced. In the inner layer, the flow is driven by the transverse turbulent transport of momentum from the outer region to the inner layer (in phase) and by the longitudinal (in the direction of wind) pressure gradient inherited from the outer flow and that is maintained in the inner layer (in phase quadrature). Therefore, fluid velocity and shear stress peak upwind of the maximum of topography. This positive offset was measured in the field on dunes with small aspect ratios (Claudin et al., 2013; Lü et al., 2021).

Under aerodynamically smooth conditions, both the turbulent and viscous boundary layers are modulated by topography and coupled. Regarding the turbulent mixing, the usual correction relative to the rough conditions over a flat bed is modeled as a decrease in both the mixing length and the turbulent viscosity near the bed, with a characteristic length scale proportional to the thickness of the viscous boundary layer (Van Driest, 1956). Such corrections are important when considering, *e.g.*, the development of dissolution and melting patterns (Appendix A.4.2). More importantly for dunes, the shear stress on the bed is controlled by the viscous boundary layer. A larger shear stress goes with a thinner viscous boundary layer, which thins out when the (negative) pressure gradient decreases. To model unusual experimental measurements of the shear stress on a wavy bed in a water channel (Zilker et al., 1977; Abrams and Hanratty, 1985), Hanratty (1981) and Frederick and Hanratty (1988) assumed that the effective pressure gradient inside the viscous boundary layer lags the outer pressure gradient by a distance proportional to the characteristic thickness of the viscous boundary layer. Under this assumption, it follows that the factors $\mathscr{A}$ and $\mathscr{B}$ decrease abruptly for a range of

wavelengths (Fig. 24). This sharp transition can explain dissolution patterns (Thorsness and Hanratty, 1979; Claudin et al., 2017). Although not directly evidenced by experimental data, this model interestingly predicts a negative phase shift between shear stress and topography for a range of wavelengths set by the characteristic thickness of the viscous boundary layer (Fig. 24). If this prediction is correct, dunes with these wavelengths cannot develop (Charru et al., 2013; Durán Vinent et al., 2019). This prediction is consistent with the general absence of dunes with wavelengths from a few to a few tens of meters on Mars, where the kinematic viscosity of the atmosphere is larger than on Earth (Lapôtre et al., 2017; Lapôtre et al., 2018; Durán Vinent et al., 2019). The fundamental origin of this anomalous flow regime is an active area of research, and is likely associated with a laminar-to-turbulent transition (Zilker et al., 1977; Frederick and Hanratty, 1988; Lapôtre et al., 2017).

#### *A.4.2. Dissolution and melting patterns as evidence for the Hanratty anomaly*

Transverse patterns may form on an ice sheet under deep flows when the ice sublimates in air or melts under water. Similar patterns are also observed in soluble rocky substrates dissolving under water flow. These erosion patterns can only appear if the rate of substrate erosion (sublimation, melting, or dissolution) is greater in the troughs than on the bumps. Dissolution increases the concentration of solutes at the solid/fluid interface, and sublimation or melting extracts heat from the fluid, which decreases temperature at the solid/fluid interface. To sustain the melting or dissolution process, heat or solute concentration must be transported towards or away from the interface. This transport may be buoyancy-driven by melting or dissolution themselves, leading to density stratification into the fluid caused by gradients in temperature or concentration (Sullivan et al., 1996; Haudin et al., 2014; Cohen et al., 2016; Favier et al., 2019; Cohen et al., 2020). In the case of a stable density stratification, differential erosion between bumps and troughs is explained by the coupling between flow and topography, which modulates the thicknesses of boundary layers (analogously to the case of dunes discussed above) and the turbulent transport of heat and concentration (Thorsness and Hanratty, 1979; Claudin et al., 2017). The existence of dissolution patterns suggests that the turbulent viscosity and diffusion of heat or concentration are more significant in troughs than over bumps.

Such patterns were reproduced experimentally in laboratory flumes over plaster (Allen, 1971; Blumberg and Curl, 1974; Villien et al., 2005) or icy (Ashton and Kennedy, 1972; Gilpin et al., 1980; Bushuk et al., 2019) beds and under turbulent flows. Based on these studies, the initial and mature patterns have wavelengths that scale with the inverse of flow velocity, *i.e.*, that are proportional to the characteristic thickness of the viscous boundary layer (Curl, 1966, 1974). Furthermore, mature patterns reach a stationary state with constant amplitude and wavelength. This pattern saturation seems to coincide with a smooth-to-rough regime transition, at which point bedform amplitude becomes much greater than the thickness of the boundary layer. These experimental observations support the existence of a particular turbulent flow regime in the smooth case for a range of wavelengths — the Hanratty anomaly.

### *A.5. Possible confinement by the atmospheric boundary layer*

A planetary atmosphere, like Earth's, displays a vertical structure. As radiation from the sun heats the ground, it leads to an unstable density stratification (with warmer, less dense air at the bottom), which in turn drives convection in the atmospheric boundary layer (ABL). Above the ABL, in the free atmosphere, density stratification is stable (*i.e.*, air density decreases with altitude). The height of the ABL, $\Lambda$, depends on the heat flux from the ground to the atmosphere and varies spatially due to, *e.g.*, lateral variations in ground albedo, and in time, *e.g.*, due to seasonal changes in sun radiative flux. Such fluctuations make it challenging to determine a characteristic height of the ABL that is relevant to dune formation, especially as giant dunes integrate flows over a long period, but only under conditions that are conducive to active sediment transport (Gunn et al., 2022). Shear stresses in excess of threshold values for sand transport tend to occur during strong diurnal convection within the boundary layer over dune fields — this convection is associated with high $\Lambda$ values (Gunn et al., 2021).

Another challenge lies in modeling wind flow over a dune under ABL confinement. In the subaqueous case, there is a coupling between the bottom topography and the water free surface, which can deform and where waves can propagate due to the gravitational restoring force. In particular, this coupling causes a transition between downstream-moving dunes and upstream-moving antidunes when the flow over the dune exceeds the velocity of water waves. In this case, flow regime is controlled by the Froude number, a dimensionless number that relates flow velocity to speed of shallow water waves. Like in the subaqueous case, gravity waves can also propagate at the interface between the ABL and the free atmosphere, where a density jump, $\Delta\rho_f$, occurs. One can thus define a Froude number, $\mathcal{F} = U/\sqrt{g\Lambda\Delta\rho_f/\rho_f}$, where $U$ is the flow velocity at altitude $\Lambda$ (Stull, 1988; Vosper, 2004; Hunt et al., 2006; Jiang, 2014).

A second Froude number, $\mathcal{F}_N$, can be defined from the strength of the vertical density stratification in the free atmosphere, $\partial_z\rho_f$. Stable stratification in the free atmosphere sets a characteristic oscillation frequency of fluid particles, the Brunt–Väisälä frequency, $N_B = \sqrt{-g\partial_z\rho_f/\rho_f}$, such that $\mathcal{F}_N = U/(\Lambda N_B)$ (Stull, 1988; Vosper, 2004; Hunt et al., 2006; Jiang, 2014). The coupling between dune dynamics and the ABL, and its dependence on these Froude numbers, remain largely unexplored. In addition to the ABL, flow confinement can result from other phenomena, such as katabatic winds. Each specific confinement scenario is likely to be characterized by different controls on $\Lambda$. Cross-wind or secondary dune patterns could possibly be induced by such confinement effects (Gadal et al., 2022).

## References


Abrams, J., Hanratty, T.J., 1985. Relaxation effects observed for turbulent flow over a wavy surface. J. Fluid Mech. 151, 443–455.

Ahlbrandt, T.S., Fryberger, S.G., 1980. Eolian Deposits in the Nebraska Sand Hills. US Geological Survey Professional Paper 1120, 1–24.

Al-Masrahy, M.A., Mountney, N.P., 2013. Remote sensing of spatial variability in aeolian dune and interdune morphology in the Rub'Al-khali, Saudi Arabia. Aeolian Res. 11, 155–170.

Allen, J.R.L., 1971. Bed forms due to mass transfer in turbulent flows: a kaleidoscope of phenomena. J. Fluid Mech. 49 (1), 49–63.

Anderson, R.S., 1987. A theoretical model for aeolian impact ripples. Sedimentology 34 (5), 943–956.

Andreotti, B., Claudin, P., Douady, S., 2002. Selection of dune shapes and velocities Part 2: A two-dimensional modeling. Euro. Phys. J. B 28, 341–352.

Andreotti, B., Claudin, P., Iversen, J.J., Merrison, J.P., Rasmussen, K.R., 2021. A lower-than-expected saltation threshold at Martian pressure and below. Proc. Natl. Acad. Sci. 118 (5), e2012386118.

Andreotti, B., Claudin, P., Pouliquen, O., 2006. Aeolian sand ripples: Experimental study of fully developed states. Phys. Rev. Lett. 96 (2), 028001.

Andreotti, B., Claudin, P., Pouliquen, O., 2010. Measurements of the aeolian sand transport saturation length. Geomorphology 123 (3–4), 343–348.

Andreotti, B., Fourrière, A., Ould-Kaddour, F., Murray, B., Claudin, P., 2009. Giant aeolian dune size determined by the average depth of the atmospheric boundary layer. Nature 457 (7233), 1120–1123.

Arens, S.M., Van der Lee, G.E.M., 1995. Saltation sand traps for the measurement of aeolian transport into the foredunes. Soil Technol. 8 (1), 61–74.

Ashton, G.D., Kennedy, J.F., 1972. Ripples on underside of river ice covers. J. Hydraul. Div. 98 (9), 1603–1624.

Aufrère, L., 1935. Essai sur les dunes du Sahara algérien. Geografiska Annaler 481–500.

Baas, A.C.W., 2007. Complex systems in aeolian geomorphology. Geomorphology 91 (3–4), 311–331.

Baas, A.C.W., Delobel, L.A., 2022. Desert dunes transformed by end-of-century changes in wind climate. Nature Clim. Change 12 (11), 999–1006.

Baas, A.C.W., Nield, J.M., 2007. Modelling vegetated dune landscapes. Geophys. Res. Lett. 34 (6).

Bagnold, R.A., 1941. The Physics of Blown Sand and Desert Dunes. Chapman and Hall, London.

Balme, M., Berman, D.C., Bourke, M.C., Zimbelman, J.R., 2008. Transverse aeolian ridges (TARs) on Mars. Geomorphology 101 (4), 703–720.
Barchyn, T.E., Hugenholtz, C.H., 2013. Reactivation of supply-limited dune fields from blowouts: A conceptual framework for state characterization. Geomorphology 201, 172–182.
Belcher, D., Veverka, J., Sagan, C., 1971. Mariner photography of Mars and aerial photography of Earth: Some analogies. Icarus 15 (2), 241–252.
Benjumea-Lopez, A.C., Hesp, P.A., 2023. Evolution of a coastal transgressive dunefield to a parabolic dunefield Canunda dunes, South Australia. Geomorphology 430, 108653.
Berman, D.C., Balme, M.R., Rafkin, S.C.R., Zimbelman, J.R., 2011. Transverse aeolian ridges (TARs) on Mars ii: distributions, orientations, and ages. Icarus 213 (1), 116–130.
Beveridge, C., Kocurek, G., Ewing, R.C., Lancaster, N., Morthekai, P., Singhvi, A.K., Mahan, S.A., 2006. Development of spatially diverse and complex dune-field patterns: Gran Desierto Dune Field, Sonora, Mexico. Sedimentology 53 (6), 1391–1409.
Bishop, S.R., Momiji, H., Carretero-González, R., Warren, A., 2002. Modelling desert dune fields based on discrete dynamics. Discrete Dyn. Nat. Soc. 7 (1), 7–17.
Blumberg, P.N., Curl, R.L., 1974. Experimental and theoretical studies of dissolution roughness. J. Fluid Mech. 65 (4), 735–751.
Bordiec, M., Carpy, S., Bourgeois, O., Herny, C., Massé, M., Perret, L., Claudin, P., Pochat, S., Douté, S., 2020. Sublimation waves: Geomorphic markers of interactions between icy planetary surfaces and winds. Earth-Sci. Rev. 211, 103350.
Bourke, M.C., 2010. Barchan dune asymmetry: Observations from Mars and Earth. Icarus 205 (1), 183–197.
Bourke, M.C., Lancaster, N., Fenton, L.K., Parteli, E.J.R., Zimbelman, J.R., Radebaugh, J., 2010. Extraterrestrial dunes: An introduction to the special issue on planetary dune systems. Geomorphology 121 (1–2), 1–14.
Bowler, J.M., 1973. Clay dunes: their occurrence, formation and environmental significance. Earth-Sci. Rev. 9 (4), 315–338.
Bristow, C.S., Duller, G.A.T., 2024. Structure and chronology of a star dune at Erg Chebbi, Morocco, reveals why star dunes are rarely recognised in the rock record. Sci. Rep. 14 (1), 4464.
Bristow, C.S., Duller, G.A.T., Lancaster, N., 2007. Age and dynamics of linear dunes in the Namib Desert. Geology 35 (6), 555–558.
Britter, R.E., Hunt, J.C.R., Richards, K.J., 1981. Air flow over a two-dimensional hill: studies of velocity speed-up, roughness effects and turbulence. Q. J. R. Meteorol. Soc. 107 (451), 91–110.
Bullard, J.E., Livingstone, I., 2002. Interactions between aeolian and fluvial systems in dryland environments. Area 34 (1), 8–16.
Bushuk, M., Holland, D.M., Stanton, T.P., Stern, A., Gray, C., 2019. Ice scallops: a laboratory investigation of the ice–water interface. Journal of fluid mechanics 873, 942–976.
Carter, R.W.G., Hesp, P.A., Nordstrom, K., 1990. Geomorphology of erosional dune landscapes. In: Coastal Dunes: Processes and Morphology. pp. 217–250.
Charnay, B., Barth, E., Rafkin, S., Narteau, C., Lebonnois, S., Rodriguez, S., Courrech du Pont, S., Lucas, A., 2015. Methane storms as a driver of Titan's dune orientation. Nat. Geosci. 8 (5), 362–366.
Charru, F., Andreotti, B., Claudin, P., 2013. Sand ripples and dunes. Annu. Rev. Fluid Mech. 45, 469–493.
Chepil, W.S., 1945. Dynamics of wind erosion: Ii. initiation of soil movement. Soil Sci. 60 (5), 397.
Claudin, P., Andreotti, B., 2006. A scaling law for aeolian dunes on Mars, Venus, Earth, and for subaqueous ripples. Earth Planet. Sci. Lett. 252, 30.
Claudin, P., Charru, F., Andreotti, B., 2011. Transport relaxation time and length scales in turbulent suspensions. J. Fluid Mech. 671, 491–506.
Claudin, P., Durán, O., Andreotti, B., 2017. Dissolution instability and roughening transition. J. Fluid Mech. 832.
Claudin, P., Wiggs, G.F.S., Andreotti, B., 2013. Field evidence for the upwind velocity shift at the crest of low dunes. Bound.-Layer Meteorol. 148 (1), 195–206.
Cohen, C., Berhanu, M., Derr, J., Courrech du Pont, S., 2016. Erosion patterns on dissolving and melting bodies. Phys. Rev. Fluids 1 (5), 050508.
Cohen, C., Berhanu, M., Derr, J., Courrech du Pont, S., 2020. Buoyancy-driven dissolution of inclined blocks: Erosion rate and pattern formation. Phys. Rev. Fluids 5 (5), 053802.
Cooke, R., Warren, A., Goudie, A., 1993. Desert Geomorphology. UCL Press.
Cooper, W.S., 1958. Coastal sand dunes of Oregon and Washington. Mem. Geol. Soc. of America 72, 169.
Cooper, W.S., 1967. Coastal dunes of California. 104, 131.
Couldrey, A.J., Benson, T., Knaapen, M.A.F., Marten, K.V., Whitehouse, R.J.S., 2020. Morphological evolution of a barchan dune migrating past an offshore wind farm foundation. Earth Surf. Process. Landf. 45 (12), 2884–2896.
Courrech du Pont, S., 2015. Dune morphodynamics. C. R. Phys. 16 (1), 118–138.
Courrech du Pont, S., Narteau, C., Gao, X., 2014. Two modes for dune orientation. Geology 42 (9), 743–746.
Creyssels, M., Dupont, P., Ould El Moctar, A., Valance, A., Cantat, I., Jenkins, J.T., Pasini, J.M., Rasmussen, K.R., 2009. Saltating particles in a turbulent boundary layer: experiment and theory. J. Fluid Mech. 625, 47–74.
Csahók, Z., Misbah, C., Rioual, F., Valance, A., 2000. Dynamics of aeolian sand ripples. Euro. Phys. J. E 3, 71–86.
Curl, R.L., 1966. Scallops and flutes. Transactions Cave Research Group of Great Britain 7 (2).
Curl, R.L., 1974. Deducing flow velocity in cave conduits from scallops. The NSS Bulletin 36 (2).
Cutts, J.A., Smith, R.S.U., 1973. Eolian deposits and dunes on Mars. J. Geophys. Res. 78 (20), 4139–4154.
Day, M., Kocurek, G., 2018. Pattern similarity across planetary dune fields. Geology 46 (11), 999–1002.
Delorme, P., Nield, J.M., Wiggs, G.F.S., Baddock, M.C., Bristow, N.R., Best, J.L., Christensen, K.T., Claudin, P., 2023. Field evidence for the initiation of isolated aeolian sand patches. Geophys. Res. Lett. e2022GL101553.
Delorme, P., Wiggs, G.F.S., Baddock, M.C., Claudin, P., Nield, J.M., Valdez, A., 2020. Dune initiation in a bimodal wind regime. J. Geophys. Res.: Earth Surf. 125 (11), e2020JF005757.
Derickson, D., Kocurek, G., Ewing, R.C., Bristow, C., 2008. Origin of a complex and spatially diverse dune-field pattern, Algodones, southeastern California. Geomorphology 99 (1–4), 186–204.
Diniega, S., Kreslavsky, M., Radebaugh, J., Silvestro, S., Telfer, M., Tirsch, D., 2017. Our evolving understanding of aeolian bedforms, based on observation of dunes on different worlds. Aeolian Res. 26, 5–27.
Dong, Z., Lv, P., Zhang, Z., Qian, G., Luo, W., 2012. Aeolian transport in the field: A comparison of the effects of different surface treatments. J. Geophys. Res.: Atmos. 117 (D9).
Dong, Z., Wei, Z., Qian, G., Zhang, Z., Luo, W., Hu, G., 2010. 'Raked' linear dunes in the Kumtagh Desert, China. Geomorphology 123 (1–2), 122–128.
Durán, O., Andreotti, B., Claudin, P., 2012. Numerical simulation of turbulent sediment transport, from bed load to saltation. Phys. Fluids 24 (10), 103306.
Durán, O., Claudin, P., Andreotti, B., 2011. On aeolian transport: Grain-scale interactions, dynamical mechanisms and scaling laws. Aeolian Res. 3, 243–270.
Durán, O., Claudin, P., Andreotti, B., 2014. Direct numerical simulations of aeolian sand ripples. Proc. Natl. Acad. Sci. 111 (44), 15665–15668.
Durán, O., Herrmann, H.J., 2006. Vegetation against dune mobility. Phys. Rev. Lett. 97 (18), 188001.
Durán, O., Moore, L.J., 2013. Vegetation controls on the maximum size of coastal dunes. Proc. Natl. Acad. Sci. 110 (43), 17217–17222.
Durán, O., Schwämmle, V., Lind, P.G., Herrmann, H.J., 2009. The dune size distribution and scaling relations of barchan dune fields. Granul. Matter 11 (1), 7–11.
Durán Vinent, O., Andreotti, B., Claudin, P., Winter, C., 2019. A unified model of ripples and dunes in water and planetary environments. Nat. Geosci. 12 (5), 345–350.
Eastwood, E., Nield, J., Baas, A., Kocurek, G., 2011. Modelling controls on aeolian dune-field pattern evolution. Sedimentology 58 (6), 1391–1406.
Elbelrhiti, H., 2012. Initiation and early development of barchan dunes: A case study of the Moroccan Atlantic Sahara desert. Geomorphology 138 (1), 181–188.
Elbelrhiti, H., Andreotti, B., Claudin, P., 2008. Barchan dune corridors: field characterization and investigation of control parameters. J. Geophys. Res.: Earth Surf. 113 (F2).
Endo, N., Taniguchi, K., Katsuki, A., 2004. Observation of the whole process of interaction between barchans by flume experiments. Geophys. Res. Lett. 31 (12).
Ewing, R.C., 2020. White Sands. Inland Dunes of North America, pp. 207–237.
Ewing, R.C., Kocurek, G., 2010. Aeolian dune-field pattern boundary conditions. Geomorphology 114 (3), 175–187.
Ewing, R.C., Lapôtre, M.G.A., Lewis, K.W., Day, M., Stein, N., Rubin, D.M., Sullivan, R., Banham, S., Lamb, M.P., Bridges, N.T., et al., 2017. Sedimentary processes of the Bagnold Dunes: Implications for the eolian rock record of Mars. J. Geophys. Res. 122 (12), 2544–2573.
Ewing, R.C., McDonald, G.D., Hayes, A.G., 2015. Multi-spatial analysis of aeolian dune-field patterns. Geomorphology 240, 44–53.
Exner, F.M., 1920. Zur physik der dünen. Hölder.
Exner, F.M., 1925. Über die Wechselwirkung zwischen Wasser und Geschiebe in Flüssen. Hölder-Pichler-Tempsky, A.-G..
Favier, B., Purseed, J., Duchemin, L., 2019. Rayleigh–Bénard convection with a melting boundary. J. Fluid Mech. 858, 437–473.
Fenton, L.K., 2006. Dune migration and slip face advancement in the Rabe Crater dune field, Mars. Geophys. Res. Lett. 33 (20).
Fenton, L.K., Michaels, T.I., Beyer, R.A., 2013. Inverse maximum gross bedform-normal transport 1: How to determine a dune-constructing wind regime using only imagery. Icarus 230, 5–14.
Fernandez-Cascales, L., Lucas, A., Rodriguez, S., Gao, X., Spiga, A., Narteau, C., 2018. First quantification of relationship between dune orientation and sediment availability, Olympia Undae, Mars. Earth Planet. Sci. Lett. 489, 241–250.
Flack, K.A., Schultz, M.P., 2010. Review of hydraulic roughness scales in the fully rough regime. J. Fluids Eng. 132 (4).
Fourrière, A., Claudin, P., Andreotti, B., 2010. Bedforms in a turbulent stream: formation of ripples by primary linear instability and of dunes by nonlinear pattern coarsening. J. Fluid Mech. 649, 287–328.
Frederick, K.A., Hanratty, T.J., 1988. Velocity measurements for a turbulent nonseparated flow over solid waves. Exp. Fluids 6 (7), 477–486.
Fryberger, S.G., 2000. Geological overview of White Sands National Monument. Available from: http://www.nps.gov/whsa.
Fryberger, S.G., Dean, G., 1979. Dune Forms and Wind Regime. A Study of Global Sand Seas 1052, 137–169.

Gadal, C., Delorme, P., Narteau, C., Wiggs, G.F.S., Baddock, M., Nield, J.M., Claudin, P., 2022. Local wind regime induced by giant linear dunes: comparison of ERA5-land reanalysis with surface measurements. Bound.-Layer Meteorol. 185 (3), 309–332.
Gadal, C., Narteau, C., Ewing, R.C., Gunn, A., Jerolmack, D., Andreotti, B., Claudin, P., 2020a. Spatial and temporal development of incipient dunes. Geophys. Res. Lett. 47 (16), e2020GL088919.
Gadal, C., Narteau, C., Courrech du Pont, S., Rozier, O., Claudin, P., 2019. Incipient bedforms in a bidirectional wind regime. J. Fluid Mech. 862, 490–516.
Gadal, C., Narteau, C., Courrech du Pont, S., Rozier, O., Claudin, P., 2020b. Periodicity in fields of elongating dunes. Geology 48 (4), 343–347.
Gao, X., Gadal, C., Rozier, O., Narteau, C., 2018. Morphodynamics of barchan and dome dunes under variable wind regimes. Geology 46 (9), 743–746.
Gao, X., Narteau, C., Gadal, C., 2021. Migration of reversing dunes against the sand flow path as a singular expression of the speed-up effect. J. Geophys. Res.: Earth Surf. 126 (5), e2020JF005913.
Gao, X., Narteau, C., Rozier, O., Courrech du Pont, S., 2015. Phase diagrams of dune shape and orientation depending on sand availability. Sci. Rep. 5 (1), 1–12.
Génois, M., Hersen, P., Bertin, E., Courrech du Pont, S., Grégoire, G., 2016. Out-of-equilibrium stationary states, percolation, and subcritical instabilities in a fully nonconservative system. Phys. Rev. E 94 (4), 042101.
Génois, M., Hersen, P., Courrech du Pont, S., Grégoire, G., 2013b. Spatial structuring and size selection as collective behaviours in an agent-based model for barchan fields. Eur. Phys. J. B 86, 1–13.
Génois, M., Courrech du Pont, S., Hersen, P., Grégoire, G., 2013a. An agent-based model of dune interactions produces the emergence of patterns in deserts. Geophys. Res. Lett. 40 (15), 3909–3914.
Gilpin, R.R., Hirata, T., Cheng, K.C., 1980. Wave formation and heat transfer at an ice-water interface in the presence of a turbulent flow. J. Fluid Mech. 99 (3), 619–640.
Goudie, A., Thomas, D.S.G., 1986. Lunette dunes in southern Africa. J. Arid Environ. 10 (1), 1–12.
Greeley, R., Iversen, J.D., 1987. Wind As a Geological Process: On Earth, Mars, Venus and Titan. Number 4. CUP Archive.
Greeley, R., Iversen, J., Leach, R., Marshall, J., White, B., Williams, S., 1984. Windblown sand on Venus: Preliminary results of laboratory simulations. Icarus 57 (1), 112–124.
Greeley, R., Leach, R., White, B., Iversen, J., Pollack, J., 1980. Threshold windspeeds for sand on Mars: Wind tunnel simulations. Geophys. Res. Lett. 7 (2), 121–124.
Guignier, L., Niiya, H., Nishimori, H., Lague, D., Valance, A., 2013. Sand dunes as migrating strings. Phys. Rev. E 87, 052206.
Gunn, A., 2023. Formation and reorganization time scales of aeolian landscapes. Geology 51 (4), 351–355.
Gunn, A., Casasanta, G., Di Liberto, L., Falcini, F., Lancaster, N., Jerolmack, D.J., 2022. What sets aeolian dune height? Nature Commun. 13 (1), 2401.
Gunn, A., Jerolmack, D.J., 2022. Conditions for aeolian transport in the Solar System. Nat. Astron. 6 (8), 923–929.
Gunn, A., Schmutz, P., Wanker, M., Edmonds, D.A., Ewing, R.C., Jerolmack, D.J., 2020. Macroscopic flow disequilibrium over aeolian dune fields. Geophys. Res. Lett. 47 (18), e2020GL088773.
Gunn, A., Wanker, M., Lancaster, N., Edmonds, D.A., Ewing, R.C., Jerolmack, D.J., 2021. Circadian rhythm of dune-field activity. Geophys. Res. Lett. 48 (5), e2020GL090924.
Hack, J.T., 1941. Dunes of the western Navajo country. Geogr. Rev. 31 (2), 240–263.
Hanratty, T.J., 1981. Stability of surfaces that are dissolving or being formed by convective diffusion. Annu. Rev. Fluid Mech. 13 (1), 231–252.
Haudin, F., Riolfo, L.A., Knaepen, B., Homsy, G.M., De Wit, A., 2014. Experimental study of a buoyancy-driven instability of a miscible horizontal displacement in a Hele-Shaw cell. Phys. Fluids 26 (4), 044102.
Hayward, R.K., Fenton, L.K., Titus, T.N., 2014. Mars global digital dune database (MGD3): Global dune distribution and wind pattern observations. Icarus 230, 38–46.
Hayward, R.K., Mullins, K.F., Fenton, L.K., Hare, T.M., Titus, T.N., Bourke, M.C., Colaprete, A., Christensen, P.R., 2007. Mars global digital dune database and initial science results. J. Geophys. Res. 112 (E11).
Hayward, R.K., Titus, T.N., Michaels, T.I., Fenton, L.K., Colaprete, A., Christensen, P.R., 2009. Aeolian dunes as ground truth for atmospheric modeling on Mars. J. Geophys. Res.: Planets 114 (E11).
Hernández-Calvento, L., Jackson, D.W., Cooper, A., Pérez-Chacón, E., 2017. Island-encapsulating eolian sedimentary systems of the Canary and Cape Verde archipelagos. J. Sediment. Res. 87 (2), 117–125.
Hersbach, H., Bell, W., Berrisford, P., Horányi, A., Muñoz-Sabater, J., Nicolas, J., Radu, R., Schepers, D., Simmons, A., Soci, C., Dee, D., 2019. Global reanalysis: goodbye ERA-Interim, hello ERA5. ECMWF Newsl (04), 17–24.
Hersen, P., 2004. On the crescentic shape of barchan dunes. Eur. Phys. J. B 37, 507–514.
Hersen, P., 2005. Flow effects on the morphology and dynamics of aeolian and subaqueous barchan dunes. J. Geophys. Res.: Earth Surf. 110 (F4).
Hersen, P., Douady, S., 2005. Collision of barchan dunes as a mechanism of size regulation. Geophys. Res. Lett. 32 (21).
Hesp, P., 2002. Foredunes and blowouts: initiation, geomorphology and dynamics. Geomorphology 48 (1–3), 245–268.
Hesp, P.A., 2013. Conceptual models of the evolution of transgressive dune field systems. Geomorphology 199, 138–149.
Hesp, P.A., Hernández-Calvento, L., Gallego-Fernández, J.B., da Silva, G.M., Hernández-Cordero, A.I., Ruz, M.-H., Romero, L.G., 2021. Nebkha or not?-Climate control on foredune mode. J. Arid Environ. 187, 104444.
Hesp, P.A., Smyth, T.A.G., 2017. Nebkha flow dynamics and shadow dune formation. Geomorphology 282, 27–38.
Hesp, P.A., Smyth, T.A.G., 2019. Anchored dunes. In: Aeolian Geomorphology: A New Introduction. pp. 157–178.
Hesp, P.A., Walker, I.J., 2021. Coastal dunes v2. In: Shroder, J.J.F. (Ed.), Treatise on Geomorphology, Volume 7. Elsevier Inc., pp. 540–591.
Hesse, P., 2019. Sand seas. In: Aeolian Geomorphology: A New Introduction. pp. 179–208.
Hills, E.S., 1940. The lunette, a new land form of aeolian origin. Aust. Geogr. 3 (7), 15–21.
Ho, T.D., Valance, A., Dupont, P., Ould El Moctar, A., 2011. Scaling laws in aeolian sand transport. Phys. Rev. Lett. 106 (9), 094501.
Holliday, V.T., Cuba, M., Lee, W., Windingstad, J., Fenerty, B., Bustos, D., 2023. Onset of dune construction based on archaeological evidence, White Sands, New Mexico. Quaternary Research 115, 58–66.
Holm, D.A., 1953. Dome-shaped dunes of the central Nejd, Saudi Arabia. Proceedings of the 19th International Geological Congress, Algiers 107–112.
Hugenholtz, C.H., Wolfe, S.A., 2005. Biogeomorphic model of dunefield activation and stabilization on the northern Great Plains. Geomorphology 70 (1–2), 53–70.
Hunt, J.C.R., Vilenski, G.G., Johnson, E.R., 2006. Stratified separated flow around a mountain with an inversion layer below the mountain top. J. Fluid Mech. 556, 105–119.
Hunter, R.E., Richmond, B.M., Rho, A.T., 1983. Storm-controlled oblique dunes of the Oregon coast. Geol. Soc. Am. Bull. 94 (12), 1450–1465.
Iversen, J.D., Rasmussen, K.R., 1994. The effect of surface slope on saltation threshold. Sedimentology 41 (4), 721–728.
Jackson, P.S., Hunt, J.C.R., 1975. Turbulent wind flow over a low hill. Quart. J. R. Met. Soc. 101, 929–955.
Jerolmack, D.J., Ewing, R.C., Falcini, F., Martin, R.L., Masteller, C., Phillips, C., Reitz, M.D., Buynevich, I., 2012. Internal boundary layer model for the evolution of desert dune fields. Nat. Geosci. 5 (3), 206–209.
Jerolmack, D.J., Reitz, M.D., Martin, R.L., 2011. Sorting out abrasion in a gypsum dune field. J. Geophys. Res.: Earth Surf. 116 (F2).
Jia, P., Andreotti, B., Claudin, P., 2017. Giant ripples on comet 67P/Churyumov–Gerasimenko sculpted by sunset thermal wind. Proc. Natl. Acad. Sci. 114 (10), 2509–2514.
Jiang, Q., 2014. Applicability of reduced-gravity shallow-water theory to atmospheric flow over topography. J. Atmos. Sci. 71 (4), 1460–1479.
Jungerius, P.D., 1984. A simulation model of blowout development. Earth Surf. Process. Landf. 9 (6), 509–512.
Kadivar, M., Tormey, D., McGranaghan, G., 2021. A review on turbulent flow over rough surfaces: Fundamentals and theories. Int. J. Thermofluids 10, 100077.
Kennedy, J.F., 1969. The formation of sediment ripples, dunes, and antidunes. Annu. Rev. Fluid Mech. 1 (1), 147–168.
Kocurek, G., Carr, M., Ewing, R., Havholm, K.G., Nagar, Y.C., Singhvi, A.K., 2007. White Sands Dune Field, New Mexico: age, dune dynamics and recent accumulations. Sediment. Geol. 197 (3–4), 313–331.
Kocurek, G., Ewing, R.C., 2005. Aeolian dune field self-organization–implications for the formation of simple versus complex dune-field patterns. Geomorphology 72 (1–4), 94–105.
Kocurek, G., Ewing, R.C., 2016. Trickle-down and trickle-up boundary conditions in eolian dune-field pattern formation. SEPM Special Publication: Autogenic Dynamics and Self-Organization in Sedimentary Systems 106, 18–39.
Kocurek, G., Ewing, R.C., Mohrig, D., 2010. How do bedform patterns arise? new views on the role of bedform interactions within a set of boundary conditions. Earth Surf. Process. Landf. 35 (1), 51–63.
Kocurek, G., Townsley, M., Yeh, E., Havholm, K.G., Sweet, M.L., 1992. Dune and dune-field development on Padre Island, Texas, with implications for interdune deposition and water-table-controlled accumulation. J. Sediment. Res. 62 (4), 622–635.
Kok, J.F., Parteli, E.J.R., Michaels, T.I., Karam, D.B., 2012. The physics of wind-blown sand and dust. Rep. Prog. Phys. 75 (10), 106901.
Kroy, K., Sauermann, G., Herrmann, H.J., 2002. Minimal model for aeolian sand dunes. Phys. Rev. E 66 (3), 031302.
Lancaster, N., 1989. Star dunes. Prog. Phys. Geogr. 13 (1), 67–91.
Lancaster, N., 1994. Dune morphology and dynamics. In: Geomorphology of Desert Environments. Springer, pp. 474–505.
Lancaster, N., 2013. Geomorphology of Desert Dunes. Routledge.
Lancaster, N., Kocurek, G., Singhvi, A., Pandey, V., Deynoux, M., Ghienne, J.-F., Lô, K., 2002. Late Pleistocene and Holocene dune activity and wind regimes in the western Sahara Desert of Mauritania. Geology 30 (11), 991–994.
Langford, R.P., Rose, J.M., White, D.E., 2009. Groundwater salinity as a control on development of eolian landscape: An example from the White Sands of New Mexico. Geomorphology 105 (1–2), 39–49.
Lapôtre, M.G.A., Ewing, R.C., Lamb, M.P., 2021. An evolving understanding of enigmatic large ripples on Mars. J. Geophys. Res. 126 (2), e2020JE006729.

Lapôtre, M.G.A., Ewing, R.C., Lamb, M.P., Fischer, W.W., Grotzinger, J.P., Rubin, D.M., Lewis, K.W., Ballard, M.J., Day, M., Gupta, S., et al., 2016. Large wind ripples on Mars: A record of atmospheric evolution. Science 353 (6294), 55–58.
Lapôtre, M.G.A., Ewing, R.C., Weitz, C.M., Lewis, K.W., Lamb, M.P., Ehlmann, B.L., Rubin, D.M., 2018. Morphologic diversity of Martian ripples: Implications for large-ripple formation. Geophys. Res. Lett. 45 (19), 10–229.
Lapôtre, M.G.A., Lamb, M.P., McElroy, B., 2017. What sets the size of current ripples? Geology 45 (3), 243–246.
Lapôtre, M.G.A., O'Rourke, J.G., Schaefer, L., Siebach, K., Spalding, C., Tikoo, S., Wordsworth, R., 2020. Probing space to understand Earth. Nature Reviews Earth & Environment 1 (3), 170–181.
Livingstone, I., Warren, A., 1996. Aeolian Geomorphology: An Introduction. Addison Wesley Longman Ltd.
Livingstone, I., Warren, A., 2019. Aeolian Geomorphology: A New Introduction. John Wiley & Sons.
Loope, D.B., Rowe, C.M., Joeckel, R.M., 2001. Annual monsoon rains recorded by Jurassic dunes. Nature 412 (6842), 64–66.
Lorenz, R.D., Wall, S., Radebaugh, J., Boubin, G., Reffet, E., Janssen, M., Stofan, E., Lopes, R., Kirk, R., Elachi, C., et al., 2006. The sand seas of Titan: Cassini RADAR observations of longitudinal dunes. Science 312 (5774), 724–727.
Lorenz, R.D., Zimbelman, J.R., 2014. Dune Worlds: How Windblown Sand Shapes Planetary Landscapes. Springer Science & Business Media.
Lü, P., Narteau, C., Dong, Z., Claudin, P., Rodriguez, S., An, Z., Fernandez-Cascales, L., Gadal, C., Courrech du Pont, S., 2021. Direct validation of dune instability theory. Proc. Natl. Acad. Sci. 118 (17).
Lü, P., Narteau, C., Dong, Z., Claudin, P., Rodriguez, S., An, Z., Gadal, C., Courrech du Pont, S., 2022. Coexistence of two dune growth mechanisms in a landscape-scale experiment. Geophys. Res. Lett. 49 (11), e2021GL097636.
Lü, P., Narteau, C., Dong, Z., Rozier, O., Courrech du Pont, S., 2017. Unravelling raked linear dunes to explain the coexistence of bedforms in complex dunefields. Nature Commun. 8 (1), 1–9.
Lucas, A., Narteau, C., Rodriguez, S., Rozier, O., Callot, Y., Garcia, A., Courrech du Pont, S., 2015. Sediment flux from the morphodynamics of elongating linear dunes. Geology 43, 1027–1030.
Lucas, A., Rodriguez, S., Narteau, C., Charnay, B., Courrech du Pont, S., Tokano, T., Garcia, A., Thiriet, M., Hayes, A.G., Lorenz, R.D., et al., 2014. Growth mechanisms and dune orientation on Titan. Geophys. Res. Lett. 41 (17), 6093–6100.
Luna, M.C.M.d.M., Parteli, E.J.R., Durán, O., Herrmann, H.J., 2011. Model for the genesis of coastal dune fields with vegetation. Geomorphology 129 (3–4), 215–224.
Lv, P., Dong, Z., Narteau, C., Rozier, O., 2016. Morphodynamic mechanisms for the formation of asymmetric barchans: improvement of the Bagnold and Tsoar models. Environ. Earth Sci. 75, 1–9.
Mainguet, M., 1984. A classification of dunes based on aeolian dynamics and the sand budget. In: Deserts and Arid Lands. Springer, pp. 31–58.
Martin, R.L., Kok, J.F., 2017. Wind-invariant saltation heights imply linear scaling of aeolian saltation flux with shear stress. Science advances 3 (6), e1602569.
Marvin, M.C., Lapôtre, M.G.A., Gunn, A., Day, M., Soto, A., 2023. Dune interactions record changes in boundary conditions. Geology.
Mason, J.A., Swinehart, J.B., Hanson, P.R., Loope, D.B., Goble, R.J., Miao, X., Schmeisser, R.L., 2011. Late Pleistocene dune activity in the central Great Plains, USA. Quat. Sci. Rev. 30 (27–28), 3858–3870.
McDonald, G.D., Harper, J.M., Ojha, L., Corlies, P., Dufek, J., Ewing, R.C., Kerber, L., 2022. Aeolian sediment transport on Io from lava–frost interactions. Nature Commun. 13 (1), 2076.
McKee, E.D., 1966. Structures of dunes at White Sands National Monument, New Mexico (and a comparison with structures of dunes from other selected areas). Sedimentology 7 (1), 3–69.
McKee, E.D., 1979. A study of global sand seas. Geological Survey Professional Paper 1052.
Melton, F.A., 1940. A tentative classification of sand dunes its application to dune history in the southern High Plains. J. Geol. 48 (2), 113–174.
Moore, L.J., Durán Vinent, O., Ruggiero, P., 2016. Vegetation control allows autocyclic formation of multiple dunes on prograding coasts. Geology 44 (7), 559–562.
Muñoz-Sabater, J., Dutra, E., Agustí-Panareda, A., Albergel, C., Arduini, G., Balsamo, G., Boussetta, S., Choulga, M., Harrigan, S., Hersbach, H., et al., 2021. ERA5-land: A state-of-the-art global reanalysis dataset for land applications. Earth Syst. Sci. Data 13 (9), 4349–4383.
Nakao-Kusune, S., Sakaue, T., Nishimori, H., Nakanishi, H., 2020. Stabilization of a straight longitudinal dune under bimodal wind with large directional variation. Phys. Rev. E 101 (1), 012903.
Neuman, C.M., Lancaster, N., Nickling, W.G., 1997. Relations between dune morphology, air flow, and sediment flux on reversing dunes, Silver Peak, Nevada. Sedimentology 44 (6), 1103–1111.
Nield, J.M., Baas, A.C.W., 2008. Investigating parabolic and nebkha dune formation using a cellular automaton modelling approach. Earth Surf. Process. Landf. 33 (5), 724–740.
Nield, J.M., Wiggs, G.F.S., 2011. The application of terrestrial laser scanning to aeolian saltation cloud measurement and its response to changing surface moisture. Earth Surf. Process. Landf. 36 (2), 273–278.
Owen, P.R., 1964. Saltation of uniform grains in air. J. Fluid Mech. 20, 225–242.
Page, K.J., 1971. Riverine source bordering sand dune. Aust. Geogr. 11 (6), 603–605.
Pähtz, T., Durán, O., 2017. Fluid forces or impacts: What governs the entrainment of soil particles in sediment transport mediated by a Newtonian fluid? Phys. Rev. Fluids 2 (7), 074303.
Pähtz, T., Durán, O., 2020. Unification of aeolian and fluvial sediment transport rate from granular physics. Phys. Rev. Lett. 124 (16), 168001.
Pähtz, T., Kok, J.F., Parteli, E.J.R., Herrmann, H.J., 2013. Flux saturation length of sediment transport. Phys. Rev. Lett. 111 (21), 218002.
Pähtz, T., Omeradžić, A., Carneiro, M.V., Araújo, N.A.M., Herrmann, H.J., 2015. Discrete element method simulations of the saturation of aeolian sand transport. Geophys. Res. Lett. 42 (6), 2063–2070.
Pähtz, T., Parteli, E.J.R., Kok, J.F., Herrmann, H.J., 2014. Analytical model for flux saturation in sediment transport. Phys. Rev. E 89 (5), 052213.
Paola, C., Voller, V.R., 2005. A generalized Exner equation for sediment mass balance. J. Geophys. Res.: Earth Surf. 110 (F4).
Parteli, E.J.R., Andrade, J.S., Herrmann, H.J., 2011. Transverse instability of dunes. Phys. Rev. Lett. 107, 188001.
Parteli, E.J.R., Durán, O., Bourke, M.C., Tsoar, H., Pöschel, T., Herrmann, H., 2014. Origins of barchan dune asymmetry: Insights from numerical simulations. Aeolian Res. 12, 121–133.
Parteli, E.J.R., Durán, O., Tsoar, H., Schwämmle, V., Herrmann, H.J., 2009. Dune formation under bimodal winds. Proc. Natl. Acad. Sci. USA 1106 (52), 22085–22089.
Pearce, K.I., Walker, I.J., 2005. Frequency and magnitude biases in the 'Fryberger' model, with implications for characterizing geomorphically effective winds. Geomorphology 68 (1), 39–55.
Phillips, J.D., Ewing, R.C., Bowling, R., Weymer, B.A., Barrineau, P., Nittrouer, J.A., Everett, M.E., 2019. Low-angle eolian deposits formed by protodune migration, and insights into slipface development at White Sands Dune Field, New Mexico. Aeolian Res. 36, 9–26.
Ping, L., Narteau, C., Dong, Z., Zhang, Z., Courrech du Pont, S., 2014. Emergence of oblique dunes in a landscape-scale experiment. Nat. Geosci. 7 (2), 99–103.
Preusser, F., Radies, D., Matter, A., 2002. A 160 000-year record of dune development and atmospheric circulation in Southern Arabia. Science 296 (5575), 2018–2020.
Pye, K., Tsoar, H., 1990. Aeolian Sand and Sand Dunes. Unwin Hyman, London.
Qian, G., Dong, Z., Zhang, Z., Luo, W., Lu, J., Yang, Z., 2015. Morphological and sedimentary features of oblique zibars in the Kumtagh Desert of northwestern China. Geomorphology 228, 714–722.
Radebaugh, J., Lorenz, R., Farr, T., Paillou, P., Savage, C., Spencer, C., 2010. Linear dunes on Titan and Earth: Initial remote sensing comparisons. Geomorphology 121 (1–2), 122–132.
Rasmussen, K.R., Iversen, J.D., Rautahemio, P., 1996. Saltation and wind-flow interaction in a variable slope wind tunnel. Geomorphology 17 (1–3), 19–28.
Reffet, E., Courrech du Pont, S., Hersen, P., Douady, S., 2010. Formation and stability of transverse and longitudinal sand dunes. Geology 39 (6), 491–494.
Reitz, M.D., Jerolmack, D.J., Ewing, R.C., Martin, R.L., 2010. Barchan-parabolic dune pattern transition from vegetation stability threshold. Geophys. Res. Lett. 37 (19).
Rodriguez, S., Mouélic, S.L., Barnes, J.W., Kok, J.F., Rafkin, S.C.R., Lorenz, R.D., Charnay, B., Radebaugh, J., Narteau, C., Cornet, T., et al., 2018. Observational evidence for active dust storms on Titan at equinox. Nat. Geosci. 11 (10), 727–732.
Rozier, O., Narteau, C., Gadal, C., Claudin, P., Courrech du Pont, S., 2019. Elongation and stability of a linear dune. Geophys. Res. Lett. 46 (24), 14521–14530.
Rubanenko, L., Lapôtre, M.G.A., Ewing, R.C., Fenton, L.K., Gunn, A., 2022. A distinct ripple-formation regime on Mars revealed by the morphometrics of barchan dunes. Nature Commun. 13 (1), 7156.
Rubin, D.M., 1984. Factors determining desert dune type. Nature 309 (5963), 91–92.
Rubin, D.M., 2012. A unifying model for planform straightness of ripples and dunes in air and water. Earth-Sci. Rev. 113 (3–4), 176–185.
Rubin, D.M., Carter, C.L., 2005. Bedforms 4.0: MATLABcode for Simulating Bedforms and Cross-Bedding. US Geological Survey.
Rubin, D.M., Carter, C.L., 2006. Bedforms and Cross-Bedding in Animation. Number 2. SEPM (Society for Sedimentary Geology).
Rubin, D.M., Courrech du Pont, S., Narteau, C., Newman, C.E., Bridges, N., Lapôtre, M.G.A., 2016. Interpretation of wind regime of Bagnold Dunes in Gale Crater, guided by third-generation models of dune formation. In: AGU Fall Meeting Abstracts, Volume 2016. pages EP43D–05.
Rubin, D.M., Hunter, R.E., 1983. Reconstructing bedform assemblages from compound crossbedding. In: Developments in Sedimentology, Volume 38. Elsevier, pp. 407–427.
Rubin, D.M., Hunter, R.E., 1985. Why deposit of longitudinal dunes are rarely recognised in the geologic record. Sedimentology 32, 147–157.
Rubin, D.M., Hunter, R.E., 1987. Bedform alignment in directionally varying flows. Science 237, 276–278.
Rubin, D.M., Hunter, R.E., 2008. A second look at western Sinai self dunes and their lateral migration. Geomorphology 93, 335–342.
Rubin, D.M., Ikeda, H., 1990. Flume experiments on the alignment of transverse, oblique, and longitudinal dunes in directionally varying flows. Sedimentology 37 (4), 673–684.
Rubin, D.M., Lapôtre, M.A.G., Stevens, A.W., Lamb, M.P., Fedo, C.M., Grotzinger, J.P., Gupta, S., Stack, K.M., Vasavada, A.R., Banham, S.G., et al., 2022. Ancient winds, waves, and atmosphere in Gale Crater, Mars, inferred from sedimentary structures and wave modeling. J. Geophys. Res. 127 (4), e2021JE007162.

Rubin, D.M., McCulloch, D.S., 1980. Single and superimposed bedforms: a synthesis of San Francisco Bay and flume observations. Sediment. Geol. 26 (1–3), 207–231.
Rubin, D.M., Rozier, O., Narteau, C., Courrech du Pont, S., 2024. Simulations of dune morphology under tri-directional wind regimes and application to dunes on Mars. Aeolian Res. 67–69, 100922.
Sandoungout, S.K., 2019. Caractérisation de la morphologie des dunes dans des écoulements unidirectionnels et alternatifs (Ph.D. thesis). Université de Bretagne occidentale-Brest.
Saye, S.E., Pye, K., Clemmensen, L.B., 2006. Development of a cliff-top dune indicated by particle size and geochemical characteristics: Rubjerg Knude, Denmark. Sedimentology 53 (1), 1–21.
Schultz, M.P., Flack, K.A., 2009. Turbulent boundary layers on a systematically varied rough wall. Phys. Fluids 21 (1), 015104.
Selmani, H., Valance, A., Ould El Moctar, A., Dupont, P., Zegadi, R., 2018. Aeolian sand transport in out-of-equilibrium regimes. Geophys. Res. Lett. 45 (4), 1838–1844.
Shao, Y., Raupach, M.R., 1992. The overshoot and equilibration of saltation. J. Geophys. Res.: Atmos. 97 (D18), 20559–20564.
Shozaki, H., Hasegawa, H., 2022. Development of longitudinal dunes under Pangaean atmospheric circulation. Clim. Past 18 (7), 1529–1539.
Smith, H.T.U., 1965. Dune morphology and chronology in central and western Nebraska. J. Geol. 73 (4), 557–578.
Sokal, R.R., 1974. Classification: Purposes, principles, progress, prospects: Clustering and other new techniques have changed classificatory principles and practice in many sciences. Science 185 (4157), 1115–1123.
Sokolòw, N.A., 1894. Die Dünen: Bildung, Entwickelung und innerer Bau. Springer, German translation from Russian assisted A. Arzruni.
Stull, R.B., 1988. An Introduction To Boundary Layer Meteorology, Volume 13. Springer Science & Business Media.
Sullivan, R., Kok, J.F., Katra, I., Yizhaq, H., 2020. A broad continuum of aeolian impact ripple morphologies on Mars is enabled by low wind dynamic pressures. J. Geophys. Res. 125 (10), e2020JE006485.
Sullivan, T.S., Liu, Y., Ecke, R.E., 1996. Turbulent solutal convection and surface patterning in solid dissolution. Phys. Rev. E 54 (1), 486.
Swann, C., Sherman, D.J., Ewing, R.C., 2020. Experimentally derived thresholds for windblown sand on Mars. Geophys. Res. Lett. 47 (3), e2019GL084484.
Taniguchi, K., Endo, N., Sekiguchi, H., 2012. The effect of periodic changes in wind direction on the deformation and morphology of isolated sand dunes based on flume experiments and field data from the Western Sahara. Geomorphology 179, 286–299.
Telfer, M.W., Hesse, P.P., Perez-Fernandez, M., Bailey, R.M., Bajkan, S., Lancaster. Morphodynamics, N., 2017. boundary conditions and pattern evolution within a vegetated linear dunefield. Geomorphology 290, 85–100.
Telfer, M.W., Parteli, E.J.R., Radebaugh, J., Beyer, R.A., Bertrand, T., Forget, F., Nimmo, F., Grundy, W.M., Moore, J.M., Stern, S.A., et al., 2018. Dunes on Pluto. Science 360 (6392), 992–997.
Thorsness, C.B., Hanratty, T.J., 1979. Stability of dissolving or depositing surfaces. AIChE J. 25 (4), 697–701.
Tsoar, H., 1983. Dynamic processes acting on a longitudinal (seif) sand dune. Sedimentology 30 (4), 567–578.
Tsoar, H., 1984. The formation of seif dunes from barchans-a discussion. Zeitschrift Geomorphol. 28 (1), 99–103.
Tsoar, H., 2005. Sand dunes mobility and stability in relation to climate. Physica A 357 (1), 50–56.
Tsoar, H., Parteli, E.J.R., 2016. Bidirectional winds, barchan dune asymmetry and formation of seif dunes from barchans: a discussion. Environ. Earth Sci. 75 (18), 1–10.
Tsoar, H., Yaalon, D.H., 1983. Deflection of sand movement on a sinuous longitudinal (self) dune: use of fluorescent dye as tracer. Sediment. Geol. 36 (1), 25–39.
Ungar, J.E., Haff, P.K., 1987. Steady state saltation in air. Sedimentology 34, 289–299.
Valance, A., Rasmussen, K.R., Ould El Moctar, A., Dupont, P., 2015. The physics of aeolian sand transport. C. R. Phys. 16 (1), 105–117.
Van Driest, E.R., 1956. On turbulent flow near a wall. Journal of the aeronautical sciences 23 (11), 1007–1011.
Villien, B., Zheng, Y., Lister, D., 2005. Surface dissolution and the development of scallops. Chem. Eng. Comm. 192 (1), 125–136.
Vosper, S.B., 2004. Inversion effects on mountain lee waves. Q. J. R. Meteorol. Soc. 130 (600), 1723–1748.
Walker, I.J., Hesp, P.A., Davidson-Arnott, R.G.D., Bauer, B.O., Namikas, S.L., Ollerhead, J., 2009. Response of three-dimensional flow to variations in the angle of incident wind and profile form of dunes: Greenwich Dunes, Prince Edward Island, Canada. Geomorphology 105, 127–138.
Walker, I.J., Nickling, W.G., 2002. Dynamics of secondary airflow and sediment transport over and in the lee of transverse dunes. Prog. Phys. Geogr. 26, 47–75.
Walker, I.J., Nickling, W.G., 2003. Simulation and measurement of surface shear stress over isolated and closely spaced transverse dunes in a wind tunnel. Earth Surf. Process. Landf. 28, 1111–1124.
Walker, I.J., Shugar, D.H., 2013. Secondary flow deflection in the lee of transverse dunes with implications for dune morphodynamics and migration. Earth Surf. Process. Landf.
Wang, X., Dong, Z., Zhang, J., Chen, G., 2002. Geomorphology of sand dunes in the Northeast Taklimakan Desert. Geomorphology 42 (3–4), 183–195.
Warren, A., 1971. Dunes in the Tenere Desert. Geogr. J. 458–461.
Warren, A., 1972. Observations on dunes and bi-modal sands in the Ténéré Desert. Sedimentology 19 (1–2), 37–44.
Warren, A., Allison, D., 1998. The palaeoenvironmental significance of dune size hierarchies. Palaeogeogr. Palaeoclimatol. Palaeoecol. 137 (3–4), 289–303.
Wasson, R.J., Hyde, R., 1983. Factors determining desert dune type. Nature 304, 337–339.
Werner, B.T., Kocurek, G., 1997. Bed-form dynamics: Does the tail wag the dog? Geology 25 (9), 771–774.
Werner, B.T., Kocurek, G., 1999. Bedform spacing from defect dynamics. Geology 27 (8), 727–730.
Wiggs, G., 2019. Desert dunes: Form and process. In: Aeolian Geomorphology: A New Introduction. pp. 133–155.
Wiggs, G.F.S., Livingstone, I., Warren, A., 1996. The role of streamline curvature in sand dune dynamics: evidence from field and wind tunnel measurements. Geomorphology 17 (1), 29–46.
Worman, S.L., Murray, A.B., Littlewood, R., Andreotti, B., Claudin, P., 2013. Modeling emergent large-scale structures of barchan dune fields. Geology 41 (10), 1059–1062.
Xu, Z., Mason, J.A., Lu, H., 2015. Vegetated dune morphodynamics during recent stabilization of the Mu Us dune field, north-central China. Geomorphology 228, 486–503.
Yan, N., Baas, A.C.W., 2017. Environmental controls, morphodynamic processes, and ecogeomorphic interactions of barchan to parabolic dune transformations. Geomorphology 278, 209–237.
Yizhaq, H., Balmforth, N.J., Provenzale, A., 2004. Blown by wind: nonlinear dynamics of aeolian sand ripples. Physica D 195 (3–4), 207–228.
Yu, X., Hörst, S.M., He, C., McGuiggan, P., Crawford, B., 2018. Where does Titan sand come from: insight from mechanical properties of Titan sand candidates. J. Geophys. Res. 123 (9), 2310–2321.
Zhang, Z., Dong, Z., Hu, G., Parteli, E.J.R., 2018. Migration and morphology of asymmetric barchans in the Central Hexi Corridor of Northwest China. Geosciences 8 (6), 204.
Zhang, D., Narteau, C., Rozier, O., Courrech du Pont, S., 2012. Morphology and dynamics of star dunes from numerical modelling. Nat. Geosci. 5, 463–467.
Zilker, D.P., Cook, G.W., Hanratty, T.J., 1977. Influence of the amplitude of a solid wavy wall on a turbulent flow, Part 1. Non-separated flows. J. Fluid Mech. 82 (1), 29–51.